Appendix

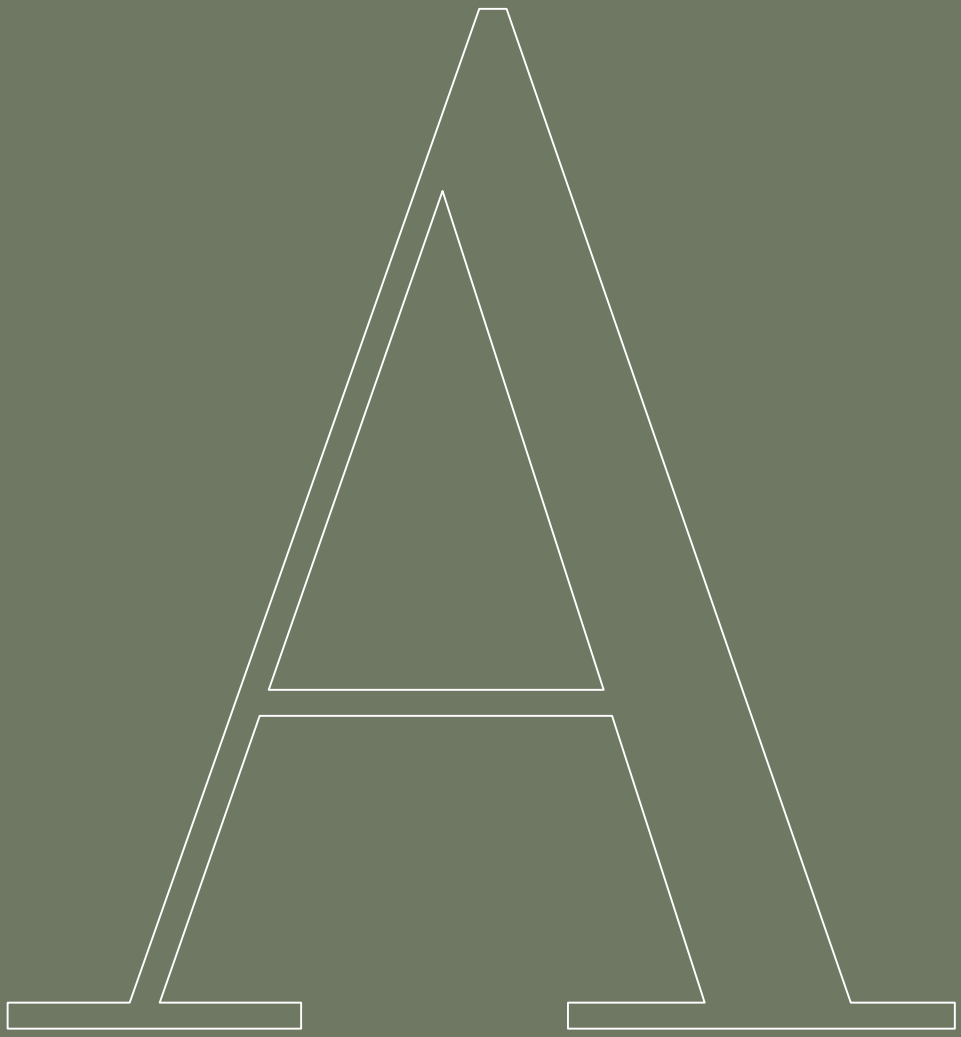

1. Detailed Description of Optical Transduction Modes

1.1 Colorimetry

The colorimetric signal readout, often referred to as spectrophotometry, is a signal reading method that detects the surface refractive index of structures to be measured by recording the color changes of sensor structures based on optical response signals. Researchers can observe changes in the shade or type of solution color during reactions to detect the target with the naked eye or use a UV–visible absorption spectrometer to read out signal changes.

Colorimetry is one of the oldest analytical methods[1]. Its roots trace back to pre-modern chemistry times, when it was employed for basic 'naked eye' quantification of color shifts, such as the transformation of tea color when lemon juice is added. The earliest documented colorimetric reaction was performed by Plinius Secundus, a Roman Empire commander and philosopher, who used gallnut extract to detect iron in hydrated copper acetate [2]. The evolution of colorimetric detection technologies was significantly shaped by the burgeoning dye and pigment industry in the late 19th century. This era witnessed the creation of tools and methods for precisely determining color and optical properties. W. A. Lampadius, in 1838, marked an early milestone with quantitative colorimetric determination, estimating nickel and iron levels in cobalt ore by comparing filtrate color with standard solutions in cylindrical tubes [3]. The earliest true colorimeter featuring a glass prism that controlled red, green, and blue light beams independently to match the color in the sample was invented by Scottish scientist James Clerk Maxwell in 1860. One of the key developments during this time was the invention of the Duboscq colorimeter by Jules Duboscq in 1870. Photoelectric colorimetry became popular in the mid-1930s, and in 1938 William Henry Summerson applied for a patent for his colorimeter containing a photocell [4].

In contemporary sensor technology, colorimetric sensors leverage the changes in color or spectral properties induced by the interaction between the receptor and the target analyte. This interaction results in measurable alterations in absorbance or reflectance spectra, providing a visual or instrument-based indication of the analyte's presence and concentration. Absorbance, the most prevalent mode of detection, operates based on the amount of monochromatic radiation absorbed by the analytes from a light beam. Conversely, transmittance is determined by the intensity of monochromatic radiation

that is not absorbed by the analytes. Both methods require similar equipment: a light source, a detector (like a photodiode), and a monochromator if necessary.

To construct a colorimetric sensor system, the chromogenic probe is clearly the key contributing factor. Traditional organic chromophores have been extensively utilized in colorimetric sensors for the detection of diverse target molecules. However, these organic probes face challenges such as relatively low molar extinction coefficient and limited aqueous compatibility that restrict their practical application.

Nanotechnology plays an important role in current colorimetric sensors development. Metal nanoparticles, mainly including gold (Au), silver (Ag), palladium (Pd), platinum (Pt) and ruthenium (Ru) are preferred over traditional organic dyes due to their localized surface plasmon resonance (LSPR) properties. These properties are influenced by factors such as color, dispersion, aggregation status, shape, and size of the nanoparticles, making them highly effective for sensitive colorimetric detection [5]. In sensors based on interparticle distance-dependent principles, the aggregation or dispersion of these nanoparticles by analytes can lead to noticeable color changes, a phenomenon attributed to LSPR effects.

Colorimetric detection stands out as a user-friendly technique, offering direct visual results without the need for additional equipment. In addition, colorimetry is regarded as the most suitable detection technique to integrate with paper based devices, due to its simplicity and compatibility with relatively low-cost reporting systems, including smartphones[6,7] and scanners[8]. This simplicity makes it the most promising transduction mode for commercialization. From healthcare to environmental monitoring[9], colorimetric sensors are increasingly finding their way into everyday devices, such as home pregnancy test, COVID-19 lateral flow test and pH strips. However, despite their widespread adoption, challenges persist in the commercialization of quantitative colorimetric sensors.

1.2 Fluorescence spectroscopy

Fluorescence spectroscopy is a technique that utilizes the emission of light by a molecule or material, referred to as a fluorophore. This emission occurs following the initial electronic excitation induced by light absorption. In the context of chemical sensors, the excitation of fluorophores by an external light source initiates the emission

of fluorescence signals. This emitted fluorescence acts as a measurable indicator, providing valuable insights into the presence and concentration of the target substance[10].

In scenarios where the target molecules naturally exhibit fluorescence properties, direct detection is feasible. However, for molecules that lack intrinsic fluorescence, a fluorescent label becomes essential. This involves using fluorophores, fluorescent molecules, or nanomaterials such as quantum dots and nanoparticles to tag the target molecules, thereby facilitating efficient detection. Fluorescence-based sensors employ several parameters [11]. These include fluorescence intensity (F), which can be measured at specific excitation and emission wavelengths, giving rise to the fluorescence emission and excitation spectra. Emission anisotropy or polarization (r or P) is determined based on fluorescence intensities at different polarizations. Furthermore, the fluorescence lifetime (τF), also known as the fluorescence-detected excited-state lifetime, characterizes how long a fluorophore stays in its excited state before returning to the ground state. All these parameters can be determined as a function of excitation and emission wavelengths. They can be used for reporting on sensor-target interactions and a variety of possibilities exist for their employment in sensor constructs.

The advent of nanotechnology has significantly enhanced the development of fluorescence-based sensors. The introduction of quantum dots [12–14] and nanoparticles [15,16] has increased the sensitivity and adaptability of these sensors, offering a broader range of applications compared to traditional fluorophores.

Fluorescence spectroscopy has a rich history, with its first fluorescent sensor for aluminum ion (Al^{3+}) detection reported by F. Goppelsroder in 1867, utilizing a fluorescent morin chelate [17]. Initially focused on metal ion detection, the scope of fluorescent sensors has expanded to include biologically and environmentally important cations, anions, small neutral molecules, and biomacromolecules such as proteins and DNA[18]. This expansion has been paralleled by advancements in microscopic imaging technologies. While the complexity of experimental setups remains a consideration, ongoing advancements and cost-effective solutions aim to address these challenges, ensuring the continued expansion of fluorescence spectroscopy applications beyond the laboratory setting [19].

1.3 Other optical transducers

In addition to well-known optical transduction methods like colorimetry and fluorescence spectroscopy, several other techniques play significant roles in chemical sensing. Plasmonic techniques, such as propagating surface plasmon resonance (SPR), and surface-enhanced Raman scattering (SERS) has already caught the scientific community's attention as a highly sensitive and promising technique in chemical sensing [20]. SPR utilizes the resonant oscillation of conduction electrons at a metal-dielectric interface for biosensing, offering label-free detection of molecular interactions. SERS, on the other hand, SERS technology is used to enhance the naturally weak Raman signal using the optical and chemical properties of nearby plasmonic nanomaterial enabling detailed molecular recognition [21]. Both techniques are acclaimed for their sensitivity, label-free detection, high reusability, short response time, and simple sample treatments, along with the use of minimal electrical components [20]. However, SPR's effectiveness in detecting small molecules can be limited due to minimal refractive index variation post-analyte recognition.

Additionally, chemiluminescence, Chemiluminescence (CL) is a phenomenon that light emission occurs from electronically excited state of a species during the chemical reaction, offers high sensitivity for detecting low analyte levels, useful in environmental and clinical diagnostics [22]. CL sensors are based on the quantitative relationship between CL readout signal and the concentration of analyte. The integration of CL with technologies like flow injection microchip and immunoassay has expanded its application scope, allowing for automated and selective analyses [23].

2. Detailed Description of Electrochemical Transduction Modes

2.1 Amperometry

Amperometry technique utilizes a three-electrode system. In this method, current is measured either at a constant potential, known as amperometry, or by scanning a potential range, known as voltammetry. The current flowing in an electrochemical cell is measured when a constant potential value is applied on the working electrode, producing a Faradic process (oxidation or reduction) of the target molecule. The current value is related to the concentration of the analyte according to the following mathematical equation:

$$i = \frac{nFAK_m(C_{bulk} - C_{x=0})}{\delta}$$

in which:

i is the limiting current [A];

n is number of exchanged electrons;

F is the Faraday constant [C mol^{-1}];

A is the working electrode area [cm^2];

K_m is the mass transport coefficient [cm s^{-1}];

C_{bulk} is the concentration of electroactive species in the bulk solution [mol cm^{-3}];

$C_{x=0}$ is the concentration of electroactive species at the surface of the electrode [mol cm^{-3}];

δ is the thickness of the diffusion layer

Amperometric sensors can be employed in various modes, including chronoamperometry and single-potential/multiple-potential amperometry. Chronoamperometry measures the steady-state current at a stepped potential within a brief time frame [24]. The steady-state current arises from alterations in the diffusion of the analyte to the substrate electrode with the receptor [25]. Single and multiple potential chronoamperometric techniques are prevalent. In single-potential amperometry, a forward potential pulse is applied, and the corresponding current response is measured, often employing linear sweep voltammetry (LSV). In multiple/double potential amperometry, the potential is swept by initially applying a forward potential and then returning it to the starting initial value within a specified time frame, typically observed in cyclic voltammetry (CCV).

Other volumetric techniques, such as controlled potential amperometry, encompass pulse voltammetry, which includes differential pulse voltammetry (DPV), square wave voltammetry (SWV), and normal pulse voltammetry (NPV), the latter not yet reported with amperometric detection. These diverse modes and techniques highlight the flexibility and applicability of amperometry, making it a powerful tool for probing electrochemical processes and quantifying analytes in various applications.

One of the earliest amperometric sensors, developed in 1953 by L. C. Clark, revolutionized the measurement of dissolved oxygen in blood [26]. This pioneering device had a profound impact on the medical community, especially in monitoring dissolved oxygen, critical for developing the now commonplace heart-lung machine[27,28]. With the evolution of nanotechnology and the introduction of novel electrode nanomaterials, amperometric sensors have found widespread applications across various domains, showcasing their adaptability and enduring relevance in modern analytical practices [29].

2.2 Potentiometry

In potentiometric sensors, the mechanism involves measuring potential changes resulting from charge accumulation at the working electrode, even in the absence of current flow between the electrodes. Utilizing a high impedance voltmeter, the potential difference or electromotive force between the working electrode and the reference electrode is measured. This potential is proportionally related to the logarithm of the analyte concentration, forming the basis of the sensor's analytical output. The equation that correlates the measured potential difference and the activity of the analyte is the Nernst equation:

$$E_{Cell} = E^0_{Cell} - \left(\frac{RT}{nF}\right) \ln Q$$

Where:

E_{Cell} is the observed cell potential at zero current [V];

E^0_{Cell} is the standard cell potential [V];

R is the universal gas constant = 8.3143 [J K^{-1} mol^{-1}];

T is the absolute temperature [K];

n is the charge number of electrode reaction;

F is the Faraday constant = 9.6487·104 [C mol^{-1}];

Q is the ratio of ion activity at the anode to ion activity at the cathode;

The reference electrode commonly used in potentiometric sensors is Ag/AgCl, ensuring a stable reference potential. Conversely, the working electrode integrates an ion-

selective or semi-permeable membrane, earning it the designation of an ion-selective electrode. The origin of ion-selective electrodes can be traced back to the mid-20th century, notably with Max Cremer's work on glass electrodes for pH measurement in 1906, laying the foundation of potentiometric sensing.

Potentiometric sensors have expanded their scope beyond pH measurement to encompass a diverse array of analytes, facilitated by customizable ion-selective membranes. With these types of electrodes, it is possible to determine a wide variety of ions, such as K^+, Na^+, Ca^{2+}, NH^{4+}, F^-, I^-, CN^-, or gases such as CO_2 or NH_3 [30,31]. In 1970, the ion-sensitive field-effect transistor (ISFET) configuration was proposed by Bergveld, marking an evolutionary step in the development of more versatile potentiometric sensors. It was found that ions can be detected by a ISFET as long as its architecture is changed by removing the metal gate and inserting the gate oxide in an aqueous solution along with a reference electrode. Their success in requiring low sample volumes and achieving extreme miniaturization has made them promise for in-field applications.

Moreover, the advent of microfabricated sensors in the late 1990s and early 2000s marked another major milestone in the field of potentiometric sensors. These sensors can be produced in large quantities at a low cost, making them ideal for numerous applications in environmental[32–34], food [35], and health[36] monitoring.

2.3 Electrochemical impedance spectroscopy

Electrochemical impedance spectroscopy (EIS) measures the current in terms of charge transfer resistance or capacitance when the resulting current is in phase or out of phase with the applied potential. EIS enables the measurement of different parameters such as impedance, phase, resistance, and capacitance at different frequencies as a measure of molecular interaction. EIS can measure the response in a full frequency span typically from 10 mHz to 100 kHz, but it can also be measured at a single frequency for the development of practical sensor. In addition, Considered one of the most sensitive electroanalytical techniques in the field of sensors, EIS does not require receptor labelling.

EIS is a powerful surface characterization method that has been discovered since the 1970s but has only been applied in the sensing field since the 2000s. This non-

destructive technique measures the response of an electrochemical system subjected to voluntary sinusoidal perturbation. Generally, this perturbation consists of a low amplitude (~10 mV) AC voltage, imposed around the equilibrium potential of the redox couple in solution, while sweeping a frequency range (f) of about ten kHz. Given that the disturbance imposed in EIS is sinusoidal (with an angular frequency $\omega = 2\pi f$ and a maximum voltage V_0), the applied voltage is written in the following form:

$$V(t) = V_0 \sin(\omega t)$$

The current response through the electrochemical system is of the same sinusoidal form with a phase shift φ and a maximum current I_0, as illustrated by the following equation:

$$I(t) = I_0 \sin(\omega t + \varphi)$$

Where, in the potentiostatic mode, $V(t)$ is the perturbation imposed at a chosen equilibrium potential with respect to the redox couple under study, and $I(t)$is the current response of the system under study.

Expressed as a complex number *Z(ω)*, the electrochemical impedance results from the ratio of the applied voltage to the measured current:

$$Z^*(\omega) = \frac{V(t)}{I(t)} = Re\left(Z(\omega)\right) + j \times Im\left(Z(\omega)\right); \text{ With } j = \sqrt{-1}$$

$Re(Z)$ is the real part of Z^* and Im(Z) is its imaginary part (often noted as Z' and $-Z''$, respectively). Hence the impedance modulus:

$$|Z| = \sqrt{(Z')^2 + (Z'')^2}$$

This mathematical formulation enables the quantification and interpretation of electrochemical impedance, offering a window into the intricate interplay of molecular entities.

To interpret the impedimetric response, two signal representations are employed—the Nyquist diagram and the Bode diagram (Figure A.1). The Nyquist diagram elucidates the interplay of Z' and Z'' in an orthonormal frame, while the Bode diagram delineates $|Z|$ and phase shift φ against the logarithm of frequency $\log(f)$. In sensing, the Nyquist representation is prevalent, especially for faradaic systems involving a soluble redox probe diffusing from solution to the electrode surface. This graphical approach proves

instrumental in unraveling the intricacies of molecular dynamics at the electrochemical interface.

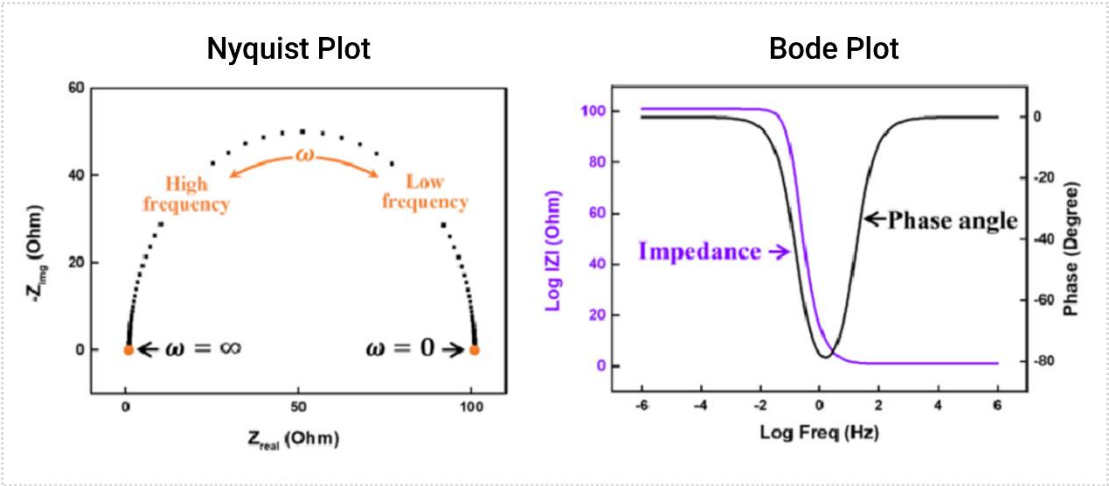

Figure A.1 Electrochemical Impedance Spectroscopy representation by Nyquist plot (left) and Bode plot (right) [37].

Nyquist plots usually include a semicircle region lying on the axis followed by a straight line. The semicircle portion (at higher frequencies) corresponds to the electron-transfer-limited process, and the straight line (at low-frequency range) represents the diffusion-limited process.

Moreover, the modifications of the electrochemical behavior of the electrode/electrolyte interface can be modeled by an equivalent electrical circuit. This modeling assigns to each point of the obtained signal a physical meaning. More concretely, each variable involved in the electrochemical process is assimilated to a real electronic component having approximately the same electronic behavior (resistance, capacitor, etc.). Consequently, many equivalent electrical circuits have been described in the literature, whose complexity varies according to the system studied [38]. Among them, the "Randles-Ershler" circuit shown above (Figure A.2) is the most used in the field of sensors.

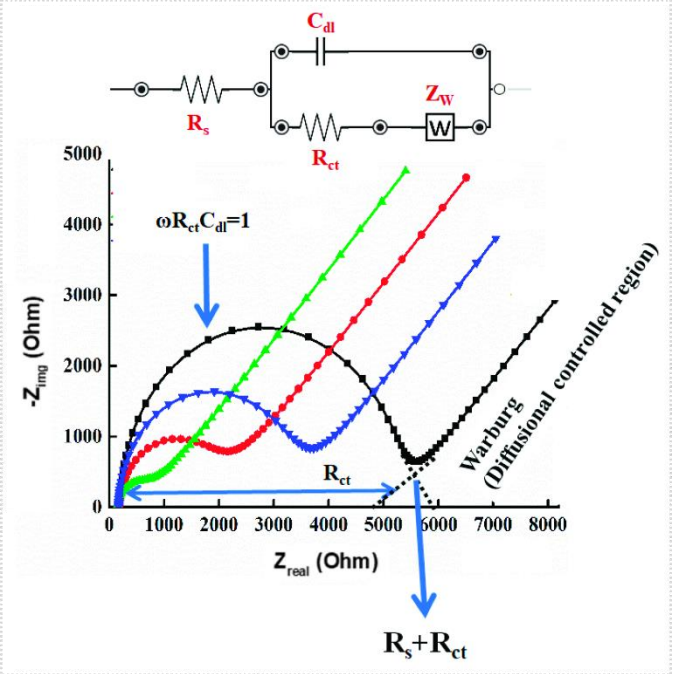

Figure A.2 Nyquist plot curves and their Randles equivalent circuit [38].

It consists of the following elements:

- Electrolyte resistance (R_s): It refers to the internal resistance of the electrochemical cell relative to the conductance of the electrolyte solution, i.e., the mobility of its ions. This results in a translation of the Nyquist signal of the Rs value.
- Charge transfer resistance (R_{ct}): This is the equivalent resistance to electron transfer between redox species if we assume that their activities are constant. This resistance therefore informs on the kinetics of the redox reactions involved.
- Warburg impedance (W): It characterizes the evolution of the faradic current according to the diffusion of electroactive species inducing variations in their activities (concentrations). It illustrates in some way the influence of the transport of matter to the surface of the electrode. At high frequencies, the diffusing reagents do not need to move very far, which minimizes the Warburg impedance. On the other hand, at low frequencies, the diffusion constraint increases this value (W).
- Constant Phase Element (CPE): These elements represent non-ideal capacitors to translate the value of the non-perfect capacitance (due to the electrode roughness) at the electrode/electrolyte interface as the ions in the solution approach the electrode surface to form a double layer. The value of the CPE depends on many

variables including electrode potential, ion types and concentrations, oxide layers, adsorption and oxide layers, impurity adsorption, temperature, etc.

Electrochemical Impedance Spectroscopy (EIS) is valued for its non-destructive nature, facilitated by the small amplitude perturbation from steady state. This technique has gained popularity owing to its remarkable sensitivity, reaching down to the femto-and attomolar ranges [39,40]. EIS stands out for its versatility, enabling impedance measurements not only in the presence of a redox couple (faradic) but also in their absence, allowing for non-faradic impedance measurements[38]. This flexibility extends its utility to label-free sensing, particularly advantageous when dealing with non-electroactive analytes [41].

But In most of the studies described in the literature, the variation of the detection signal is attributable to changes in the resistance of the electrode to electronic transfer (R_{ct}), provided by the redox probe in solution. Common benchmark redox probes include anionic $[Fe(CN)_6]^{3-/4-}$, cationic $[Ru(NH_3)_6]^{2+/3+}$, or neutral $[Fc(MeOH)^{0/+}]$.

Resistive impedance is certainly a very powerful characterization and detection tool thanks to the wealth of information it provides from simple experiments. However, this technique is not without drawbacks. A high sensitivity could sometimes be correlated with a non-specific response or a false positive result, due to a contaminated surface, repetitive measurements or after several immersions in the buffer between measurements. In addition, EIS is limited by the faradaic regime in solution i.e., the need to add a redox probe to the buffer. This can potentially affect the stability and activity of the assembled electrode. For example, Vogt et al.[42] demonstrated the deterioration of the surface of a gold electrode by free CN^- ions during impedance measurements in a typical $[Fe\ (CN)_6]^{3-/4-}$ solution. On the other hand, the modeling of certain electrochemical systems by equivalent circuits is sometimes very complex, since the model electrical circuit is often ot the only one possible.

3. Detailed Description of Hybrid Transduction Modes

3.1 Electrochemiluminescence

Electrochemiluminescence (ECL) is a sensing technique that converts electrical energy into light, typically through an electrode system. This process is marked by the transition of molecular species, formed by the electrochemical reaction, from an excited

state to a ground state, or the high-energy transmission of electrons within these molecular species. The resulting luminescence from the surface of the electrode is usually measured using a photodetector. The roots of ECL can be traced back to 1929 when Harvey discovered the luminescence of aminophthalichydrazid in the process of an electrochemical reaction and termed this phenomenon as galvano-luminescence[43]. Hercules then observed chemiluminescence during electrolysis of aromatic hydrocarbons at the cathode and discussed its possible mechanism in 1964, which can be seen as the first detailed report about ECL[44]. Since these pioneering works, ECL has evolved into a valuable technique with diverse applications in the field of analytical and sensing methodologies. As previously mentioned, Electrochemiluminescence (ECL) arises from the interactions among electrode species, and based on different reaction mechanisms, it can be broadly classified into two predominant categories: the annihilation pathway and the co-reactant pathway (see Figure A.3).

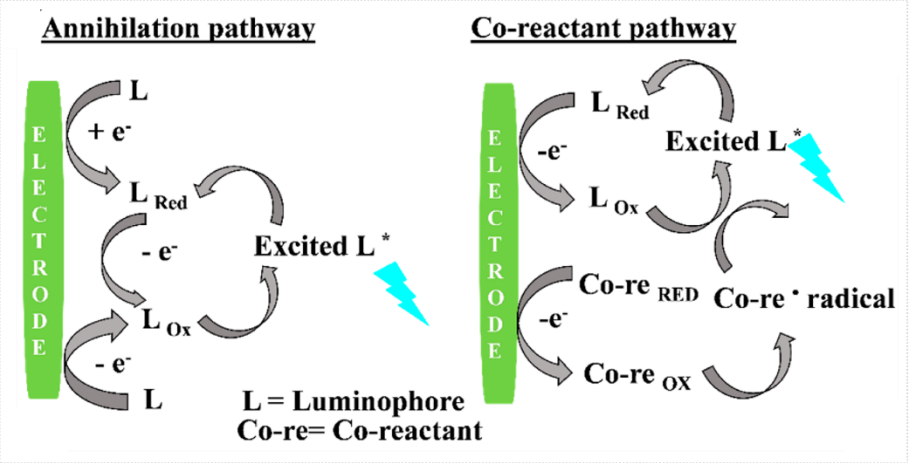

Figure A.3 ECL mechanisms: Annihilation and co-reactant pathway [45].

In the annihilation pathway, the generation of ECL requires only a single emitter. An alternating voltage is applied to the electrode surface, leading to the creation of oxidized and reduced free radicals of the luminescent species. These free radicals then undergo an annihilation reaction, resulting in the formation of excited-state luminescent species. The subsequent relaxation of these excited-state species leads to the emission of visible light [46]. Conversely, the co-reactant pathway involves both an emitter and a co-reactant. In this pathway, the ECL reagent and co-reactant experience simultaneous oxidation or reduction. The co-reactant rapidly decomposes, producing high-energy free radical intermediates. The ECL reagent reacts with these high-energy free radicals,

forming excited-state molecules that emit luminescence. Essentially, the co-reactant plays a crucial role in initiating the generation of high-energy intermediates that subsequently contribute to the luminescent process [47]. The classic co-reactants include oxalate, cerium(III) sultate, and tri-n-propylamine (TPA) [48].

In its role as a sensing transduction mode, the presence of the target analyte can affect the concentration of the luminophore or co-reactor, thereby changing the ECL signal intensity and allowing the detection of the target molecule [49]. With the combination of optical and electrochemical methods, ECL represents many advantages such as a wide dynamic range, excellent spatiotemporal controllability, and high sensitivity, bringing ECL from a basic investigation to various practical applications especially in bioassays[50,51]. ECL analysis technologies have been commercialized, such as the Elecsys® technology from Roche and the MULTI-ARRAY® Technology from Meso Scale Diagnostics[52].

3.2 Photoelectrochemistry

Photoelectrochemistry (PEC) is a technique that transforms light (photons) into electric signals by exciting electrons in a photoactive material. This leads to the generation of photocurrents, representing the reverse process of electrochemiluminescence, where light is utilized for excitation, and photocurrent functions as the detection signal.

In a typical PEC cell, three essential components work in tandem: (a) a light-harvesting nanomaterial assembled on a transparent conducting substrate as the working electrode (WE), (b) a metal electrocatalyst as the counter electrode (CE), and (c) suitable electrolyte between the WE and CE. The photoelectrochemical process unfolds as follows: When light with sufficient energy irradiates the nanomaterial, electrons transition from the valence band (*VB*) to the conduction band (*CB*), generating electron-hole pairs (e^--h^+) (Figure 7).

If the analyte in the reaction cell is an electron acceptor (oxidant), it combines with electrons in the conduction band of the nanomaterial. The external circuit carries these electrons to quench the photogenerated holes of the nanomaterial, forming a cathodic photocurrent. Conversely, if the analyte in the reaction cell is an electron donor (reductant), it provides electrons to quench the photogenerated holes of the

nanomaterial. Simultaneously, electrons in the conduction band of the nanomaterial are transferred to the external circuit, resulting in an anodic photocurrent (see Figure A.4).

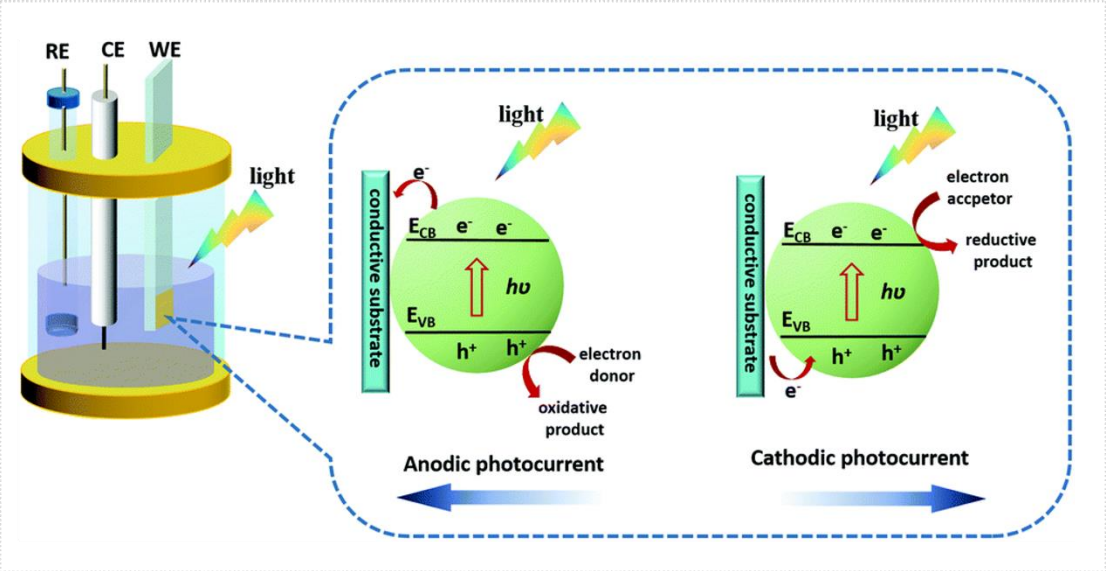

Figure A.4 Diagram of PEC sensing with the traditional three electrode system and the photocurrent generation mechanism [53].

A crucial aspect of PEC is the careful selection of photoactive materials, spanning inorganic, organic, or hybrid semiconductors. Previous reports categorize these materials into semiconductors and semiconductor-based heterojunctions.

Photoelectrochemistry traces its roots back to 1839 when Becquerel observed a photocurrent—a flow of electrons—between illuminated electrodes in a solution [54]. However, it wasn't until 1972 when Fujishima and Honda pioneered the use of light-irradiated titanium dioxide (TiO_2) for water oxidation, a process referred to as water splitting [55]. This landmark discovery revitalized interest in photoelectrochemistry, propelling its applications into various domains, notably sensing. PEC exhibits sensitivity comparable to electrochemiluminescence. Its advantage lies in the separation of excitation (light) and detection (photocurrent), ensuring high sensitivity with low background signal. Additionally, PEC instruments are simpler and more cost-effective compared to conventional optical methods or electrochemiluminescence. PEC sensors operate in potentiometric or current modes, contributing to their widespread adoption in various fields over the past two decades, including medical research, environmental monitoring, and food safety [56].

3.3 Electrochemical quartz crystal microbalance (EQCM)

EQCM is a sensitive analytical technique used to measure mass changes on an electrode's surface during electrochemical reactions. This system typically employs electrodes made of gold (Au) or platinum (Pt). The core principle involves an electrode-coupled oscillator circuit linked to a frequency counter [57]. The EQCM detects changes in the resonant frequency of the quartz crystal microbalance (QCM), which are correlated with mass alterations resulting from electrochemical processes on the electrode surface [58]. This technology allows the monitoring of surface-related electrochemical phenomena. EQCM transduction mode is gaining more and more attention when coupled with imprinted polymers as a recognition part in the sensors.

EQCM has been also commonly applied diversly in environmental, pharmaceutical and biomedical sensing. However, EQCM still faces challenges like environmental sensitivity and the need for precise calibration.

The Electrochemical Quartz Crystal Microbalance (EQCM) is an advanced analytical technique utilized to measure subtle mass changes on electrode surfaces during electrochemical reactions. Employing electrodes typically made of gold or platinum, EQCM operates on the principle of an electrode-coupled oscillator circuit connected to a frequency counter. It detects variations in the quartz crystal's resonant frequency, correlating them with mass shifts linked to electrochemical activity on the electrode's surface. This makes EQCM a valuable tool for monitoring surface-related electrochemical phenomena such as electrodeposition and corrosion. Its use, particularly when combined with imprinted polymers for recognition in sensor design, is gaining attention. The versatility of EQCM extends to environmental, pharmaceutical, and biomedical sensing applications. Despite its growing popularity, EQCM confronts challenges like environmental sensitivity and the necessity for accurate calibration, which are crucial for maintaining its precision and reliability in diverse sensing contexts.

References

[1] R. T. Eskew, *Color Res. Appl.* **2002**, *27*, 377.

[2] S. Kumar, P. Bhushan, A. K. Agarwal, S. Bhattacharya, in *Pap. Microfluid.*, Springer, Singapore, **2019**, pp. 1–5.

[3] W. A. Lampadius, *J. für Prakt. Chemie* **1838**, *13*, 385–397.

[4] Y. Kumari Shrestha, S. Krishna Shrestha, in *Adv. Color. [Working Title]*, IntechOpen, **2023**.

[5] I. H. El-Sayed, X. Huang, M. A. El-Sayed, *Nano Lett.* **2005**, *5*, 829–834.

[6] A. W. Martinez, S. T. Phillips, E. Carrilho, S. W. Thomas, H. Sindi, G. M. Whitesides, *Anal. Chem.* **2008**, *80*, 3699–3707.

[7] G. G. Morbioli, T. Mazzu-Nascimento, A. M. Stockton, E. Carrilho, *Anal. Chim. Acta* **2017**, *970*, 1–22.

[8] A. W. Martinez, S. T. Phillips, M. J. Butte, G. M. Whitesides, *Angew. Chemie Int. Ed.* **2007**, *46*, 1318–1320.

[9] G. M. Fernandes, W. R. Silva, D. N. Barreto, R. S. Lamarca, P. C. F. Lima Gomes, J. Flávio da S Petruci, A. D. Batista, *Anal. Chim. Acta* **2020**, *1135*, 187–203.

[10] Z. Gryczynski, I. Gryczynski, J. R. Lakowicz, in *Methods Enzymol.*, Methods Enzymol, **2003**, pp. 44–75.

[11] D. Wu, A. C. Sedgwick, T. Gunnlaugsson, E. U. Akkaya, J. Yoon, T. D. James, *Chem. Soc. Rev.* **2017**, *46*, 7105–7123.

[12] X. Tong, S. Shi, C. Tong, A. Iftikhar, R. Long, Y. Zhu, *TrAC - Trends Anal. Chem.* **2020**, *131*, DOI 10.1016/j.trac.2020.116008.

[13] Y. Du, S. Guo, *Nanoscale* **2016**, *8*, 2532–2543.

[14] C. J. Murphy, *Anal. Chem.* **2002**, *74*, 520 A-526 A.

[15] N. Fontaine, A. Picard-Lafond, J. Asselin, D. Boudreau, *Analyst* **2020**, *145*, 5965–5980.

[16] L. Zhang, E. Wang, *Nano Today* **2014**, *9*, 132–157.

[17] A. W. Czarnik, American Chemical Society. Division of Organic Chemistry., D. C. . American Chemical Society. Meeting (204th : 1992 : Washington, *Fluorescent Chemosensors for Ion and Molecule Recognition : Developed from a Symposium Sponsored by the Division of Organic Chemistry of the American Chemical Society at the 204th Meeting of the American Chemical Society, Washington, DC, August 23-28, 199*, American Chemical Society, **1993**.

[18] S. O. Fakayode, C. Lisse, W. Medawala, P. N. Brady, D. K. Bwambok, D. Anum, T. Alonge, M. E. Taylor, G. A. Baker, T. F. Mehari, J. D. Rodriguez, B. Elzey, N. Siraj, S. Macchi, T. Le, M. Forson, M. Bashiru, V. E. Fernand Narcisse, C. Grant, *Appl. Spectrosc. Rev.* **2024**, DOI 10.1080/05704928.2023.2177666.

[19] Y.-H. Shin, M. Teresa Gutierrez-Wing, J.-W. Choi, *J. Electrochem. Soc.* **2021**, *168*, 017502.

[20] A. M. Shrivastav, U. Cvelbar, I. Abdulhalim, *Commun. Biol.* **2021**, *4*, 1–12.

[21] O. R. Bolduc, J. F. Masson, *Anal. Chem.* **2011**, *83*, 8057–8062.

[22] H. Zhu, X. Huang, Y. Deng, H. Chen, M. Fan, Z. Gong, *TrAC - Trends Anal. Chem.* **2023**, *158*, 116879.

[23] L. Zhao, J. Xu, L. Xiong, S. Wang, C. Yu, J. Lv, J. M. Lin, *TrAC Trends Anal. Chem.* **2023**, *166*, 117213.

[24] D. Grieshaber, R. MacKenzie, J. Vörös, E. Reimhult, *Sensors* **2008**, *8*, 1400–1458.

[25] C. Lefrou, P. Fabry, J. C. Poignet, *Electrochem. Basics, with Examples* **2012**, 1–353.

[26] L. C. CLARK, R. WOLF, D. GRANGER, Z. TAYLOR, *J. Appl. Physiol.* **1953**, *6*, 189–193.

[27] L. C. Clark, C. Lyons, *Ann. N. Y. Acad. Sci.* **1962**, *102*, 29–45.

[28] L. C. Clark, G. Sachs, *Ann. N. Y. Acad. Sci.* **1968**, *148*, 133–153.

[29] R. Seeber, F. Terzi, *J. Solid State Electrochem.* **2011**, *15*, 1523–1534.

[30] E. Zdrachek, E. Bakker, *Anal. Chem.* **2019**, *91*, 2–26.

[31] E. Bakker, E. Pretsch, *TrAC Trends Anal. Chem.* **2005**, *24*, 199–207.

[32] G. Lisak, *Environ. Pollut.* **2021**, *289*, 117882.

[33] M. L. Bouhoun, P. Blondeau, Y. Louafi, F. J. Andrade, *Chemosensors* **2021**, *9*, 96.

[34] C. L. Baumbauer, P. J. Goodrich, M. E. Payne, T. Anthony, C. Beckstoffer, A. Toor, W. Silver, A. C. Arias, *Sensors* **2022**, *22*, 4095.

[35] M. E. Draz, H. W. Darwish, I. A. Darwish, A. S. Saad, *Food Chem.* **2021**, *346*, 128911.

[36] M. Cuartero, M. Parrilla, G. A. Crespo, *Sensors (Switzerland)* **2019**, *19*, 363.

[37] W. Choi, H. C. Shin, J. M. Kim, J. Y. Choi, W. S. Yoon, *J. Electrochem. Sci. Technol.* **2020**, *11*, 1–13.

[38] H. S. Magar, R. Y. A. Hassan, A. Mulchandani, *Sensors* **2021**, *21*, 6578.

[39] A. A. Ensafi, M. Amini, B. Rezaei, *Microchim. Acta* **2018**, *185*, DOI 10.1007/s00604-018-2810-x.

[40] A. R. Cardoso, F. T. C. Moreira, R. Fernandes, M. G. F. Sales, *Biosens. Bioelectron.* **2016**, *80*, 621–630.

[41] R. Patel, M. Vinchurkar, A. Mohin Shaikh, R. Patkar, A. Adami, F. Giacomozzi, R. Ramesh, B. Pramanick, L. Lorenzelli, M. Shojaei Baghini, *Bioelectrochemistry* **2023**, *150*, 108370.

[42] S. Vogt, Q. Su, C. Gutiérrez-Sánchez, G. Nöll, *Anal. Chem.* **2016**, *88*, 4383–4390.

[43] N. Harvey, *J. Phys. Chem.* **1929**, *33*, 1456–1459.

[44] D. M. Hercules, *Science* **1964**, *145*, 808–809.

[45] E. Martínez-Periñán, C. Gutiérrez-Sánchez, T. García-Mendiola, E. Lorenzo, *Biosens. 2020, Vol. 10, Page 118* **2020**, *10*, 118.

[46] H. Zhang, H. Jiang, X. Liu, X. Wang, *Anal. Chim. Acta* **2024**, *1285*, 341920.

[47] S. Rebeccani, A. Zanut, C. I. Santo, G. Valenti, F. Paolucci, *Cite This Anal. Chem* **2021**, *2022*, 348.

[48] X. Gou, Z. Xing, C. Ma, J.-J. Zhu, *Cite This Chem. Biomed. Imaging* **2023**, *2023*, 414–433.

[49] X. Liu, S. Zhao, L. Tan, Y. Tan, Y. Wang, Z. Ye, C. Hou, Y. Xu, S. Liu, G. Wang, *Biosens. Bioelectron.* **2022**, *201*, 113932.

[50] W. Zhu, J. Dong, G. Ruan, Y. Zhou, J. Feng, *Angew. Chemie Int. Ed.* **2023**, *62*, e202214419.

[51] A. Zanut, A. Fiorani, S. Canola, T. Saito, N. Ziebart, S. Rapino, S. Rebeccani, A. Barbon, T. Irie, H. P. Josel, F. Negri, M. Marcaccio, M. Windfuhr, K. Imai, G. Valenti, F. Paolucci, *Nat. Commun.* **2020**, *11*, DOI 10.1038/s41467-020-16476-2.

[52] L. Li, Y. Chen, J. J. Zhu, *Anal. Chem.* **2017**, *89*, 358–371.

[53] Z. Qiu, D. Tang, *J. Mater. Chem. B* **2020**, *8*, 2541.

[54] A. Devadoss, P. Sudhagar, C. Terashima, K. Nakata, A. Fujishima, *J. Photochem. Photobiol. C Photochem. Rev.* **2015**, *24*, 43–63.

[55] A. Fujishima, K. Honda, *Nature* **1972**, *238*, 37–38.

[56] Y. Wang, Y. Rong, T. Ma, L. Li, X. Li, P. Zhu, S. Zhou, J. Yu, Y. Zhang, *Biosens. Bioelectron.* **2023**, *236*, 115400.

[57] J. P J, K. Prabakaran, J. Luo, D. H. M G, *Sensors Actuators A Phys.* **2021**, *331*, 113020.

[58] D. A. Buttry, M. D. Ward, *Chem. Rev.* **1992**, *92*, 1355–1379.

Appendix

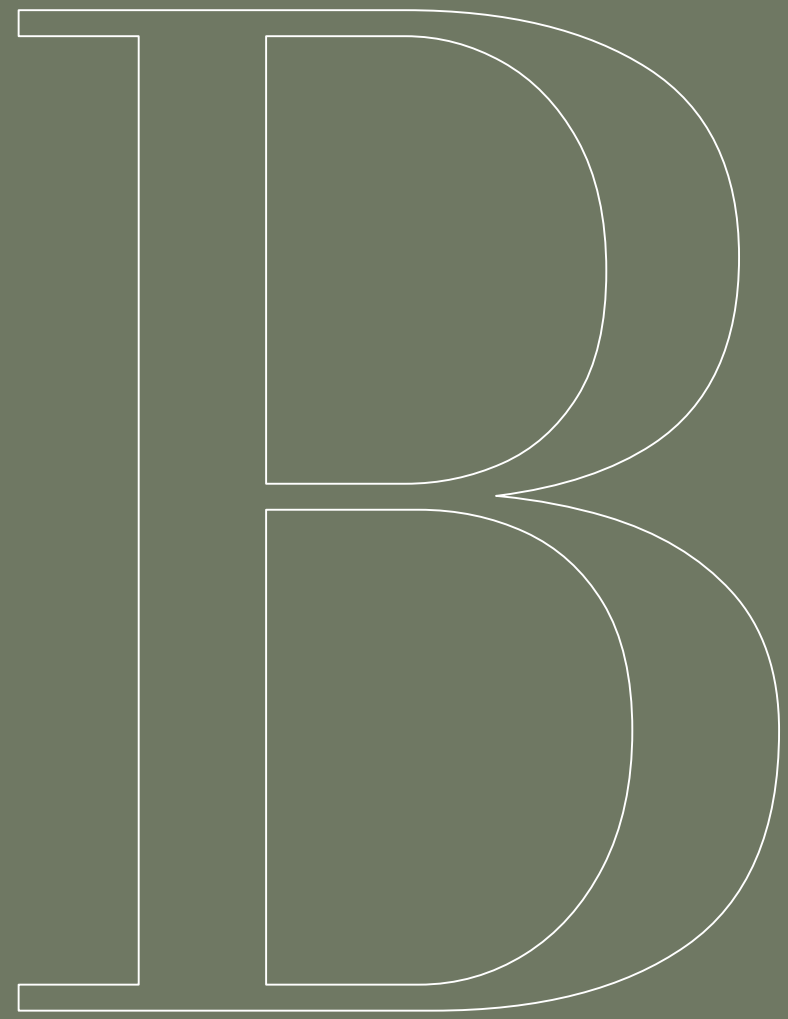

1. Supramolecular chemistry

Supramolecular chemistry also known as '*chemistry beyond the molecule*' is an interdisciplinary branch of science (spans the fields of chemistry, physics, and biology) that deals with the assembly and interaction between two or more components. This description was made by Jean-Marie Lehn, who won the Nobel Prize for his work in this field in 1987 [1]. Lehn's use of "beyond molecule" expression relates to the fact that, in contrast to classical chemistry, which deals with the creation of individual molecules from atoms, supramolecular chemistry focuses on the reversible non-covalent interactions between molecules resulting into organized molecular "arrays". As a contemporary terminology, Jonathan W. Steed et al. coined the term 'Lego^{TM} chemistry,' in which each Lego^{TM} brick symbolizes a molecular building block and these blocks are linked together by reversible intermolecular interactions (bonds) to form a supramolecular aggregate [2].

Explicitly, supramolecular chemistry is based on noncovalent interactions such as hydrogen bonding, polar attractions, van der Waals forces, and hydrophilic-hydrophobic interactions to organize and hold supramolecular assemblies together. Although these interactions are weak in comparison to covalent bonds, their multiplicity results in an extraordinary level of structural complexity.

In fact, nature was always a major source of inspiration for supramolecular chemistry. Enzyme-substrate, protein-ligand, and antibody-antigen are all rooted in non-covalent interactions, shape recognition, and complementary binding sites, albeit with a high degree of specificity [3]. Consequently, supramolecular structures have found extensive utility as artificial recognition units.

However, precise control over the formation and dissociation of the assembly in response to a range of triggers remains challenging as this property is very much akin to the substrate–catalyst (Lock–key specificity) binding in many biological systems. These biomimetic properties make synthetic host–guest systems attractive tools for the creation of therapeutics and diagnostics. Supramolecular chemistry can be divided into two broad categories: host-guest chemistry and self-assembly chemistry. The two approaches will be detailed in the following sections.

1.1 Host-guest chemistry

Host-guest chemistry represents a prominent facet of supramolecular chemistry, where host molecules form complexes with guest molecules or ions. Typically, host-guest complexes feature a larger cavitand molecule acting as the 'host' (H), encapsulating a compatible smaller molecule called 'guest' (G) within its cavity (Figure B.1). One definition of hosts and guests was given by Donald Cram, who said '*The host component is defined as an organic molecule or ion whose binding sites converge in the complex…The guest component is any molecule or ion whose binding sites diverge in the complex'* [4]. The Host guest complexation relies primarily on non-covalent forces, such as hydrogen bonds and van der Waals forces, and hydrophobic interactions. Despite the relatively modest strength of these interactions individually, their collective impact leads to substantial alterations in the physicochemical properties of the guests. In biology, one of the most notable examples of host-guest interactions unfolds in the dynamic relationship between enzymes and their substrates. Enzymes envelop substrates, giving rise to a reversible complex formation.

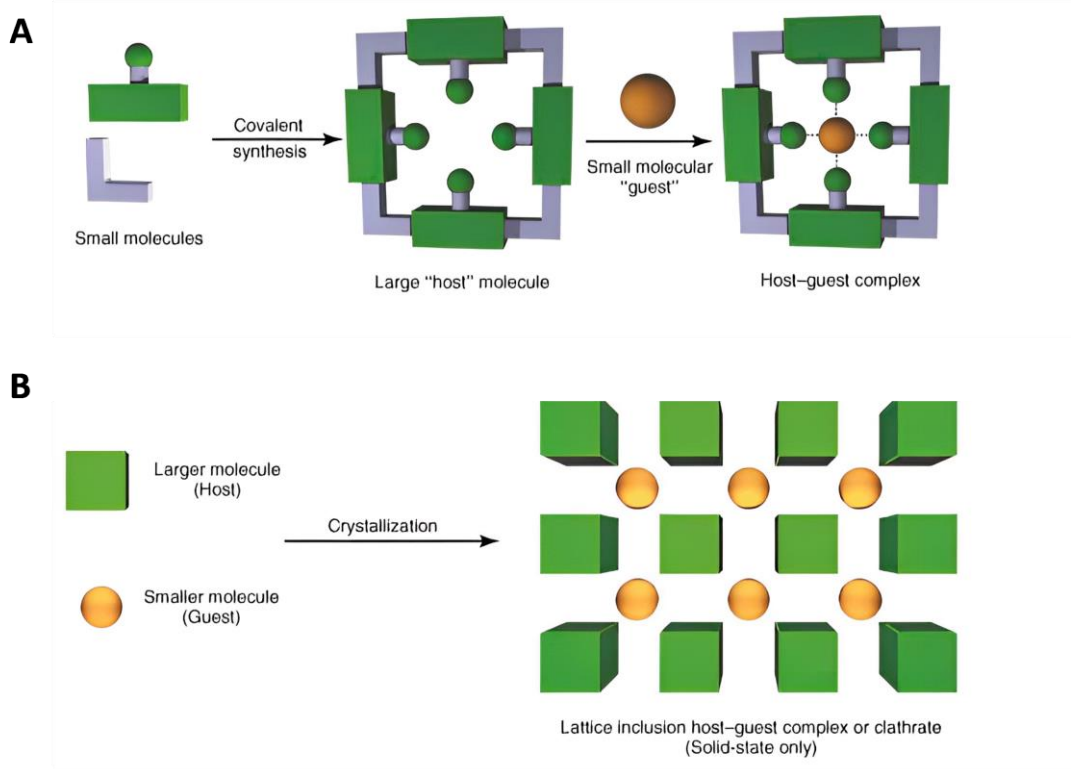

Figure B.1 Key design approaches encountered in supramolecular chemistry. (A) molecular host synthesis and associated host guest complexation, (B) solid state formation of host guest lattice inclusion complex [2].

Over the past few decades, dating back to the mid-20th century, extensive efforts have been devoted to crafting noncovalently linked host-guest complexes employing classical synthetic macrocyclic host molecules. Among all the reported macrocycles, crown ethers, cyclodextrins and calixarenes are the most well-known macrocycles and were considered as the first-, second-, and third-generation macrocycles, respectively. They are the most studied and have been used in a wide range of advanced applications including sensing [5], transport [6], catalysis [7] and drug/gene delivery [8].

In more recent times, a new generation of macrocycles has emerged offering a fresh perspective on molecular recognition and encapsulation. Notably, Cucurbit[n]urils, discovered in the mid-20th century, Pillarenes, in the early 2000s, and Trianglamine, in 2008 [9], have significantly enriched the landscape of macrocyclic host molecules. These macrocycles bring distinct and unique architectural designs, adding to the diversity of macrocyclic host molecules (Figure B.2). Their introduction has ignited substantial research interest and led to their recognition as highly promising components with a broad spectrum of applications in modern chemistry.

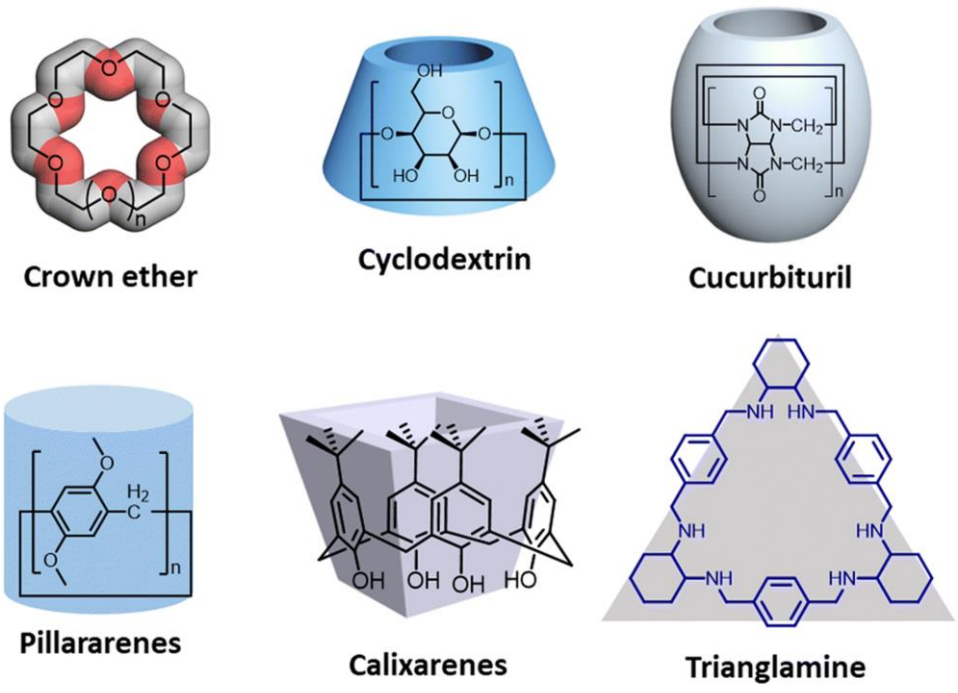

Figure B.2 Selected structures of macrocyclic hosts.

In the solid state, molecules can be strategically arranged to create structures with external (extrinsic) voids, a characteristic observed in materials like metal-organic frameworks (MOFs) [10], covalent organic frameworks (COFs) [11], and hydrogen-bonded organic frameworks (HOFs) [12]. These structures with extrinsic cavities serve as versatile supramolecular hosts, capable of accommodating a diverse array of guests, ranging from inorganic anions and monatomic cations to more intricate molecules such as hormones and pheromones (Figure 1B). Such compounds are commonly referred to as clathrates, a term derived from the Greek word 'klethra,' signifying 'bars' or 'enclosures.'

The formation of host-guest complexes is distinguished by its ability to occur without altering the fundamental structure and valence of the original molecules. This is primarily due to the fact that a strong chemical bond between the host and guest is not always necessary, as it would typically demand a high degree of matching and adaptability in terms of spatial geometry, electric charge, hydrophilicity, and symmetry between the host and guest molecules. Consequently, the foundation of supramolecular systems lies in molecular and site recognition, where recognition becomes the pivotal process. Recognition involves the selective binding between a given receptor and an agent, leading to the realization of specific functions and properties within these complexes.

1.2 Self-assembly

Self-assembly is a process in which the basic structural units (molecules , nanomaterials…) spontaneously form ordered structures. The process of self-assembly is not a simple superposition of the weak forces among a large number of atoms, ions, and molecules, but a complex synergistic effect, in which the individual components spontaneously self-sort at the same time and gather to form a compact and ordered assembly.

Much like Host-Guest inclusion, molecular self-assembly is controlled by molecular recognition, which is driven by weak and reversible non-covalent interactions, such as hydrogen bonds. Molecular recognition ensures a high degree of order in the self-assembled systems, and structural stability and integrity are maintained by non-covalent interactions (Figure B.3).

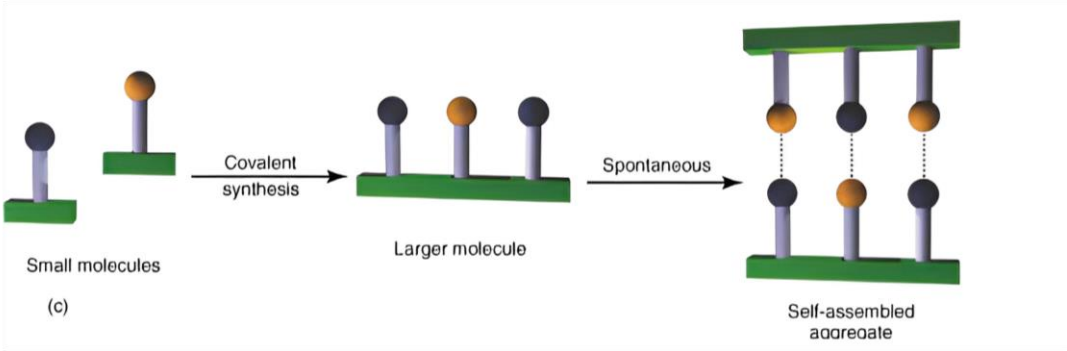

Figure B.3 Self-assembly between complementary molecules [2].

Molecular self-assembly can be categorized into two main processes. First, there's the assembly of infinite network structures, exemplified by nanotubes, Langmuir-Blodgett films, cable hydrocarbons, and rotating hydrocarbons [13]. Second, we have another molecular assembly method known as the templating effect [14], where molecules organize themselves, particularly evident in processes occurring at silicon interfaces [15].

Many supramolecular species designed and developed by chemists draw inspiration from biological systems. For instance, deoxyribonucleic acid (DNA) consists of two strands that self-assemble through hydrogen bonds and aromatic stacking interactions, forming the iconic double helical structure. This natural example has inspired scientists to mimic this structure and tailor artificial materials with similar structural intricacies and functionalities [16]. This includes DNA cubes [17], protein nanosheets [18], protein cages [19], and so on, for medical use.

2. β-Cyclodextrins

Cyclodextrins (CDs), also referred to as cyclomaltoses, cycloamyloses, or Schardinger dextrins, constitute a group of cyclic oligosaccharides derived from starch or starch derivatives through the action of the bacterial enzyme cyclodextrin glycosyltransferase (CGTase) [20]. Cyclodextrins (CDs) are composed of six or more glucopyranose monomers linked together through α-1,4-glycosidic bonds as presented in Figure B.4. The CD family includes several members, with the most prominent ones being α-CD (consisting of six glucopyranose units), β-CD (comprising seven glucopyranose units), and γ-CD (containing eight glucopyranose units) [21].

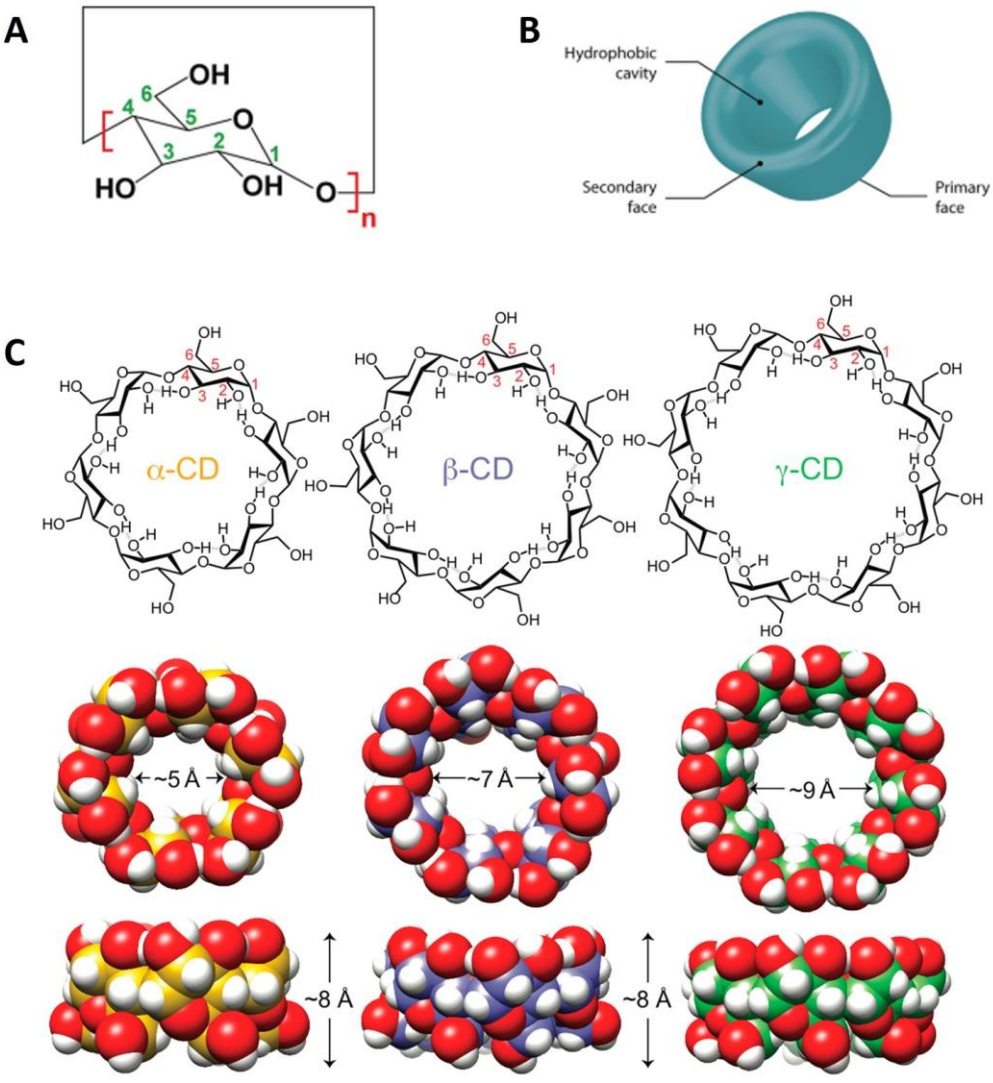

Figure B.4 Cyclodextrin (CD) structures of (A) the monomer unit, (B) the overall shape, and (C) the structures of α-, β-, and γ-CDs [21].

The history of cyclodextrins is rooted in the late 19th and early 20th centuries. In 1891, the French pharmacist and chemist Antoine Villiers made a significant discovery when he identified α- and β-cyclodextrins as digestion products of potato starch, a result achieved through the use of the bacterium Bacillus amylobacter [22]. However, it was the Austrian microbiologist Franz Schardinger who earned the moniker of the "founding father" of cyclodextrin chemistry [23]. In the early 20th century, Schardinger isolated what he termed "crystalline dextrins" from various starch sources after digestion by Bacillus macerans, a bacterial species still commonly used today for cyclodextrin production. It was in the 1940s that German chemist Freudenberg and his colleagues made another pivotal contribution, discovering γ-cyclodextrin and elucidating the cyclic oligosaccharide structure of cyclodextrin molecules [21]. This newfound knowledge paved the way for the preparation of cyclodextrin-inclusion complexes. In 1953, Freudenberg, Cramer, and Plieninger secured the first patent related to cyclodextrins, marking the inception of their application in drug formulations [24].

Today, cyclodextrins play a vital role in pharmaceuticals, cosmetics, food science, and many other industries, where their unique molecular properties enable innovative solutions and advancements in modern science and technology [25]. In fact, the production of cyclodextrins reached over 10,000 metric tons/year, where around 70, 15, 5, and 10% of which are β-cyclodextrin, α-cyclodextrin, γ-cyclodextrin, and other cyclodextrin derivatives, respectively [26].

Their distinctive molecular structure underpins remarkable properties. CDs possess a hydrophilic outer surface, thanks to the presence of free hydroxyl groups along the molecule's exterior. In contrast, their inner portion is less hydrophilic, even bordering on hydrophobic, due to the arrangement of ether oxygen atoms in the glycosidic hemiacetals and carbon-hydrogen atoms. This unique structural duality allows CDs to be soluble in water while being capable of forming complexes with hydrophobic guest molecules.

This low-polarity central void within CDs has the exceptional ability to encapsulate various guest molecules of suitable size, shape, structure, and dimensions, resulting in stable associations without the need for covalent bonds. Furthermore, the presence of hydroxyl groups allows for direct substitution reactions and chemical modifications at different positions, yielding a diverse range of polymerized derivatives tailored for

specific applications. During the COVID-19 pandemic, researchers exploited the biocompatibility of cyclodextrins to a significant extent. Their versatile applications included acting as encapsulating agents for antiviral drugs, serving as adjuvants to stabilize proteins and other molecules implicated in the infection, enhancing the efficacy of vaccines, functioning as cholesterol trappers to destabilize the virus capsid, acting as carriers for RNA therapies, demonstrating antiviral properties themselves, and even finding utility in anticoagulant therapies [27].

Among the three main cyclodextrins (α-CD, β-CD, and γ-CD), β-CD stands out as the most extensively used and studied. This preference can be attributed to its unique characteristics. In fact, β-CD possesses an intermediate-sized cavity, effectively accommodating a diverse range of guest molecules such as benzene rings and naphthalene molecules. Its balanced hydrophilic-hydrophobic nature allows it to be soluble in water and form stable inclusion complexes with hydrophobic guests. α-CD is smaller and more hydrophilic, while γ-CD is larger and less soluble in water, limiting its utility in certain applications. β-CD's stability, combined with its commercial availability, makes it a top choice in numerous applications, including pharmaceuticals, food science, and more.

The introduction of functional groups, such as -SH, -NH_2, and -COOH, provides additional binding sites, resulting in improved properties. Various β-CD derivatives, including carboxymethyl-β-CD, amino-β-CD, hydroxypropyl-β-CD, and thiolated β-CD, can be linked to a wide array of substrate materials via diverse chemical bonds.

2.1 β-Cyclodextrin based sensors

β-Cyclodextrin (β-CD) has emerged as an asset in sensing technology, primarily due to its exceptional ability to encapsulate guest molecules through non-covalent interactions. This unique property serves as the foundation for its application as a recognition moiety in sensors.

In fact, β-CD was found to offer a compelling alternative to traditional biological recognition moieties such as antibodies and enzymes. A noteworthy example of this is β-CD's high affinity for specific molecules, like cholesterol [28] and L-tyrosine [29], which has led scientists to develop chemical sensors replacing their respective enzymes, HMG-CoA reductase, and Tyrosine hydroxylase. Indeed, this strategic shift towards β-

CD-based sensors has resulted in notable advantages, including increased stability, robustness, and cost-effectiveness of developed sensors. These β-CD-based sensors stand in contrast to traditional biosensors, which frequently contend with challenges like biological element denaturation and higher costs. β-CD's capacity for selective binding with specific molecules has empowered researchers to develop chemical sensors characterized by exceptional specificity with minimal interference from other substances. Furthermore, one of its remarkable features is its capacity for functionalization, which allows for seamless integration into various nanostructures and the incorporation of different nanomaterials. This versatility greatly expands the scope and potential of β-CD-based sensors.

In the design of β-CD-based sensors, a crucial consideration revolves around effectively labeling the host-guest interactions. Diverse strategies have been devised to monitor these complexations, with the choice depending on the specific sensing approach and transduction mode employed. These β-CD-based sensors can be broadly classified into two main categories: Direct Sensing and Indicator Displacement Assay.

2.1.1 Direct Sensing

In the paradigm of direct sensing, the analyte is directly bound to the receptor to lead to a signal change. In the first scenario, direct sensing involves the analyte binding directly to the receptor, resulting in a noticeable change in the signal. This is particularly applicable when the analyte inherently possesses an active signal, whether it be electrochemical or optical. Upon confinement within the cyclodextrin cavity, the interaction triggers a variation in the signal, serving as a detectable indicator.

In the second scenario, direct sensing is employed even when the targeted analyte lacks an inherent active signal. In such cases, a labeling process is necessary. Cyclodextrin is linked to an active probe, a choice that depends on the specific transduction mode employed by the sensors (Figure B.5). The inclusion of the analyte within the cyclodextrin cavity brings about a discernible variation in the probe signal, enabling detection even when the analyte itself lacks an inherent signal.

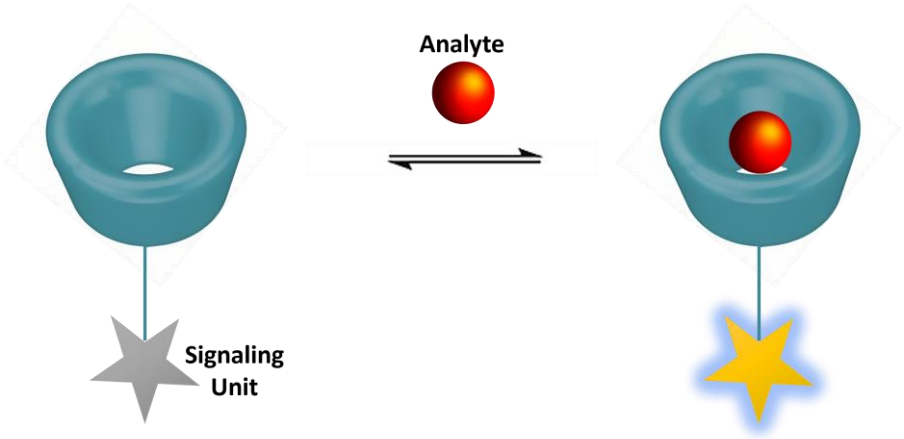

Figure B.5 Illustration of the receptor−reporter direct sensing approach of molecular sensing.

2.1.2 Indicator Displacement Assay

Competitive binding, a fundamental concept in supramolecular chemistry, involves multiple guest molecules competing for binding to a common host (receptor). This approach leverages the reversible nature of molecular recognition, enabling the establishment of distinct equilibria between the host and multiple guests. Consequently, it yields binding selectivity. Competitive binding has a rich history of application in sensing, particularly in biochemistry [30], exemplified by competitive binding immunoassays, competitive enzyme inhibition assays, and DNA intercalation assays, among others.

However, within the past two decades, the utilization of synthetic receptors in competitive binding assays has gained significant prominence. One such strategy is the "indicator displacement assay" (IDA), which has emerged as a standard method for molecular sensing, complementing the direct sensing approach discussed earlier. IDA hinges on the competition between an indicator molecule and an analyte for binding to a common receptor.

In a typical IDA experiment, an indicator molecule initially binds to the receptor in our case the β-CD moiety, forming the sensing ensemble. Subsequently, the analyte is introduced, leading to the displacement of the indicator from the sensing ensemble. Importantly, the free and bound states of the indicator exhibit distinct properties, often manifesting as variation in their proper signal (see Figure B.6).

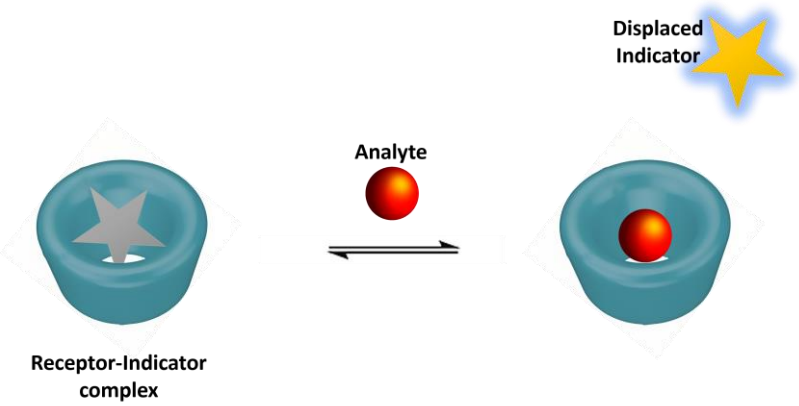

Figure B.6 Illustration of the indicator displacement assay (IDA).

The choice of indicator in an IDA depends on the intended transduction mode, which may involve electroactive, fluorescent, or other probes. To achieve desirable sensitivity in an IDA, it is crucial that the binding constant of the analyte to the receptor closely matches that of the indicator to the receptor. This balance ensures the assay's effectiveness in discriminating and quantifying the analyte of interest.

2.2 β-CD-based optical sensors

The utilization of β-cyclodextrin (β-CD) in optical assays has a rich history dating back to the 1970s, with pioneers like Ueno and colleagues making noteworthy contributions in 1979 [31]. Their pioneering work laid the foundation for what are now commonly referred to as "turn-off" fluorescent chemical sensors. These researchers successfully developed fluorophore-modified β-CDs, which served as integral components in monitoring a diverse range of analytes. Within these sensors, a key feature is the attenuation of fluorescence intensity upon the formation of complexes with guest molecules [32] as illustrated in Figure B.7 A. This innovative approach has seen the integration of various fluorophore compounds such as dansyl [33], dimethylaminobenzoyl [32], naphthyl [34], pyrene, and anthracene moieties.

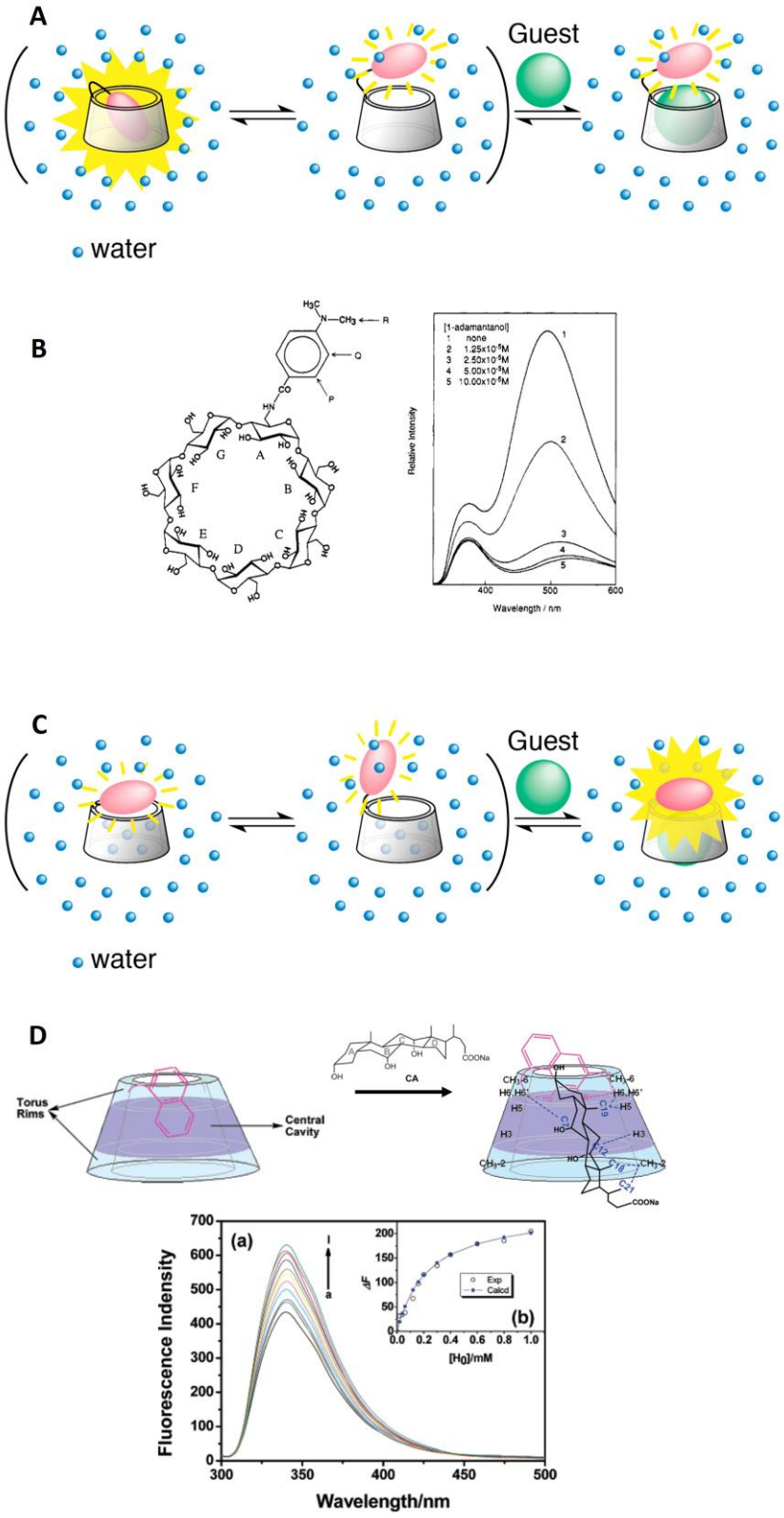

Figure B.7 (A) An equilibrium model for turn-off CD chemosensor in aqueous solution; (B) DMAB/β-CD based chemosensor for the detection of 1-adamantanol with the corresponding fluorescence spectra [32] (C) An equilibrium model for turn-on CD chemosenor in aqueous solution; (D) Naphtalene/β-CD based chemosensor for the detection of cholic acid sodium salt and with the corresponding fluorescence spectra [35].

As an example from one of Ueno's studies [32], a p-(dimethylamino)benzoyl (DMAB) modified β-cyclodextrin (β-CD) was utilized to detect and monitor 1-adamantanol as the target analyte (see figure B.7 B). Upon the inclusion of the target analyte within the modified cyclodextrin, the DMAB moiety experiences a shift in its location, transitioning from the hydrophobic inner cavity of DMAB-β-CD to the polar environment of the surrounding bulk water. This alteration in the environment significantly impacts the twisted intramolecular charge transfer (TICT) excited state of DMAB, leading to a notable decrease in the fluorescence signal. This effect can be attributed to the high polarity of the environment, which affects DMAB's fluorescence properties.

In addition, a class of "turn-on" sensors has emerged, where fluorescence intensity is amplified through the formation of host-guest complexes, as depicted in Figure B.7 C. A pivotal design feature involves introducing a rigid spacer between the β-cyclodextrin (β-CD) and the fluorophore, preventing the formation of self-inclusion complexes within the fluorophore-CD conjugates. Consequently, the fluorophore is ensconced within a hydrophilic environment, leading to the suppression of fluorescence. However, the ingenious strategy comes into play with the introduction of a hydrophobic guest molecule into the cavity of the fluorophore-CD conjugate. This inclusion of a hydrophobic guest molecule relocates the fluorophore to a more hydrophobic environment, resulting in a significant increase in fluorescence intensity.

Several "turn-on" fluorescent chemical sensors, exemplified by compounds like 4-amino-7-nitrobenz-2-oxa-1,3-diazole-CD [36], napthol-CD and hydroxyquinoline-CD conjugates [35], have been reported.

To elaborate further, in a study conducted by [35] a Naphtalene-modified β-cyclodextrin (β-CD) was introduced as a fluorescent turn On chemosensor for the detection of cholic acid sodium salt (see Figure B.7 D). Interestingly, it was observed that the transfer of the chromophore group from the central cavity of the β-CD to the more hydrophobic torus rim resulted in a significant enhancement of fluorescent intensities and an extension of fluorescent lifetimes. The naphthalene group does not entirely exit the cavity, it shifts from the central cavity to the hydrophobic portion of the narrow torus rim. As a result, the relative fluorescent intensities of the host naphthalene experience a remarkable enhancement upon complexation with bile salts. In simpler terms, β-CDs can simultaneously accommodate both the fluorescent sidearms and bile salt guests

within their extended cavities, facilitating multipoint cooperative binding. This observation enabled the establishment of a direct correlation between the enhancement of the Naphtalene fluorescence signal and the concentration of the salt, offering a robust foundation for quantitative analysis.

In addition, various chromophore compounds have been integrated into β-cyclodextrin (β-CD) such as metal Complex Chromophores, Azo dyes [37]. However, such traditional fluorescent labels often face challenges such as insufficient brightness, poor stability, and photobleaching [38].

As a remedy, nanotechnology has been employed to enhance β-CD-based optical sensors. Fluorescent nanoparticles, including Gold Nanoparticles (AuNPs) [39–41], Silver Nanoparticles (AgNPs) [42–45] and upconversion nanoparticles (UCNPs) [46,47] have shown improved brightness and photostability, making them a viable alternative to traditional fluorescent probes.

For instance, a cholesterol assay was developed using mercapto-β-cyclodextrin capped gold nanoclusters as a fluorescent probe [48]. The host–guest interaction between cholesterol and cyclodextrin enhances the fluorescence of gold nanoclusters directly, without the involvement of additional dyes or quenchers (Figure B.8). This Turn ON probe exhibits a linear response to cholesterol within the concentration range of 10.0 ~ 100.0 μM, with a remarkable detection limit of 5.77 μM.

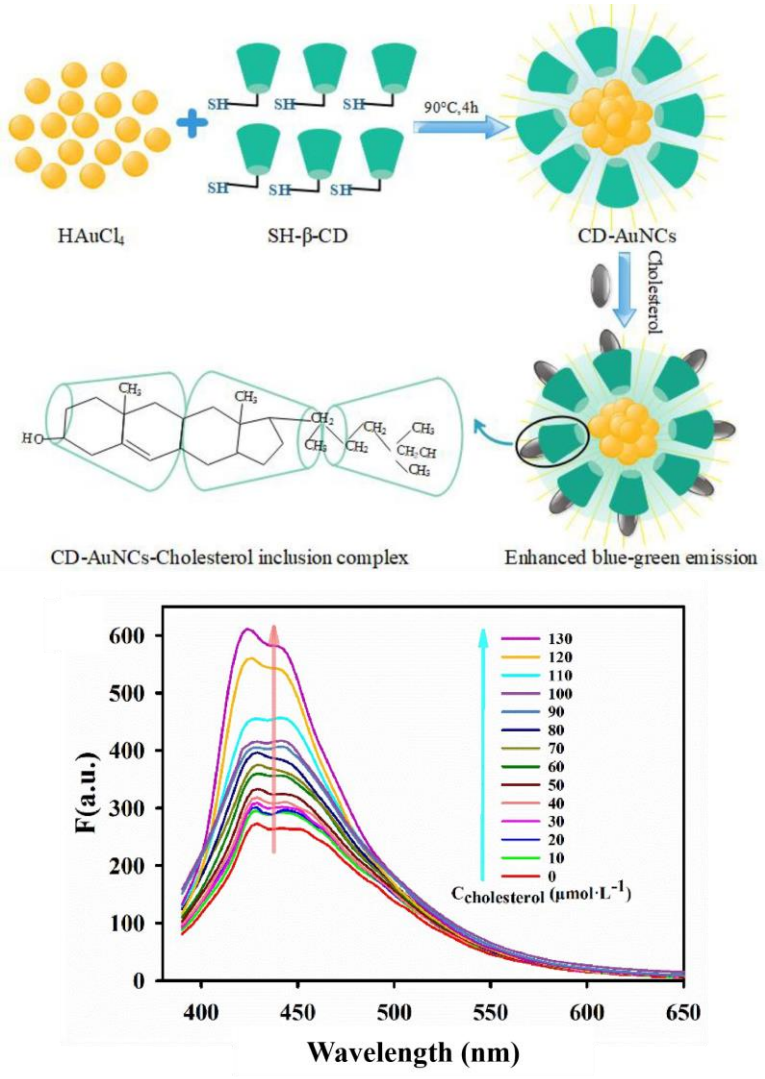

Figure B.8 Schematic diagram for the synthesis of CD-AuNCs and the fluorescence enhancement caused by different concentration of cholesterol upon host–guest interaction [48].

Similarly, Silver nanoclusters were modified with thiolated cyclodextrin (SH-β-CD) to develop a "Turn off" fluorescent and colorimetric sensor for the detection of intracellular alkaline phosphatase (ALP) in human serum samples[42].

As presented in Figure B.9, β-CD-AgNCs were applied as fluorescent probes for ALP sensing on the basis of inner filter effect. NPP acted as the effective enzyme catalytic substrate of ALP to produce NP and NP can efficiently quench the fluorescence of β-CD-AgNCs through IFE beneficial from the host-guest interaction between β-CD and NP. This β-CD-AgNCs based system for ALP activity analysis showed a linear range of 0.02–10.0 U L^{-1} and a detection limit as low as 0.0046 U L^{-1}.

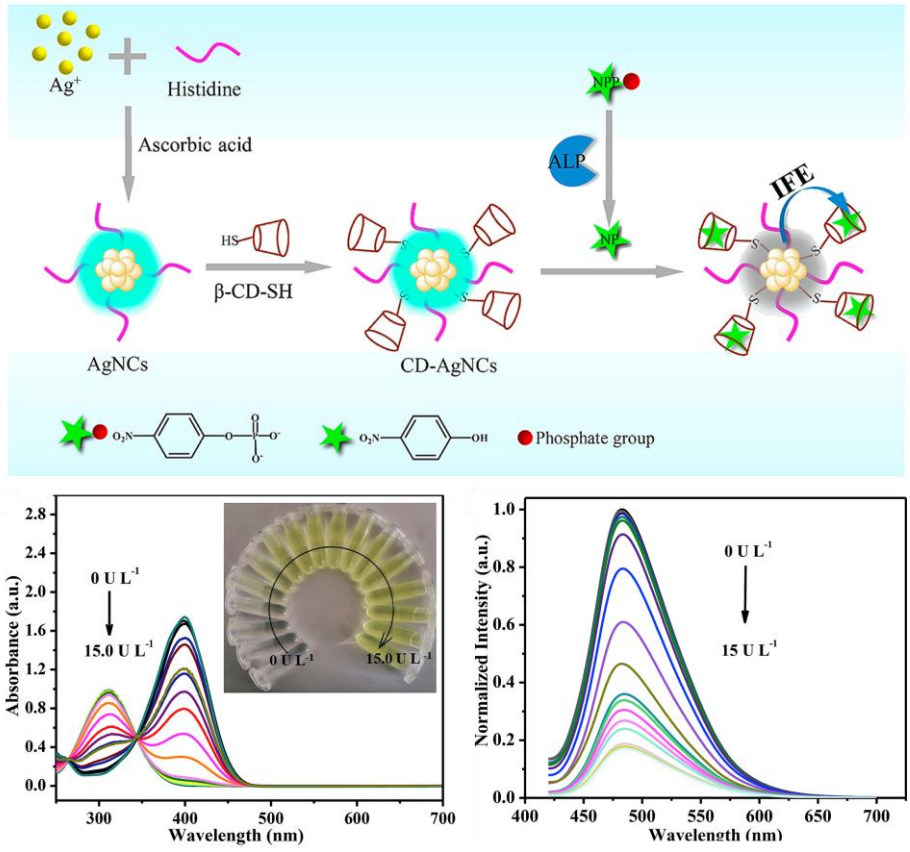

Figure B.9 Schematic representation of the β-CD-AgNCs based system for ALP activity analysis and the corresponding UV–vis absorption spectra and Fluorescence response of the sensor with varied amounts of ALP addition [42].

Nevertheless, it's worth noting that the cost associated with these nanoparticles can be a limiting factor when it comes to commercialization. In response to this cost challenge, researchers have turned to quantum dots (QDs) as a cost-effective alternative. QDs are nanostructures with exceptional optical properties and are relatively straightforward to synthesize. These fluorescent nanodots present an economical and efficient option for the development of optical sensors, offering the potential to balance performance with affordability in commercial applications.

Quantum dots (QDs) have been effectively employed with β-cyclodextrin (β-CD) to advance optical sensor technology. QDs, with their unique optical properties, have played a significant role in overcoming the limitations of conventional fluorescent labels. They exhibit superior brightness, excellent stability, broad absorption spectra with narrow emission peak, and resistance to photobleaching. One of the remarkable features of QDs is their adaptability through functionalization, allowing for tailored applications. These fluorescent nanodots have been incorporated with β-CD to create hybrid systems that offer enhanced sensing capabilities.

Various types of quantum dots, such as Carbon Quantum Dots (CQDs) [49], Cadmium Telluride Quantum Dots (CdTe) [50], Zinc Sulfide Quantum Dots (ZnSQDs) [51], and molybdenum disulfide quantum dots (MoS_2QDs) [52], have been anchored to Cyclodextrin for the development of optical sensors.

For example, Durán et all developed an optical sensor for vanillin in food samples using CdSe/ZnS quantum dots (QDs) modified with β-cyclodextrin (β-CD)[51]. It was found that the interaction between vanillin and β-CD–CdSe/ZnS-QDs complex produced the quenching of the original fluorescence of β-CD–CdSe/ZnS-QDs according to the Stern–Volmer equation (Figure B.10). This allowed the monitoring of vanillin in synthetic and food samples with a limit of detection of 0.99 µg mL−1.

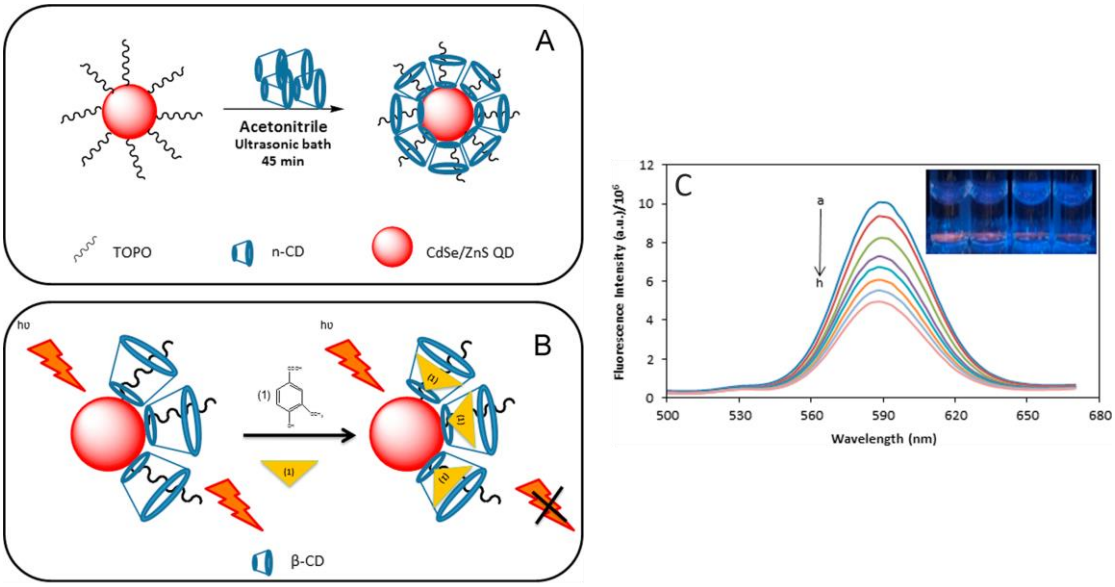

Figure B.10 Schematic illustration of (A) surface modification of TOPO–CdSe/ZnS-QDs with n-cyclodextrins (B) Host–guest interaction between β-CD–CdSe/ZnS-QDs and vanillin and (C) Fluorescence spectra of β-CD–CdSe/ZnS-QDs with different concentrations of vanillin [51].

In a letter authored by Freeman and colleagues [53], they describe a novel approach where they functionalized CdSe/ZnS quantum dots (QDs) with β-cyclodextrin (β-CD) for both general optical sensing and chiroselective sensing of various substrates, utilizing either fluorescence resonance energy transfer (FRET) or electron transfer (ET) mechanisms. The sensing approach is depicted in Figure B.11.

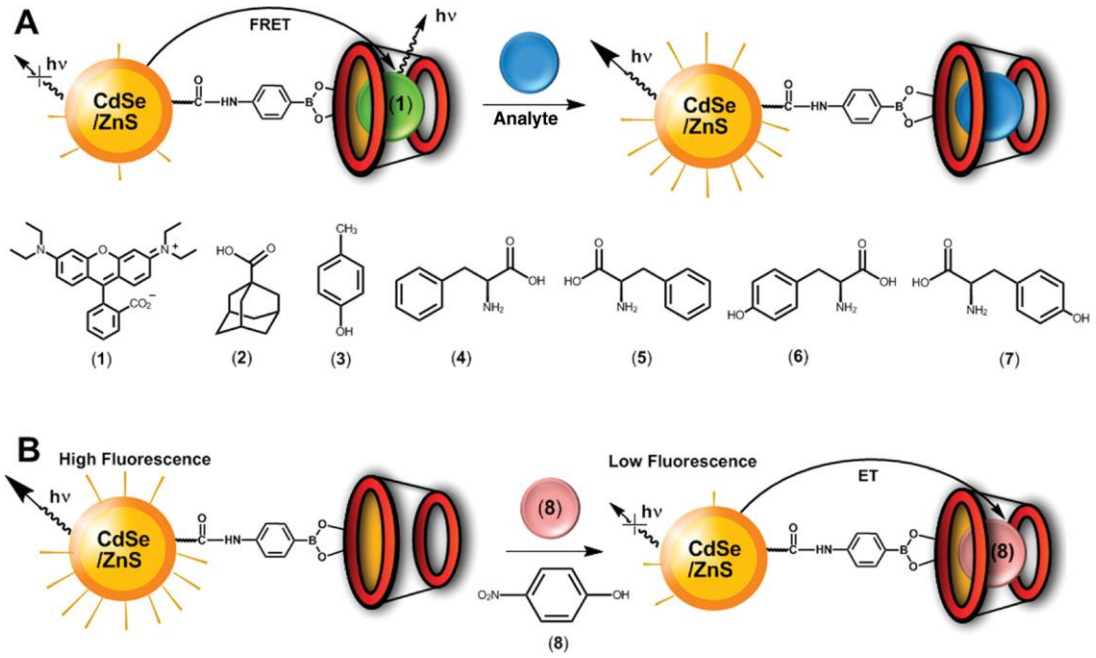

Figure B.11 (A) Sensing of Substrates by a Competitive FRET Assay Using β-Cyclodextrin-Modified CdSe/ZnS QDs with Receptor-Bound Rhodamine B (1) and (B) Direct Analysis of Substrates by the β-Cyclodextrin-Modified CdSe/ZnS QDs Using an Electron Transfer Quenching Route [53].

The FRET mechanism, facilitated by the interaction between the QDs and Rhodamine B incorporated within the β-CD receptor sites, enables the competitive analysis of substances such as adamantanecarboxylic acid and p-hydroxytoluene. Additionally, the β-CD-modified QDs, with dye incorporation, are employed for the chiroselective optical discrimination between d,l-phenylalanine and d,l-tyrosine. Furthermore, these receptor-functionalized QDs find application in the optical detection of p-nitrophenol through an ET quenching route.

In addition to fluorescence, other optical methods was used in β-cyclodextrin (β-CD)-based sensors, such as absorption spectroscopy, colorimetry [54,55], and surface plasmon resonance [56,57].

In summary, β-CD-based optical sensors have a rich history and have evolved to encompass both "turn-off" and "turn-on" fluorescent chemical sensors. Nanotechnology, with the incorporation of fluorescent nanoparticles and quantum dots, has addressed traditional fluorescent label limitations, offering improved brightness and stability. These sensors find diverse applications, from food quality control to chiroselective discrimination of enantiomers, showcasing their versatility and potential in the field of supramolecular sensing.

2.3 β-CD based electrochemical sensors

β-Cyclodextrins (β-CDs) have found valuable applications in the development of electrochemical sensors. To achieve this, β-CDs have been combined with various materials with the aim of immobilizing them onto electrode surfaces. In designing β-CD-based electrochemical sensors, similar strategies to those employed in β-CD-based optical sensors have been applied. Particularly, when dealing with electroactive analytes, β-CDs have been employed to capture the target analyte and confine it in close proximity to the electrode surface. However, this confinement is suitably weak to facilitate efficient electron transfer, enabling the oxidation or reduction of the analyte. This process generates an electric current, typically, which can be correlated with the concentration of the analyte.

To further enhance the sensitivity of these sensors, β-CDs have been combined with a diverse range of nanomaterials. These include carbon-based nanomaterials such as graphene and carbon nanotubes, metal nanoparticles [58,59], conducting polymers [60–63], and MXenes [64,65], among others. For instance, an electrochemical sensor was developed to detect minute levels of Bisphenol A (BPA) in water (Figure B.12) [66]. This sensor harnessed the potential of chemically modified multiwall carbon nanotubes (MWCNTs) in conjunction with β-cyclodextrin (β-CD) on a screen-printed carbon electrode (SPCE) [66]. The result was an impressive limit of detection for BPA, determined to be as low as 13.76 nM.

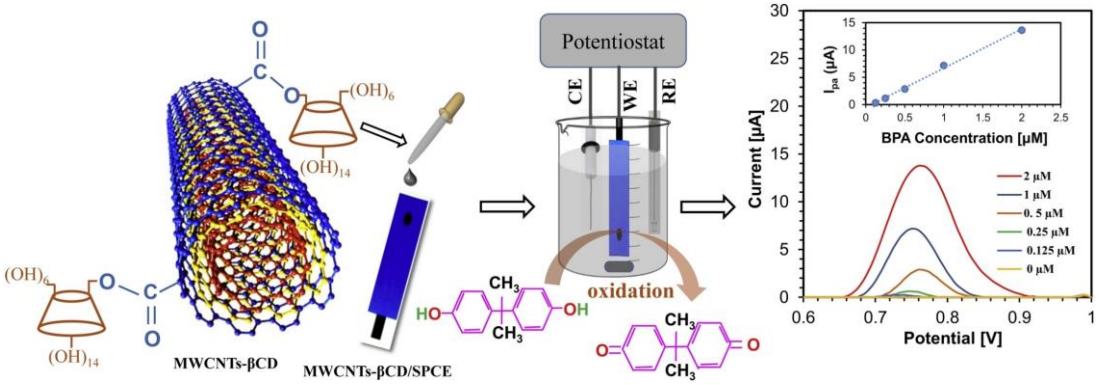

Figure B.12 Schematic of the modification of screen-printed carbon electrode with MWCNTs- β-CD and the detection of Bisphenol A using Linear Sweep Voltammetry [66].

The improved sensing performance of this sensor can be attributed to the host-guest interaction capability of MWCNTs-βCD with BPA. This is made possible by the combined effects of the hydrophilic nature of β-CD and the large surface area of

MWCNTs. These factors synergize to enhance the sensor's selectivity and sensitivity, making it a powerful tool for detecting BPA in water at extremely low concentrations.

In addition, the use of β-cyclodextrin (β-CD) has demonstrated exceptional selectivity in electrochemical sensors. In a study published by Qin et al., the simultaneous determination of ascorbic acid, dopamine, and uric acid was achieved [67]. This was made possible through the utilization of a conductive β-cyclodextrin polymer on a screen-printed electrode modified with reduced graphene oxide as presented in Figure B.13.

A noteworthy advantage of this approach is that all these analytes are electroactive, eliminating the need for additional probes. Instead, β-CD played a central role in capturing dopamine (DA), ascorbic acid (AA), and uric acid (UA), ensuring the generation of distinct electrochemical signals.

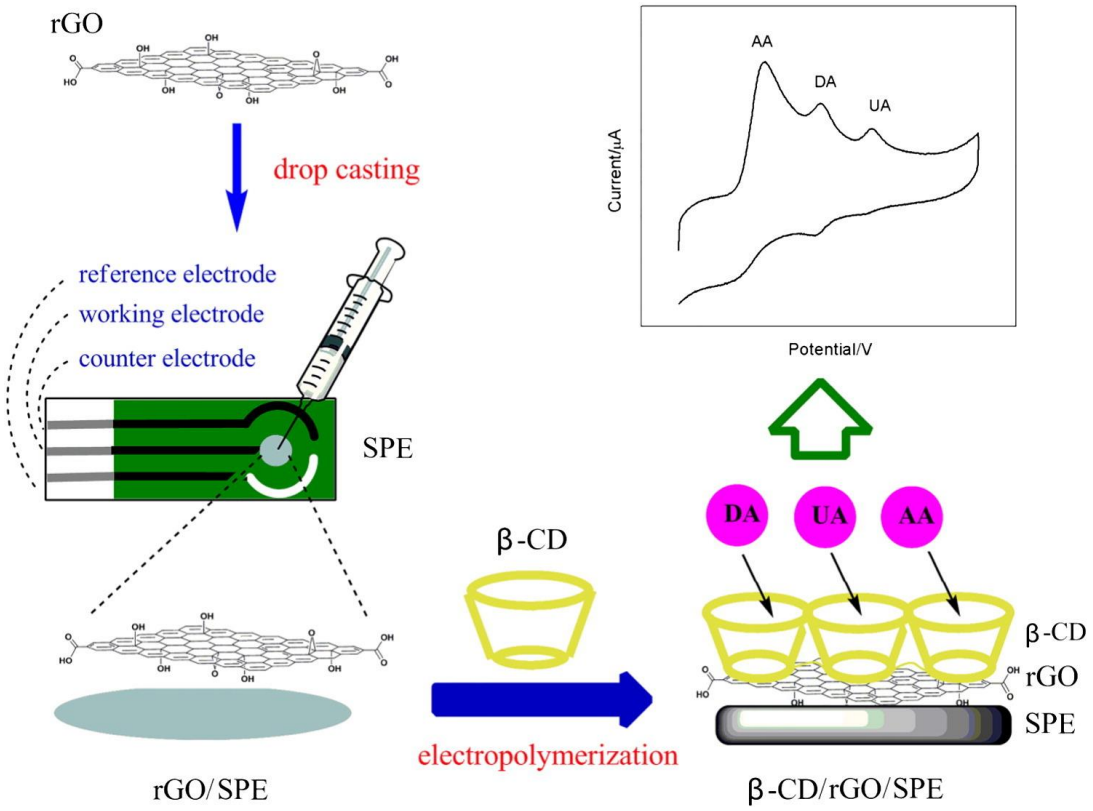

Figure B.13 Schematic illustration of the surface functionalization of screen printed electrode with rGO/β-CD and its use for the simultaneous detection of DA, AA, and UA [67].

Furthermore, it's crucial to emphasize that β-CD was electropolymerized on the surface of the reduced graphene oxide (RGO)/electrode. Remarkably, β-CD can undergo electropolymerization using electrochemical techniques such as cyclic voltammetry (CV) [68,69] (Figure B.14). This simplifies its integration into electrode surfaces, modernizing the sensor design process.

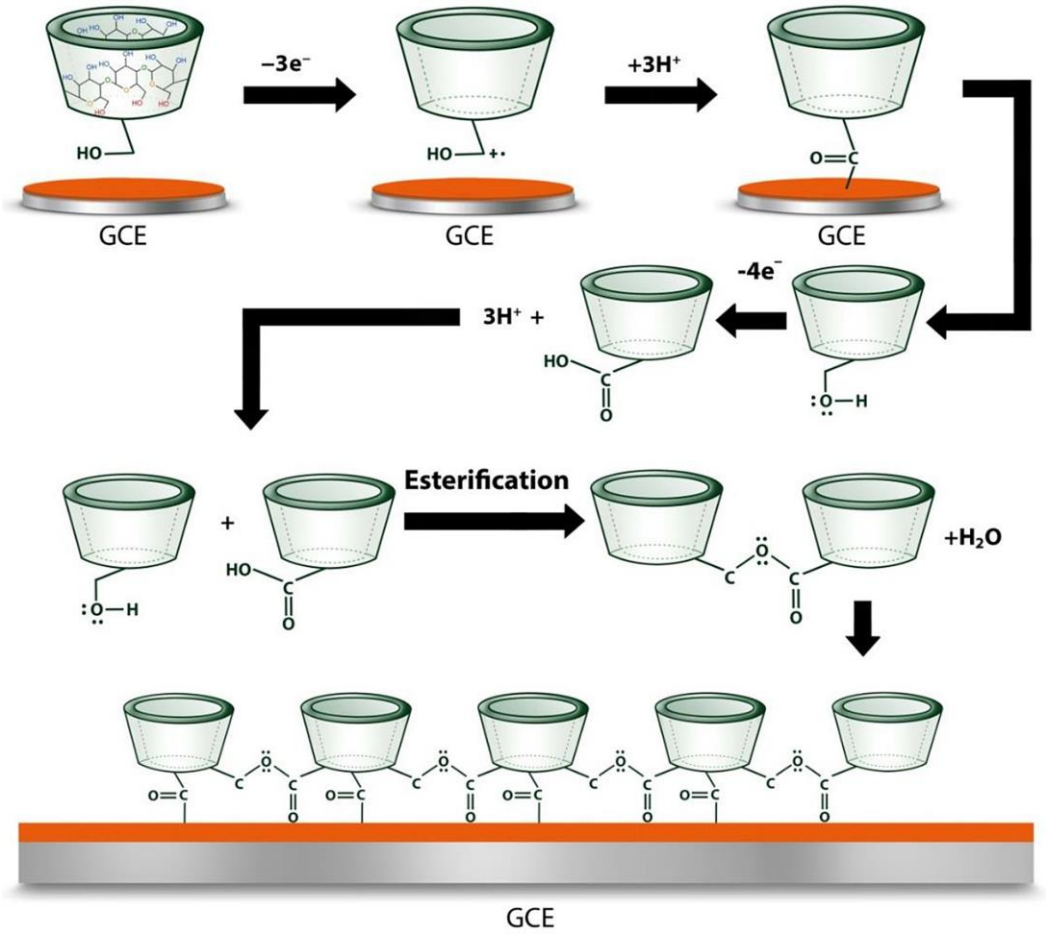

Figure B.14 Mechanism of electropolymerization procedure of β-CD on the glassy carbon electrode[70].

In cases where the target analyte lacks inherent electroactivity, researchers have adopted a different strategy by employing labeled cyclodextrin. This strategy involves using redox indicators and nanomaterials to facilitate electrochemical monitoring of host-guest inclusion phenomena.

For example, in a study led by Agnihotri et al. [71] Methylene Blue (MB) was utilized as a redox indicator. As can be seen in figure 15, MB forms a unique inclusion complex with β-CD, serving as the foundation for an cholesterol-sensing matrix. In this arrangement, the MB molecules are displaced by cholesterol molecules and released into the buffer solution. This displacement is then detected through electrochemical

means, employing the Differential Pulse Voltammetric (DPV) technique as detailed in Figure B.15.

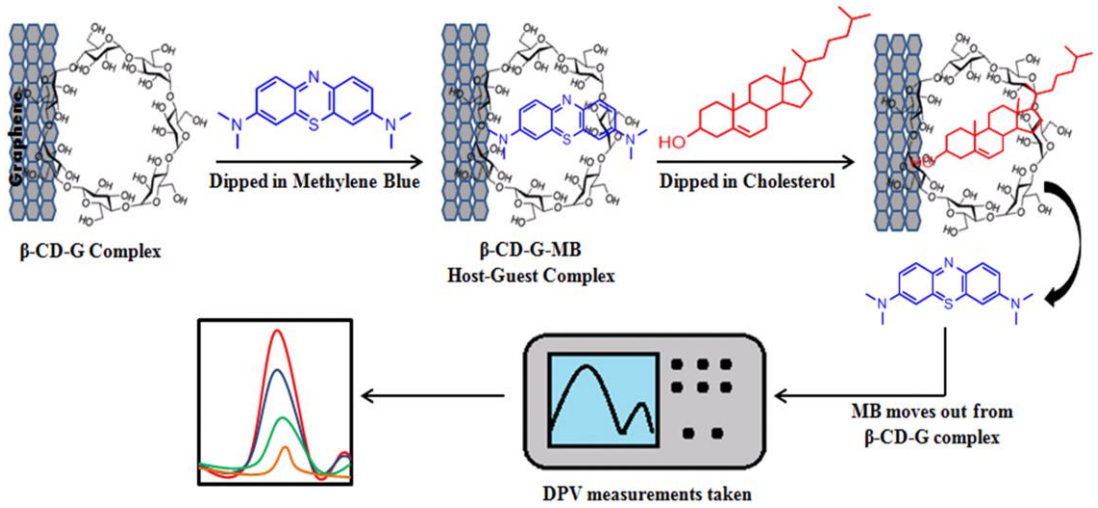

Figure B.15 Demonstrating the mechanism of cholesterol sensing, using Grp-β-CD as the working matrix and methylene blue as redox indicator [71].

The progression of MB displacement by cholesterol is visibly apparent through a continuous increase in the electrochemical signal of MB observed during DPV. This increase correlates directly with the rising concentration of the target cholesterol. This innovative approach showcases the versatility of β-CD-based electrochemical sensors, allowing for the detection of non-electroactive analytes through a host-guest inclusion mechanism, expanding the range of potential applications. Other redox indicators, such as ferrocene [72,73] and rhodamine B [74,75] , have also been effectively employed in similar fashion.

In conclusion, β-CD-based sensors represent a powerful and versatile tool in analytical chemistry. By capitalizing on the host-guest inclusion properties of β-CDs and their compatibility with various nanomaterials, these sensors offer enhanced sensitivity and selectivity. They enable the efficient detection of electroactive analytes and expand their applicability to non-electroactive substances through innovative strategies like redox indicators. The marriage of β-CDs with nanotech has opened doors to novel sensor designs and applications, holding promise for advancements in fields ranging from environmental monitoring to healthcare diagnostics.

References

[1] J. -M Lehn, *Angew. Chemie Int. Ed. English* **1988**, *27*, 89–112.

[2] J. W. Steed, D. R. Turner, K. J. Wallace, *Core Concepts in Supramolecular Chemistry and Nanochemistry*, John Wiley, **2007**.

[3] L. You, D. Zha, E. V Anslyn, *Chem. Rev.* **2015**, *115*, 7840–7892.

[4] D. J. Cram, *Angew. Chemie Int. Ed. English* **1988**, *27*, 1009–1020.

[5] R. Pinalli, A. Pedrini, E. Dalcanale, *Chem. Soc. Rev.* **2018**, *47*, 7006–7026.

[6] S. Chen, Y. Wang, T. Nie, C. Bao, C. Wang, T. Xu, Q. Lin, D. H. Qu, X. Gong, Y. Yang, L. Zhu, H. Tian, *J. Am. Chem. Soc.* **2018**, *140*, 17992–17998.

[7] C. Wang, L. Xu, Z. Jia, T.-P. Loh, *Chinese Chem. Lett.* **2023**, 109075.

[8] M. J. Webber, R. Langer, *Chem. Soc. Rev.* **2017**, *46*, 6600–6620.

[9] Y. Wang, H. Wu, J. F. Stoddart, *Acc. Chem. Res.* **2021**, *54*, 2027–2039.

[10] X. T. Liu, B. Bin Qian, D. S. Zhang, M. ;Hui Yu, Z. Chang, X. H. Bu, *Coord. Chem. Rev.* **2023**, *476*, 214921.

[11] X. Wu, Z. Liu, H. Guo, Y. L. Hong, B. Xu, K. Zhang, Y. Nishiyama, W. Jiang, S. Horike, S. Kitagawa, G. Zhang, *ACS Appl. Mater. Interfaces* **2021**, *13*, 37172–37178.

[12] Q. Huang, W. Li, Z. Mao, L. Qu, Y. Li, H. Zhang, T. Yu, Z. Yang, J. Zhao, Y. Zhang, M. P. Aldred, Z. Chi, *Nat. Commun. 2019 101* **2019**, *10*, 1–8.

[13] K. Ariga, *Molecules* **2021**, *26*, 1621.

[14] M. Rycenga, P. H. C. Camargo, Y. Xia, *Soft Matter* **2009**, *5*, 1129–1136.

[15] B. Baris, V. Luzet, E. Duverger, P. Sonnet, F. Palmino, F. Cherioux, *Angew. Chemie - Int. Ed.* **2011**, *50*, 4094–4098.

[16] L. A. Churchfield, F. A. Tezcan, *Acc. Chem. Res.* **2019**, *52*, 345–355.

[17] K. E. Bujold, J. Fakhoury, T. G. W. Edwardson, K. M. M. Carneiro, J. N. Briard, A. G. Godin, L. Amrein, G. D. Hamblin, L. C. Panasci, P. W. Wiseman, H. F. Sleiman, *Chem. Sci.* **2014**, *5*, 2449–2455.

[18] X. Li, S. Qiao, L. Zhao, S. Liu, F. Li, F. Yang, Q. Luo, C. Hou, J. Xu, J. Liu,

ACS Nano **2019**, *13*, 50.

[19] E. Sasaki, D. Böhringer, M. Van De Waterbeemd, M. Leibundgut, R. Zschoche, A. J. R. Heck, N. Ban, D. Hilvert, *Nat. Commun.* **2017**, *8*, DOI 10.1038/ncomms14663.

[20] Z. Li, M. Wang, F. Wang, Z. Gu, G. Du, J. Wu, J. Chen, *Appl. Microbiol. Biotechnol.* **2007**, *77*, 245–255.

[21] S. Wüpper, K. Lüersen, G. Rimbach, *Biomolecules* **2021**, *11*, 1–21.

[22] G. Crini, *Chem. Rev.* **2014**, *114*, 10940–10975.

[23] G. Crini, *J. Incl. Phenom. Macrocycl. Chem.* **2020**, *97*, 19–28.

[24] T. Loftsson, D. Duchêne, *Int. J. Pharm.* **2007**, *329*, 1–11.

[25] N. Sharma, A. Baldi, *Drug Deliv.* **2016**, *23*, 739–757.

[26] R. nan Zhao, B. wei Zhu, Y. Xu, S. feng Yu, W. jun Wang, D. hong Liu, J. ning Hu, *Carbohydr. Polym.* **2023**, *319*, 121198.

[27] P. F. Garrido, M. Calvelo, A. Blanco-González, U. Veleiro, F. Suárez, D. Conde, A. Cabezón, Á. Piñeiro, R. Garcia-Fandino, *Int. J. Pharm.* **2020**, *588*, 119689.

[28] L. Alonso, P. Cuesta, J. Fontecha, M. Juarez, S. E. Gilliland, *J. Dairy Sci.* **2009**, *92*, 863–869.

[29] M. Shanmugam, D. Ramesh, V. Nagalakshmi, R. Kavitha, R. Rajamohan, T. Stalin, *Spectrochim. Acta - Part A Mol. Biomol. Spectrosc.* **2008**, *71*, 125–132.

[30] S. Sinn, J. Krämer, F. Biedermann, *Chem. Commun.* **2020**, *56*, 6620–6623.

[31] A. Ueno, H. Yoshimura, R. Saka, T. Osa, *J. Am. Chem. Soc.* **1979**, *101*, 2779–2780.

[32] K. Hamasaki, H. Ikeda, A. Nakamura, A. Ueno, F. Toda, I. Suzuki, T. Osa, *J. Am. Chem. Soc.* **1993**, *115*, 5035–5040.

[33] F. Hamada, Y. Kondo, R. Ito, I. Suzuki, T. Osa, A. Ueno, *J. Incl. Phenom. Mol. Recognit. Chem.* **1994**, *15*, 273–279.

[34] S. R. McAlpine, M. A. Garcia-Garibay, *J. Am. Chem. Soc.* **1998**, *120*, 4269–4275.

[35] Y. Liu, J. Shi, D. S. Guo, *J. Org. Chem.* **2007**, *72*, 8227–8234.

[36] H. Ikeda, T. Murayama, A. Ueno, *Org. Biomol. Chem.* **2005**, *3*, 4262–4267.

[37] P. Ncube, R. W. Krause, B. B. Mamba, *Sensors* **2011**, *11*, 4598–4608.

[38] C. M. Stawicki, T. E. Rinker, M. Burns, S. S. Tonapi, R. P. Galimidi, D. Anumala, J. K. Robinson, J. S. Klein, P. Mallick, *Sci. Rep.* **2021**, *11*, DOI 10.1038/s41598-021-99084-4.

[39] X. Li, D. Liu, Z. Wang, *Biosens. Bioelectron.* **2011**, *26*, 2329–2333.

[40] Z. Su, S. Wei, X. Shi, X. Wang, L. Zhang, X. Bu, H. Xu, Y. Liu, M. Jin, B. Pang, C. Zhao, *Anal. Chim. Acta* **2023**, *1239*, 340672.

[41] P. Sumathi, S. Suganthi, R. Sivaraj, G. T. Selvan, P. M. Selvakumar, I. V. M. V. Enoch, *Microchem. J.* **2019**, *150*, DOI 10.1016/j.microc.2019.104066.

[42] M. Wang, S. Wang, L. Li, G. Wang, X. Su, *Talanta* **2020**, *207*, DOI 10.1016/j.talanta.2019.120315.

[43] X. Qiu, J. Gu, T. Yang, C. Ma, L. Li, Y. Wu, C. Zhu, H. Gao, Z. Yang, Z. Wang, X. Li, A. Hu, J. Xu, L. Zhong, J. Shen, A. Huang, G. Chen, *Spectrochim. Acta - Part A Mol. Biomol. Spectrosc.* **2022**, *276*, DOI 10.1016/j.saa.2022.121212.

[44] V. Bhardwaj, S. A. Kumar, S. K. Sahoo, *ACS Appl. Bio Mater.* **2020**, *3*, 7021–7028.

[45] R. Rajamanikandan, M. Ilanchelian, *Mater. Today Commun.* **2018**, *15*, 61–69.

[46] C. Ma, T. Bian, S. Yang, C. Liu, T. Zhang, J. Yang, Y. Li, J. Li, R. Yang, W. Tan, *Anal. Chem.* **2014**, *86*, 6508–6515.

[47] N. Wang, X. Yu, K. Zhang, C. A. Mirkin, J. Li, *J. Am. Chem. Soc.* **2017**, *139*, 12354–12357.

[48] W. Xiao, Z. Yang, J. Liu, Z. C. Chen, H. Li, *Microchem. J.* **2022**, *175*, 107125.

[49] C. Tang, Z. Qian, Y. Huang, J. Xu, H. Ao, M. Zhao, J. Zhou, J. Chen, H. Feng, *Biosens. Bioelectron.* **2016**, *83*, 274–280.

[50] Z. Zhang, J. Zhou, Y. Liu, J. Tang, W. Tang, *Nanoscale* **2015**, *7*, 19540–19546.

[51] G. M. Durán, A. M. Contento, Á. Ríos, *Talanta* **2015**, *131*, 286–291.

[52] Y. Yi, W. Zeng, G. Zhu, *Talanta* **2021**, *222*, 121703.

[53] R. Freeman, T. Finder, L. L. Bahshi, I. Willner, *Nano Lett.* **2009**, *9*, 2073–2076.

[54] A. Haynes, P. Halpert, M. Levine, *ACS Omega* **2019**, *4*, 18361–18369.

[55] S. S. John Xavier, C. Karthikeyan, G. Gnana Kumar, A. R. Kim, D. J. Yoo, *Anal. Methods* **2014**, *6*, 8165–8172.

[56] N. Hayashi, R. Chen, M. Hiraoka, T. Ujihara, H. Ikezaki, *J. Agric. Food Chem.* **2010**, *58*, 8351–8356.

[57] Y. Lu, H. Li, X. Qian, W. Zheng, Y. Sun, B. Shi, Y. nan Zhang, *Opt. Fiber Technol.* **2020**, *56*, 102187.

[58] S. Wu, S. Fan, S. Tan, J. Wang, C. P. Li, *RSC Adv.* **2018**, *8*, 775–784.

[59] Y. Lu, Y. Zhou, J. Xia, S. Zhong, Y. Liu, Q. Chen, H. Chen, *Chempluschem* **2022**, *87*, e202200385.

[60] Y. F. Hu, Z. H. Zhang, H. Bin Zhang, L. J. Luo, S. Z. Yao, *Talanta* **2011**, *84*, 305–313.

[61] M. Ben Ali, R. Kalfat, H. Sfihi, H. Ben Ouada, J. M. Chovelon, N. Jaffrezic-Renault, *Mater. Sci. Eng. C* **1998**, *6*, 53–58.

[62] T. Nie, L. Lu, L. Bai, J. Xu, K. Zhang, O. Zhang, Y. Wen, L. Wu, *Int. J. Electrochem. Sci.* **2013**, *8*, 7016–7029.

[63] J. Bae, K. Shin, O. S. Kwon, Y. Hwang, J. An, A. Jang, H. J. Kim, C. S. Lee, *J. Ind. Eng. Chem.* **2019**, *79*, 19–28.

[64] X. Tu, F. Gao, X. Ma, J. Zou, Y. Yu, M. Li, F. Qu, X. Huang, L. Lu, *J. Hazard. Mater.* **2020**, *396*, 122776.

[65] Q. Wang, H. Xin, Z. Wang, *Biosensors* **2022**, *12*, 657.

[66] M. Y. Ali, A. U. Alam, M. M. R. Howlader, *Sensors Actuators B Chem.* **2020**, *320*, 128319.

[67] Q. Qin, X. Bai, Z. Hua, *J. Electroanal. Chem.* **2016**, *782*, 50–58.

[68] A. C. Pereira, A. E. F. Oliveira, G. B. Bettio, *Chem. Pap.* **2019**, *73*, 1795–1804.

[69] Casulli, Taurino, Carrara, Hayashita, *C — J. Carbon Res.* **2019**, *5*, 78.

[70] S. Sardaremelli, M. Hasanzadeh, H. Razmi, *J. Mol. Recognit.* **2021**, *34*, e2884.

[71] N. Agnihotri, A. D. Chowdhury, A. De, *Biosens. Bioelectron.* **2015**, *63*, 212–217.

[72] A. B. Ganganboina, R. an Doong, *Microchim. Acta* **2018**, *185*, 1–11.

[73] Z. Hua, Q. Qin, X. Bai, C. Wang, X. Huang, *Sensors Actuators, B Chem.* **2015**, *220*, 1169–1177.

[74] Y. Yi, D. Zhang, Y. Ma, X. Wu, G. Zhu, *Anal. Chem.* **2019**, *91*, 2908–2915.

[75] X. Zhang, L. Wu, J. Zhou, X. Zhang, J. Chen, *J. Electroanal. Chem.* **2015**, *742*, 97–103.

Appendix

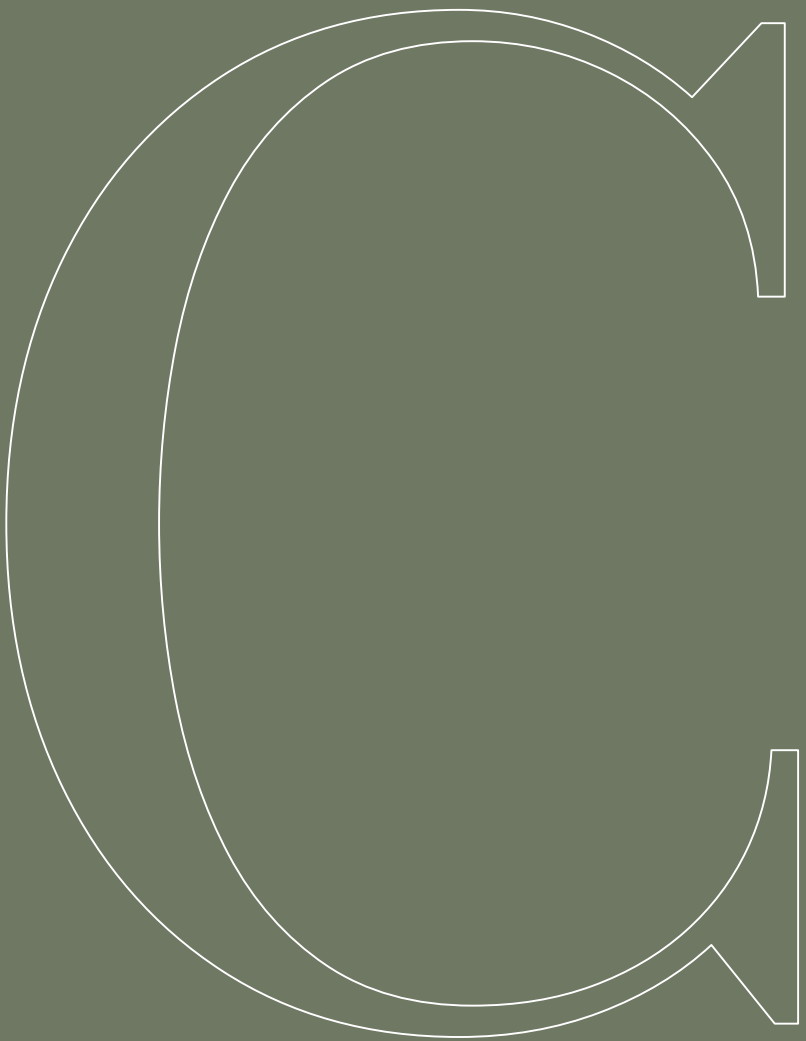

1. Insights into Nitrate sensing

Nitrate is a naturally occurring chemical form of nitrogen in ecosystems and is an essential part of the nitrogen cycle, formed during the nitrification process carried out by microorganisms [1]. It also serves as a crucial component of synthetic fertilizers, benefiting plant growth and food production for humans and animals [2]. Dietary nitrates have positive effects on the human body, improving blood flow, reducing blood pressure, and preventing cardiovascular diseases by being converted into nitric oxide [3]. However, human activities have significantly impacted the global nitrogen cycle. Intensive farming and extensive fertilizer use contribute to nitrate leaching from soil into water bodies, leading to the contamination of drinking water sources. Other sources, such as leaky cesspools, sewage treatment plants, manure runoff, and fossil fuel combustion, also contribute to elevated nitrate levels in water [4]. Despite its benefits, excessive nitrate exposure can have detrimental effects on both human health and the environment. High nitrate intake through drinking water and food has been linked to adverse health effects, including potential harm to the human endocrine system and the development of nitrosamines, associated with diseases such as Alzheimer's and Parkinson's [5,6]. Infants and young children, with immature digestive systems, are particularly vulnerable to "Methemoglobinemia" or "Blue Baby Syndrome," where hemoglobin binds with nitrite, impairing its function [7].

From an environmental perspective, increased nitrate levels in water bodies lead to eutrophication, exacerbating CO_2 levels and contributing to acidification. This process can create "dead zones" where aquatic life cannot survive. Soil's nitrate contributes to the release of greenhouse gas nitrous oxide, amplifying global warming and air pollution [8].

Addressing these multi-faceted concerns necessitates the monitoring and maintenance of nitrate levels in water and food. Regulatory authorities, such as the World Health Organization (WHO), recommend a maximum contaminant level of 50 mg L^{-1} NO_3^- in drinking water to safeguard public health [9]. However, in recent years, underground water has shown an alarming increase in nitrate content. Therefore, the control and removal of nitrate in aquatic ecosystems and plants are of highest importance to minimize/avoid its undesirable environmental effects and to prevent any adverse effects on human health.

2. Analytical methods for Nitrate determination

Various analytical methods have been developed for the determination of nitrate in different samples. Conventional techniques include spectrophotometric methods [10], chromatographic methods [11,12], electrophoretic methods [13,14], colorimetry [15,16], and fluorescence analysis [17,18]. While these methods offer high sensitivity (nM or ppb detection levels), they have certain limitations. For instance, spectrophotometric methods are subject to interferences from organic matter and ionic species, limiting their application in certain sample types. Chromatographic methods, such as high-performance liquid chromatography (HPLC) and gas chromatography (GC), require specialized columns, expensive eluent materials, and detection modes to overcome interferences from ions with similar retention times. Additionally, most chromatographic methods involve sample pre-treatments or derivatization steps, which add complexity and time to the analyses.

In recent years, there has been growing interest in the development of innovative nitrate assays that offer rapid, cost-effective, and user-friendly solutions, making them more suitable for in-site detection. Nitrates, being electroactive species, can be selectively reduced by applying a suitable potential. Consequently, electrochemical nitrate sensors have been extensively investigated as a promising tool for nitrate sensing [19]. The first attempt for electrochemical nitrate reduction was reported by Faraday since 1834 [20]. His work marked the beginning of investigations into this electrochemical process. Over several decades, researchers have developed a spectrum of electrochemical sensors, which can be categorized as enzymatic and non-enzymatic electrochemical nitrate sensors.

2.1 Enzymatic-Based Electrochemical Nitrate Biosensors

An enzyme-based electrode functions as a chemical transducer, intertwining an electrochemical procedure with the catalytic activity of an immobilized enzyme on the transducer surface. Such enzyme, nitrate reductase (NiR), which facilitates the reduction of nitrate, has gained attention as a key bio-recognition element for constructing biosensors designed to detect nitrate [21].

The utilization of NiR as the biocatalyst ensures specificity and sensitivity to the electrochemical sensor, enabling accurate nitrate quantification. However, the primary

challenge in enzymatic-based sensors is to successfully immobilize the enzyme onto the electrode surface. Traditionally, direct immobilization of enzymes onto bulk material surfaces causes denaturation, reducing their bioactivity [22]. As a result, the use of nanomaterials emerges as a viable strategy, as evidenced by the increased specific surface area and free surface energy inherent in nanomaterials, allowing for robust NiR enzyme adsorption and providing a biocompatible microenvironment.

Various nanomaterials have been used in the development of enzymatic nitrate sensors, with conductive polymers taking center stage. Conductive polymers have two advantages: they effectively immobilize enzymes while also allowing them to regenerate. Polypyrrole (PPy) [23,24], poly(3,4-ethylenedioxythiophene) (PEDOT) [25], and polydimethylsiloxane (PDMS) [26] are among the polymers studied for enzymatic nitrate sensors. The NiR enzyme is typically immobilized on the surface of polymer matrices via electropolymerization. This method was successfully used to develop an amperometric biosensor for detecting low levels of nitrate in freshwater [25]. When subjected to the most appropriate electropolymerization conditions, the PEDOT nanowire displayed a well-defined morphology, resulting in the sensor achieving outstanding specificity, rapid response time, and high sensitivity.

To enhance the enzyme's analytical capabilities, some researchers have chosen to incorporate additional nanomaterials, such as carbon-based materials. In this context, Ali and coworkers [27] developed a microfluidic impedimetric nitrate sensor. They achieved this by incorporating the NiR enzyme within a matrix of PEDOT nanofibers that had been modified using Graphene oxide (GO) nanosheets (Figure C.1 A). This sensor demonstrated remarkable precision in detecting and quantifying nitrate concentrations in soil extracts. It stood out for its heightened sensitivity and broad linear detection range. Furthermore, this study reaffirmed the strong interactions between the NiR enzyme and the GO nanosheets. The combined structure of GO nanosheets adhering to the PEDOT nanofibers through π–π interactions led to an increased electrochemical surface area, facilitating the attachment of the NiR enzyme. This catalytic process generated a higher number of electrons, inducing significant impedance fluctuations at the transducer in proportion to the nitrate concentration.

Likewise, another investigation conducted by Ali and his team [58] introduced a novel approach (Figure C.1 B). They created a bioelectrode that involved a covalent immobilized NiR enzyme onto a composite material composed of wrinkled-ridged

graphene oxide (GO) nanosheets and pre-stretched PDMS. This bioelectrode displayed the benefits of incorporating GO nanosheets into the polymer matrix for immobilizing the NiR enzyme. As depicted in Figure C.1 B , the oxygenated functional groups present on the GO nanosheets facilitated robust covalent linkages between the NiR enzyme and the GO surface. This interaction significantly amplified the catalytic transformation of nitrate into nitrite. However, despite its commendable sensitivity, this sensor exhibited a relatively limited linear detection range.

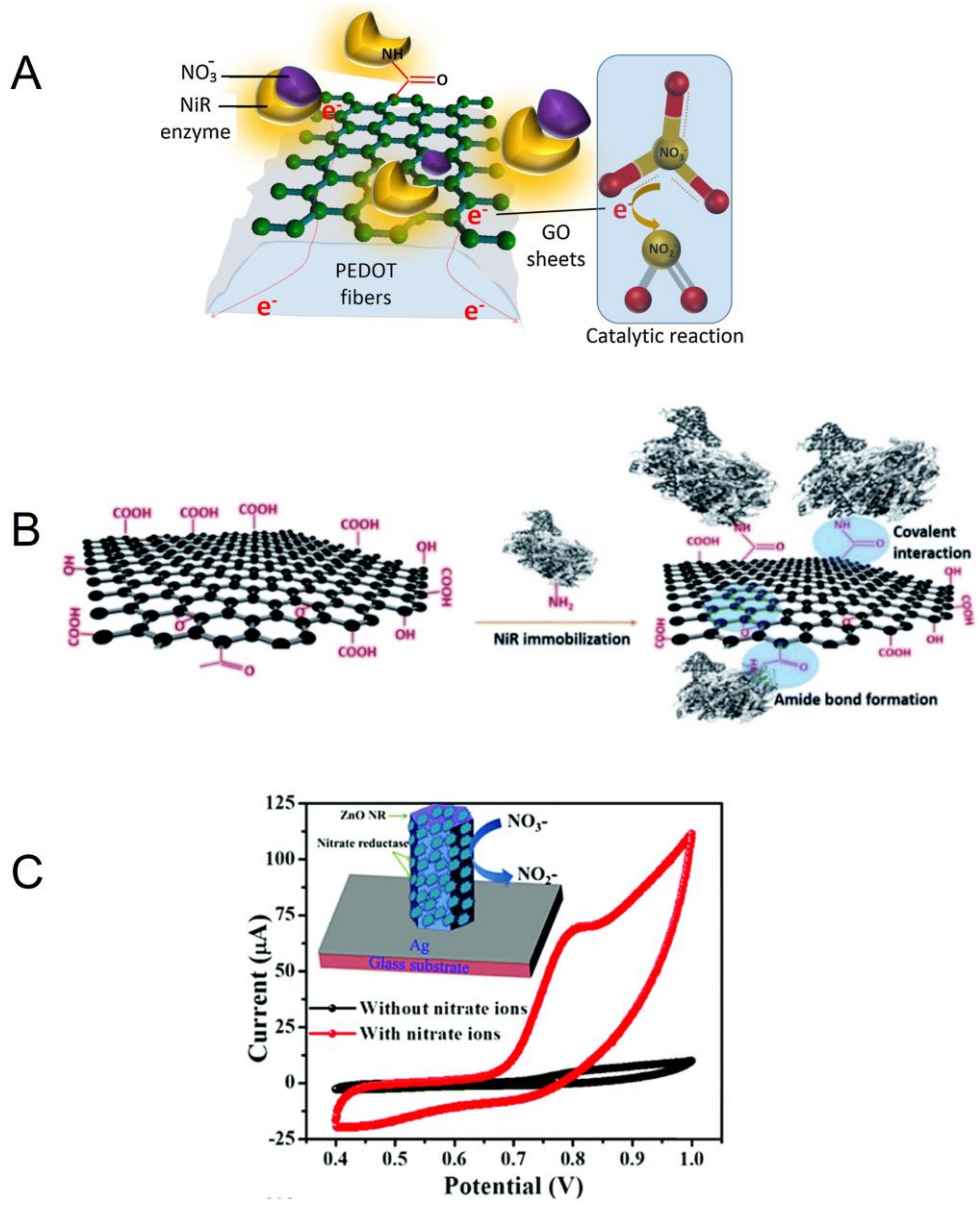

Figure C.1 (A) Schematic illustration of the surface immobilization of PEDOT nanofibers-GO with NiR enzyme to realize electrochemical nitrate detection by catalytic conversion of nitrate to nitrite. (B) Surface functionalization of graphene oxide nanosheets with nitrate reductase moieties (C) CV curves of NiR/ZnO NiRs/Ag/glass electrode in the absence/ presence of 1.0 mM nitrate ions.

Metallic nanomaterials have also received attention in the development of nitrate biosensors [28]. Zinc oxide (ZnO) has received attention due to its biocompatibility and high isoelectric point (IEP 9.5), which allows for the electrostatic immobilization of enzymes with lower isoelectric points. Ahmad et al [29] created a nitrate biosensor by directly growing ZnO nanorods on an Ag electrode and physically immobilizing the NiR enzyme via adsorption (see Figure C.1 C). This novel approach produced a biosensor with a broad linear range (1-3400 μM), a low detection limit (1 μM), and remarkable stability over a month at 4 °C. This success can be attributed to the unique design, which capitalized on the advantages of ZnO's properties, demonstrating its potential for advancing biosensor technology.

Overall, enzymatic-based nitrate biosensors have demonstrated improved analytical flexibility, stability, and sensitivity. These remarkable analytical performance owe much to the unique properties of nanomaterials, specifically their large surface-to-volume ratio, exceptional electrical conductivity, and excellent biocompatibility. Despite these advances, challenges for enzymatic nitrate sensors remain due to the inherent nature of biologically active catalysts. These difficulties include weakening enzymatic activity after immobilization and usage, as well as constraints related to specific pH ranges, temperature fluctuations, and humidity conditions [30]. The vulnerability to interference from oxygen reduction [31], combined with higher production costs, serves as additional inhibiting factors for enzymatic nitrate sensors, potentially limiting their commercialization.

2.2 Non-enzymatic electrochemical nitrate sensors

The challenges posed by enzymatic sensors have driven significant research into non-enzymatic electrochemical nitrate sensors, resulting in notable progress in this area.

Ion selective electrodes presented an excellent monitoring option to develop potentiometric nitrate sensors. Ion-selective electrodes are cheap and simple analytical devices that have been successfully used to monitor many ionic types in aqueous solutions. They can be used both in laboratory conditions and directly in field conditions [32]. That made them among the most developed and commercialized methods for nitrate detection [33]. Traditionally, Nitrate’s ISEs comprise an ion-sensitive membrane embedded with a nitrate-specific ionophore or ion-exchanger, an inner filling solution,

and an inner reference electrode, all linked to a high impedance potentiometer [34–36]. This specific type of ISE is referred to as the liquid-contact ISEs (LC-ISEs).

However, LC-ISEs encounter challenges in terms of miniaturization and integration. Issues such as freezing or drying (>40◦C) of the electrolyte and electrolyte leakage are commonly observed, leading to the necessity for calibration and maintenance [37]. This set of challenges does not satisfy the requirements for in situ environmental analysis. The evolution beyond these challenges led to the development of solid-contact ISEs (SC-ISEs). These sensors eliminate the need for inner filling solutions entirely and operate as ion-to-electron transducers. The sensing membrane in SC-ISEs is positioned between the sample solution and a solid contact (SC), allowing for direct interaction without the complications posed by liquid electrolytes. This innovative design enhances stability, facilitates miniaturization, and addresses maintenance issues, making SC-ISEs promising tools for various applications, including nitrate detection [38].

The majority of ion-to-electron transducers are made of conducting polymers [39,40], carbon nanomaterials [41,42], or their composite materials [43,44], which provide excellent sensing performance. However, many researcher noticed the formation of an unwanted water layer at the interface disrupts potential stability, leading to mechanical failure and delamination. In addition, water may already exist during the manufacturing process, such as during the drop-casting of aqueous/organic solution or electrodeposition in aqueous solution. This phenomenon effectively reverts the sensor to a liquid contact configuration, causing potential drift and jeopardizing long-term functionality. In addition, SC-ISEs shows susceptibility to external interferences such as light, gases (CO_2, O_2), and redox couples. These interferences can impact the stability and potential response of SC-ISEs, potentially leading to inaccuracies in measurements.

Amperometry stands as another prevalent category of electrochemical sensing methods, pivoting around the principle of current measurements. Within this framework, amperometric nitrate sensing hinges on the electrocatalytic reduction of nitrate, using catalytic properties of a diverse spectrum of nanomaterials. In essence, these nanomaterials act as enzyme mimics, often referred to as nanozymes [45]. This enzyme-like catalytic behavior enables various reactions, offering an attractive alternative to traditional enzymatic methods [46].

While in enzymatic nitrate biosensors, the reduction of nitrate is achieved through a single-step process, yielding nitrite as the outcome (Eq.1) . The non-enzymatic electrochemical reduction of nitrate may follow a multielectron transfer process. This can result in the formation of a spectrum of intermediates and final products, which is heavily influenced by experimental variables such as the electrode's modification material, the chosen supporting electrolyte, the pH of the medium, and the applied electric potential. A summary of the general reactions that can occur during the electrocatalytic reduction of nitrate is given by the following equations (Eq 1-9).

In acidic medium

$$NO_3^- + 2H^+ + 2e^- \rightarrow NO_2^- + H_2O \quad \text{Eq.1}$$

$$NO_2^- + 8H^+ + 6e^- \rightarrow NH_4^+ + 2H_2O \quad \text{Eq.2}$$

$$NO_3^- + 10H^+ + 8e^- \rightarrow NH_4^+ + 3H_2O \quad \text{Eq.3}$$

In neutral or alkaline medium

$$NO_3^- + H_2O + 2e^- \rightarrow NO_2^- + 2OH^- \quad \text{Eq.4}$$

$$NO_2^- + 5H_2O + 6e^- \rightarrow NH_3 + 7OH^- \quad \text{Eq.5}$$

$$NO_2^- + 4H_2O + 4e^- \rightarrow NH_2OH + 5OH^- \quad \text{Eq.6}$$

$$NH_2OH + H_2O + 2e^- \rightarrow NH_3 + 2OH^- \quad \text{Eq.7}$$

$$2NO_2^- + 3H_2O + 4e^- \rightarrow N_2O + 6OH^- \quad \text{Eq.8}$$

$$2NO_2^- + 4H_2O + 6e^- \rightarrow N_2 + 8OH^- \quad \text{Eq.9}$$

Over the past two decades, metallic nanomaterials were identified to possess catalytic properties for nitrate ion reduction and have gained significant attention. This spectrum encompasses a range of materials, from noble metals (such as gold Au [47] palladium (Pd) [48] and silver [49]), to versatile transitional metals (like copper (Cu) and zinc (Zn) [50]) along with alloys/bimetals-based nanomaterials.

Silver was intensively investigated as a powerful electrocatalyst for nitrate reduction, particularly within a neutral pH environment. A notable study by Hu et al. [51] involved the preparation of three-dimensional dendritic silver nanostructures on a gold microelectrode through electrodeposition (Figure C.2 A). These nanostructured silver materials displayed robust catalytic properties for nitrate detection, as evidenced by their compelling analytical performance. This included maintaining good stability over

a substantial 100 measurement cycles, a broader linear detection range spanning from 2 µM to 1000 µM, and a significantly lowered limit of detection (LOD) of 2 µM in comparison to other nitrate sensors designed for use in fresh water. Additionally, an exploration of pH effects ranging from 5 to 9 revealed that the highest current response was achieved at pH 7, indicating the promising potential of silver nanostructured materials for voltammetric nitrate analysis in neutral matrices.

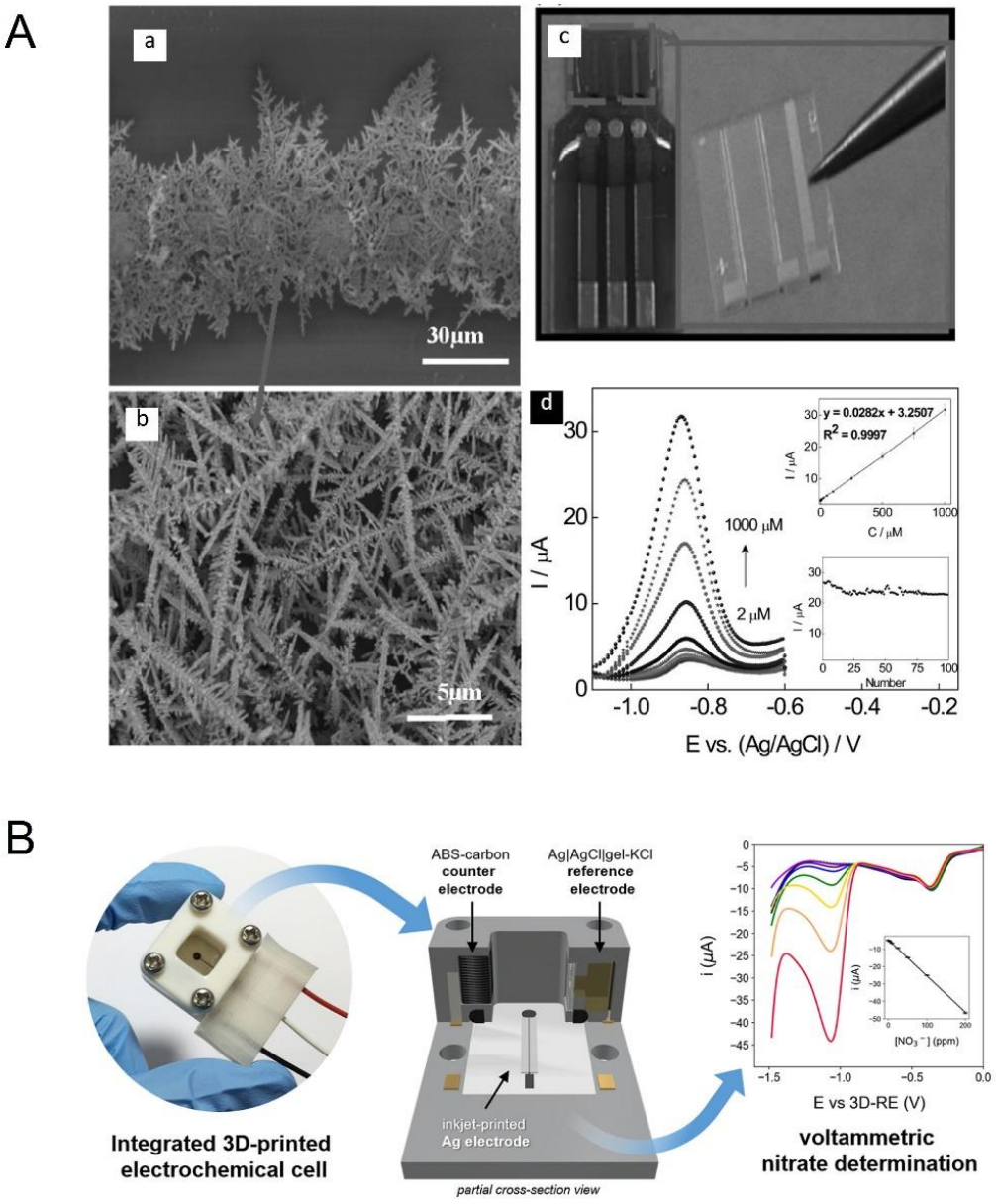

Figure C.2 (A) SEM images of dendritic silver nanostructure with different widths (a,b). Photo of microelectrode chip after encapsulation (c). Square wave voltammograms recorded in the presence of NaNO3 solutions (d). (B) Design of 3D-printed electrochemical cell with integrated counter electrode , reference electrode and disposable inkjet-printed working electrode with a graph of the Linear sweep voltammograms of NO_3^- standards.

In a more recent work [52], Sibug-Torres, S. M and her team have succeeded in fabricating a reusable 3D-printed electrochemical cell with integrated reference and counter electrodes, and a replaceable inkjet-printed silver working electrode (Figure C.2 B). Silver was electrodeposited on the working electrode and formed a dendritic nanostructure. Nitrate ions in synthetic brackish water samples (pH 8.0) were detected using linear sweep voltammetry with a LOD of 1.40 ppm and a sensitivity of 0.2086 μA ppm^{-1}. Measurements done with different electrode batches confirmed the intra- and inter-electrode reproducibility without much interference by ions (cations and anions) commonly found in such samples.

As with other noble metals examined in nitrate sensing, the high cost linked with silver has directed researchers to shift their attention towards a more economically feasible option for nitrate sensing applications. Copper, a transitional metal, has emerged as a suitable candidate due to its significant electrocatalytic activity, stability, and cost-effectiveness. Notably, copper stands out as one of the foremost metals known for its robust NO_3^- reduction activity.

Copper of various structures, such as nanoclusters [53], microarrays [54], nanowire arrays [55,56], nanosheets [57], nanoparticles [58], etc. has been employed in voltammetric or amperometric sensors for nitrate detection especially acidic media. These diverse copper configurations have consistently demonstrated superior electrocatalytic activity when compared to bare copper electrodes. This enhancement can be attributed to their increased specific surface area, which in turn translates into improved analytical performance in the development of nitrate sensor. For instance, Liang J. et al. employed a copper nanowire-based electrode, fabricated through thermal annealing, resulting in the formation of a stable and porous nanowire network (Figure C.3 A). They achieved an impressive low detection limit, as low as 1.35 μM, for nitrate detection in water [59]. In contrast, a combination of copper microspheres (CuMSs) and a polyaniline (PANI) film exhibited a less sensitive analytical performance, yielding a detection limit of 8 μM [60].

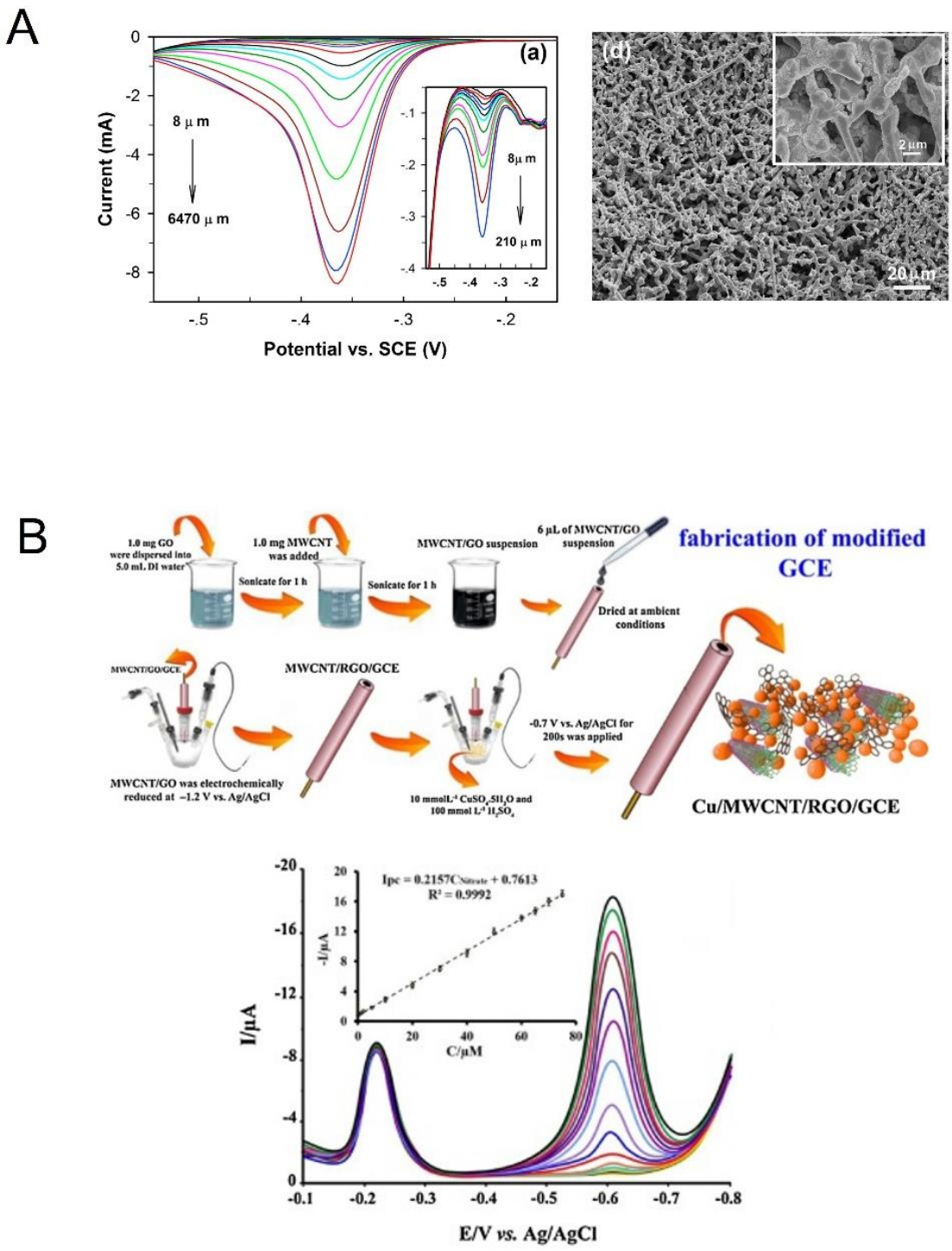

Figure C.3 (A) DPV curves recorded at Copper electrode for different concentrations of nitrate (pH = 2) and a SEM images of Cu nanowire film. (B) Preparation of GCE and Fabrication of the sensor, and SWVs of nitrate in the presence of nitrite ions (50 μM).

To achieve superior analytical performance, researchers have adopted the effective strategy of blending copper with various nanomaterials. In a study conducted by Hasan Bagheri and colleagues [61], they developed a nanocomposite consisting of copper metal nanoparticles, multiwall carbon nanotubes, and reduced graphene oxide for the purpose of nitrate detection in water (Figure C.3 B). Under optimized experimental conditions, this sensor exhibited exceptional catalytic activity in the electro-reduction of nitrate ions, particularly at a pH level of 3.0. The sensor highlighted a remarkable increase in cathodic peak currents when compared to an unmodified glassy carbon electrode (GCE). Through the application of square wave voltammetry (SWV), this fabricated sensor demonstrated a wide dynamic concentration range, spanning from 0.1 to 75 μM, while achieving detection limits as low as 20 nM.

In summary, extensive research has been conducted in recent decades to advance nitrate sensing technology. Numerous efforts have been dedicated to the development of sensors for accurate nitrate determination. With the continuous progress of nanotechnology, researchers have been actively exploring various nanostructured materials as alternatives to traditional enzymatic sensing methods. These materials offer significant advantages, including robust catalytic activity, excellent electrical conductivity, and outstanding biocompatibility. Among the nanomaterials investigated for enhancing conventional nitrate detection electrodes, nanostructured metals, particularly copper, have emerged as particularly promising candidates. Copper exhibits exceptional catalytic activity in nitrate reduction, along with high conductivity, all while remaining cost-effective and affordable. Given this context, our primary goal has centered on exploring the potential of copper to create a versatile sensor capable of both electrochemical and photoelectrochemical nitrate detection with precise accuracy.

References

[1] M. M. M. Kuypers, H. K. Marchant, B. Kartal, *Nat. Rev. Microbiol.* **2018**, *16*, 263–276.

[2] E. Rembiałkowska, *J. Sci. Food Agric.* **2007**, *87*, 2757–2762.

[3] N. G. Hord, Y. Tang, N. S. Bryan, *Am. J. Clin. Nutr.* **2009**, *90*, 1–10.

[4] R. Poulsen, N. Cedergreen, T. Hayes, M. Hansen, *Environ. Sci. Technol.* **2018**, *52*, 3869–3887.

[5] J. Molina, F. J. Jiménez-Jiménez, J. Navarro, E. Ruiz, J. Arenas, F. Cabrera-Valdivia, A. Vázquez, P. Fernández-Calle, L. Ayuso-Peralta, M. Rabasa, F. Bermejo, *J. Neurol. Sci.* **1994**, *127*, 87–89.

[6] M. Ikeda, I. Sato, T. Yuasa, T. Miyatake, S. Murota, *J. Neural Transm.* **1995**, *100*, 263–267.

[7] D. S. Powlson, T. M. Addiscott, N. Benjamin, K. G. Cassman, T. M. de Kok, H. van Grinsven, J.-L. L'hirondel, A. A. Avery, C. van Kessel, *J. Environ. Qual.* **2008**, *37*, 291–295.

[8] W. de Vries, *Curr. Opin. Environ. Sci. Heal.* **2021**, *21*, DOI 10.1016/j.coesh.2021.100249.

[9] M. R. Khan, S. M. Wabaidur, Z. A. Alothman, R. Busquets, M. Naushad, *Talanta* **2016**, *152*, 513–520.

[10] A. Daniel, D. Birot, M. Lehaitre, J. Poncin, *Anal. Chim. Acta* **1995**, *308*, 413–424.

[11] H. Kodamatani, S. Yamazaki, K. Saito, T. Tomiyasu, Y. Komatsu, *J. Chromatogr. A* **2009**, *1216*, 3163–3167.

[12] K. Tirumalesh, *Talanta* **2008**, *74*, 1428–1434.

[13] J. E. Melanson, C. A. Lucy, in *J. Chromatogr. A*, Elsevier, **2000**, pp. 311–316.

[14] L. Gao, J. S. Pulido, R. M. Hatfield, R. F. Dundervill, C. A. McCannel, S. A. Shippy, *J. Chromatogr. B Anal. Technol. Biomed. Life Sci.* **2007**, *847*, 300–304.

[15] M. B. Shinn, *Ind. Eng. Chem. - Anal. Ed.* **1941**, *13*, 33–35.

[16] D. A. Cataldo, M. H. Haroon, L. E. Schrader, V. L. Youngs, *Commun. Soil Sci.*

Plant Anal. **1975**, *6*, 71–80.

[17] K. K. Karali, L. Sygellou, C. D. Stalikas, *Talanta* **2018**, *189*, 480–488.

[18] X. Q. Zhan, D. H. Li, H. Zheng, J. G. Xu, *Anal. Lett.* **2001**, *34*, 2761–2770.

[19] H. Ryu, D. Thompson, Y. Huang, B. Li, Y. Lei, *Sensors and Actuators Reports* **2020**, *2*, 100022.

[20] M. Farady, *Philos. Trans. R. Soc. London* **1834**, *124*, 77–122.

[21] S. Cosnier, C. Innocent, Y. Jouanneau, *Anal. Chem.* **1994**, *315*, 147–60.

[22] L. Rassaei, F. Marken, M. Sillanpää, M. Amiri, C. M. Cirtiu, M. Sillanpää, *TrAC - Trends Anal. Chem.* **2011**, *30*, 1704–1715.

[23] F. Can, S. Korkut Ozoner, P. Ergenekon, E. Erhan, *Mater. Sci. Eng. C* **2012**, *32*, 18–23.

[24] S. B. Adeloju, M. Sohail, *Electroanalysis* **2011**, *23*, 987–996.

[25] A. A. Gokhale, J. Lu, R. R. Weerasiri, J. Yu, I. Lee, *Electroanalysis* **2015**, *27*, 1127–1137.

[26] M. A. Ali, W. Hong, S. Oren, Q. Wang, Y. Wang, H. Jiang, L. Dong, *RSC Adv.* **2016**, *6*, 67184–67195.

[27] M. A. Ali, H. Jiang, N. K. Mahal, R. J. Weber, R. Kumar, M. J. Castellano, L. Dong, *Sensors Actuators, B Chem.* **2017**, *239*, 1289–1299.

[28] M. A. Ali, Y. Jiao, S. Tabassum, Y. Wang, H. Jiang, L. Dong, in *TRANSDUCERS 2017 - 19th Int. Conf. Solid-State Sensors, Actuators Microsystems*, Institute Of Electrical And Electronics Engineers Inc., **2017**, pp. 238–241.

[29] R. Ahmad, K. S. Bhat, M.-S. Ahn, Y.-B. Hahn, *New J. Chem.* **2017**, *41*, 10992–10997.

[30] J. Massah, K. Asefpour Vakilian, *Biosyst. Eng.* **2019**, *177*, 49–58.

[31] N. Plumeré, *Anal. Bioanal. Chem.* **2013**, *405*, 3731–3738.

[32] V. I. Adamchuk, E. D. Lund, B. Sethuramasamyraja, M. T. Morgan, A. Dobermann, D. B. Marx, *Comput. Electron. Agric.* **2005**, *48*, 272–294.

[33] Y. Shao, Y. Ying, J. Ping, *Chem. Soc. Rev.* **2020**, *49*, 4405–4465.

[34] A. Hulanicki, R. Lewandowski, M. Maj, *Anal. Chim. Acta* **1974**, *69*, 409–414.

[35] A. Consalteri, A. Rigato, L. Clamor, P. Giandon, *J. Food Compos. Anal.* **1992**, *5*, 252–256.

[36] Y. Zhong, W. Yan, J. Chen, Z. Shangguan, *Sci. Rep.* **2014**, *4*, 7223.

[37] A. N. Mallya, P. C. Ramamurthy, *ECS J. Solid State Sci. Technol.* **2018**, *7*, Q3054–Q3064.

[38] C. L. Baumbauer, P. J. Goodrich, M. E. Payne, T. Anthony, C. Beckstoffer, A. Toor, W. Silver, A. C. Arias, *Sensors* **2022**, *22*, 4095.

[39] C. Wardak, *Electroanalysis* **2014**, *26*, 864–872.

[40] K. Pietrzak, C. Wardak, R. Łyszczek, *Electroanalysis* **2020**, *32*, 724–731.

[41] M. Cuartero, G. Crespo, T. Cherubini, N. Pankratova, F. Confalonieri, F. Massa, M. Lou Tercier-Waeber, M. Abdou, J. Schäfer, E. Bakker, *Anal. Chem.* **2018**, *90*, 4702–4710.

[42] Y. Liu, Y. Liu, Z. Meng, Y. Qin, D. Jiang, K. Xi, P. Wang, *Talanta* **2020**, *208*, DOI 10.1016/j.talanta.2019.120374.

[43] B. Paczosa-Bator, L. Cabaj, R. Piech, K. Skupień, *Anal. Chem.* **2013**, *85*, 10255–10261.

[44] M. A. Ali, X. Wang, Y. Chen, Y. Jiao, N. K. Mahal, S. Moru, M. J. Castellano, J. C. Schnable, P. S. Schnable, L. Dong, *ACS Appl. Mater. Interfaces* **2019**, *11*, 29195–29206.

[45] Y. Zu, H. Yao, Y. Wang, L. Yan, Z. Gu, C. Chen, L. Gao, W. Yin, *VIEW* **2021**, *2*, 20200188.

[46] J. Wu, X. Wang, Q. Wang, Z. Lou, S. Li, Y. Zhu, L. Qin, H. Wei, *Chem. Soc. Rev.* **2019**, *48*, 1004–1076.

[47] M. P. N. Bui, J. Brockgreitens, S. Ahmed, A. Abbas, *Biosens. Bioelectron.* **2016**, *85*, 280–286.

[48] M. R. Mahmoudian, Y. Alias, W. J. Basirun, P. Mengwoi, F. Jamali-Sheini, M. Sookhakian, M. Silakhori, *J. Electroanal. Chem.* **2015**, *751*, 30–36.

[49] K. Fajerwerg, V. Ynam, B. Chaudret, V. Garçon, D. Thouron, M. Comtat,

Electrochem. commun. **2010**, *12*, 1439–1441.

[50] M. B. Gumpu, N. Nesakumar, B. L. Ramachandra, J. B. B. Rayappan, *J. Anal. Chem.* **2017**, *72*, 316–326.

[51] J. Hu, J. Sun, C. Bian, J. Tong, X. Shanhong, *Electroanalysis* **2013**, *25*, 546–556.

[52] S. M. Sibug-Torres, L. P. Go, V. C. G. Castillo, J. L. R. Pauco, E. P. Enriquez, *Anal. Chim. Acta* **2021**, *1160*, 338430.

[53] A. K. M. S. Inam, M. A. Costa Angeli, B. Shkodra, A. Douaki, E. Avancini, L. Magagnin, L. Petti, P. Lugli, *ACS Omega* **2021**, *6*, 33523–33532.

[54] I. S. Da Silva, W. R. De Araujo, T. R. L. C. Paixão, L. Angnes, *Sensors Actuators, B Chem.* **2013**, *188*, 94–98.

[55] B. Patella, R. R. Russo, A. O'Riordan, G. Aiello, C. Sunseri, R. Inguanta, *Talanta* **2021**, *221*, 121643.

[56] A. M. Stortini, L. M. Moretto, A. Mardegan, M. Ongaro, P. Ugo, *Sensors Actuators, B Chem.* **2015**, *207*, 186–192.

[57] B. Hafezi, M. R. Majidi, *Anal. Methods* **2013**, *5*, 3552–3556.

[58] M. Sookhakian, M. A. Mat Teridi, G. B. Tong, P. M. Woi, M. Khalil, Y. Alias, *ACS Appl. Nano Mater.* **2021**, *4*, 12737–12744.

[59] J. Liang, Y. Zheng, Z. Liu, *Sensors Actuators, B Chem.* **2016**, *232*, 336–344.

[60] Y. Li, H. Han, D. Pan, P. Zhang, *J. Electrochem. Soc.* **2019**, *166*, B1038–B1043.

[61] H. Bagheri, A. Hajian, M. Rezaei, A. Shirzadmehr, *J. Hazard. Mater.* **2017**, *324*, 762–772.

Appendix

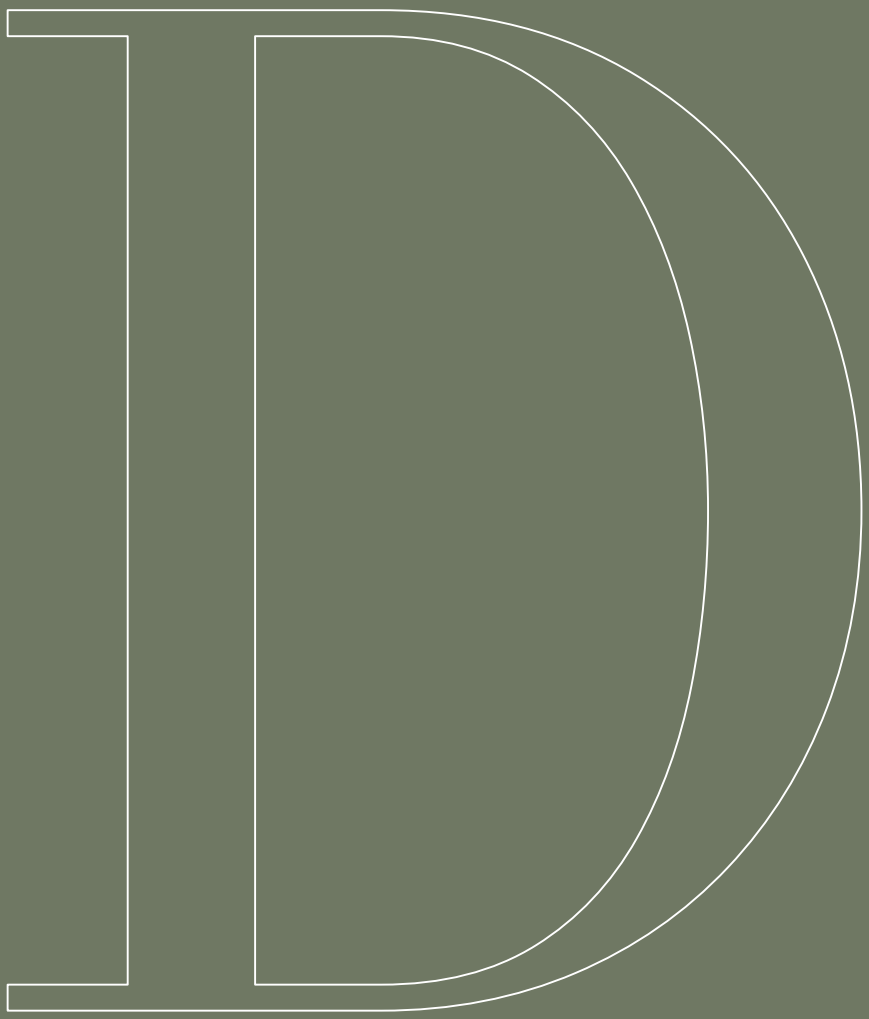

1. Introduction to Mesoporous Silica: Properties and Evolution

Porous nanomaterials are a broad class of materials that are characterized by their nano-sized pores. Since ancient times, civilizations have been using the unique properties of porous materials for a range of applications. For instance, Egyptians utilized porous activated charcoal in inks, while Western Africans employed porous clay minerals as antidiarrheal medicine[1]. In the 21st century, significant advancements in material science and nanotechnology have enabled us to master the design and synthesis of synthetic porous nanomaterials with desired structural and chemical features. These breakthroughs have been made possible by the ability to observe, measure, manipulate, assemble, control, and manufacture matter at the nanometer scale. Porous materials have a high surface area to volume ratio, which makes them incredibly useful in a variety of applications, from catalysis [2] and adsorption[3] to drug delivery, sensing[4], and energy storage [5]. The size and distribution of the pores within these materials can greatly influence their properties and, consequently, their potential applications.

Among the various types of porous nanomaterials, mesoporous nanomaterials hold a unique position due to their intermediate pore size. Mesoporous nanomaterials, as classified by the International Union of Pure and Applied Chemistry (IUPAC), have pore sizes ranging from 2 to 50 nanometers [6]. These materials occupy an intermediate position between microporous materials, which have pore sizes less than 2 nm, and macroporous materials, with pore sizes greater than 50 nm (Figure D.1).

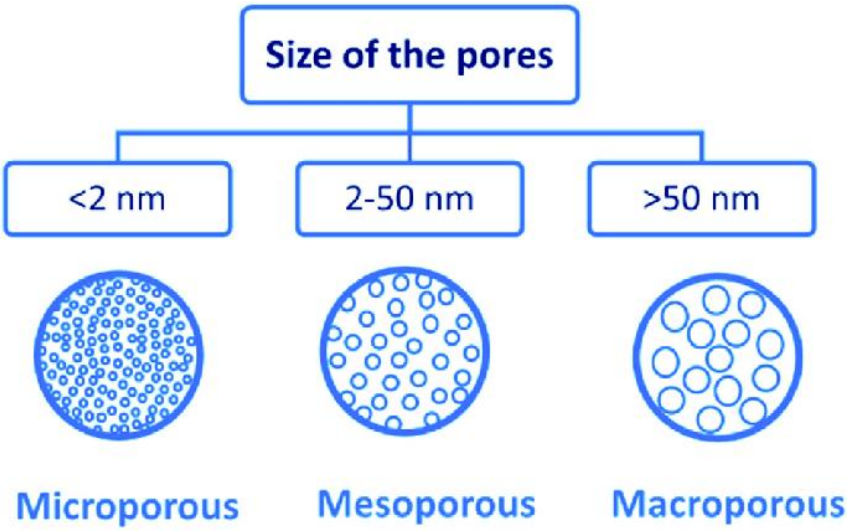

Figure D.1 Schematic representing difference between microporous, mesoporous, and macroporous materials based on their pore size [7].

The term "mesoporous" is derived from the Greek word "mesos", meaning middle, reflecting their intermediate pore size. These materials are characterized by their high surface area and porosity in the meso dimension, which distinguishes them from other porous materials. The synthesis of mesoporous materials marked a significant milestone in material science. It allowed for the creation of materials with pore sizes larger than those of zeolites, which are typically limited to around 1.5 nm [8]. This breakthrough has led to the development of a new class of materials characterized by a moderate pore size, accommodating more complex chemicals, molecular complexes, and even biomolecular materials.

2. Mesoporous silica nanomaterials

Mesoporous silica nanomaterials are a specific subclass of mesoporous nanomaterials predominantly composed of silica or silicon dioxide (SiO_2). Silica, abundant in nature and found in various forms like sand and quartz, serves as a fundamental component in the composition of many glass and ceramic materials. Silica possesses unique chemical properties, including great thermal and chemical stability. Its pore structure remains stable at high temperatures, over 1200 K. Additionally, silica walls are inert to most etching agents, whether acidic or basic, apart from hydrofluoric acid and concentrated basic solutions. These characteristics make silica an ideal building block for the creation of mesoporous materials. The versatile nature of silica as a building block has enabled researchers to successfully synthesize mesoporous silica in diverse shapes and mesostructures.

In the natural world, diatoms, unicellular microalgae found in phytoplankton and phytobenthon deposited on the bottom of seas or lakes over centuries, provide a fascinating model for the robust structure of mesoporous silica. Diatoms have a distinctive feature, the frustule, a 3D-structured silica shell organized to the ten-nanometer scale (Figure D.2) [9]. This shell serves as a mechanical defense against the environment or predators. Simultaneously, it requires porosity to allow nutrients and metabolites to diffuse in and out, and transparent for the photosynthetic activity of the cell. These microorganisms have inspired the design and processes in nanotechnology and especially in mesoporous silica nanomaterials.

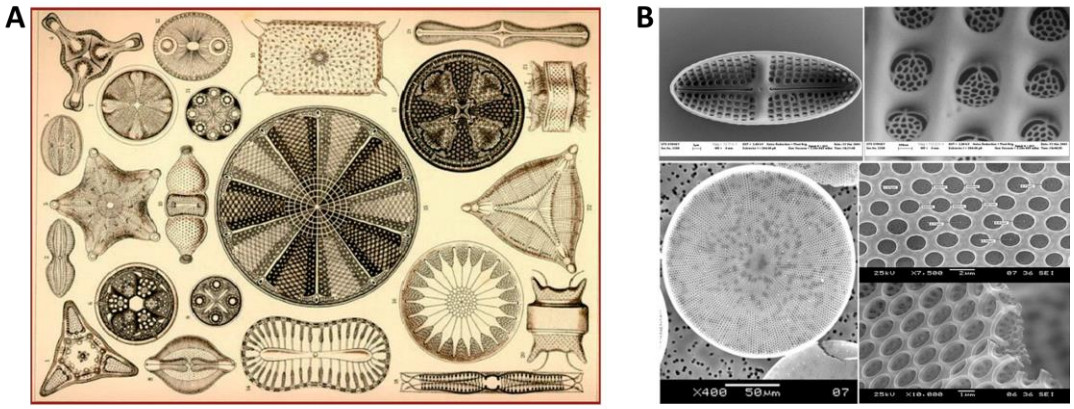

Figure D.2 (A) The diversity of diatom frustules represented by Haeckel in 'Kunstformen der Natur' in 1904 [9]. (B) Hierarchical distribution of pores in diatom frustules; Top: *Achnanthes subsessilis* (based on the work of Butcher et al. [10]) ; Bottom: *Coscinodiscus walesii* (based on the work of De Stefano et al. [11]).

The genesis of synthetic mesoporous silica dates to 1990 in Japan, where Yanagisawa et al. synthesized a novel alkyltrimethylammonium-kanemite complex, a precursor to mesoporous silica [12]. They discovered that the SiO_2 layers in the complex condensed into a three-dimensional network, constituting an early form of mesoporous silica. A significant leap occurred in 1992 when Kresge et al. at Mobil Research and Development Corporation unveiled the M41S family of mesoporous silicas. They utilized a liquid crystal template approach on aluminosilicate gels, unveiling MCM-41 (Mobil Crystalline Material) as part of their findings. MCM-41, with its hexagonal array, features pore diameters of 2.5 to 6 nm, using cationic surfactants as the templating agent. This discovery catalyzed further research, leading to the identification of other mesostructures like MCM-48, with its cubic form, and MCM-50, noted for its lamellar arrangement. Building upon Kresge's pioneering contributions, subsequent research has introduced a multitude of new mesoporous silica classes. Notably, Zhao et al. in 1998 aimed to increase the pore size within silica by using an amphiphilic triblock copolymer as a templating agent. Their work culminated in SBA-15, a hexagonally ordered mesoporous silica material conceived at the University of California, Santa Barbara. SBA-15 is distinguished from MCM-41 by its larger pores, thicker walls, and enhanced hydrothermal stability, broadening its utility. Today, the mesoporous silica landscape is a testament to the relentless pursuit of innovation, with families such as HMS, FSM, MSU, KIT, FDU, JLU, TUD, COK, and HMM enriching the catalog of these versatile materials (as detailed in Table D-1). The precise tailoring of mesoporous silica's size,

structure—from hexagonal to cubic and lamellar—and morphology—spanning rods to spheres and more elaborate shapes—continues to be driven by the synergistic relationship between surfactants and silica precursors. This symbiosis of organic and inorganic components is the keystone of mesoporous silica's adaptability.

Table D-1 Overview of selected mesoporous silica.

Mesoporous Silica family	Mesostructure Type	Syngony	Space group	Schematic Illustration
M41S	MCM-41	2D hexagonal	P6mm	
	MCM-48	3D cubic	Ia3d	
	MCM-50	Lamellar	p2	
SBA	SBA-11	3D cubic	Pm3̄m	
	SBA-12	3D hexagonal	$P6_3/mmc$	
	SBA-15	2D hexagonal	P6mm	
	SBA-16	3D cubic cages	Im3̄m	
KIT	KIT 1	3D disordered	/	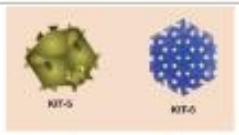
	KIT-5	3D Cage-like	Fm3̄m	
	KIT-6	3D bicontinous cubic	Ia3d	
COK	COK-12	2D Hexagonal	P6m	
FDU	FDU 1	3D cubic cages	Im3̄m	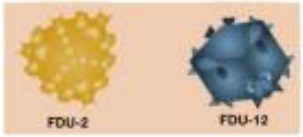
	FDU 2	3D cubic	Fd3̄m	
	FDU 5	3D bicontinuous cubic	Ia3̄d	
	FDU 12	3D cubic	Fm3̄m	

3. Mesoporous silica synthesis

3.1 Sol-gel method

Mesoporous silica nanomaterials are commonly prepared by sol-gel method in aqueous solution. This method is considered as; 'chimie douce' due to its low operation temperature and aqueous-based fabrication process, as opposed to more classical industrial techniques for glass and ceramic manufacturing, which require very high temperatures [13]. The sol-gel method involves a two-step process comprising hydrolysis followed by the condensation of silane precursors. Typical precursors of this process are alkoxysilanes ($Si(OR)_4$), with OR corresponding to different alkoxy groups, typically methoxy (tetramethoxysilane/TMOS $Si(OCH_3)_4$) and ethoxy (tetraethoxysilane/TEOS $Si(OCH_2H_5)_4$). The reactions forming part of the sol-gel process are depicted in equations 1-3.

The hydrolysis of alkoxysilane forming silanol and alcohol is presented in Eq. 1, in which n represents the degree of hydrolysis that reaches completion at n = 4.

$$Si(OR)_4 + n\,H_2O \rightarrow Si(OR)_{4-n}(OH)_n + n\,ROH \quad (Eq.\ 1)$$

The subsequent reactions can be categorized into water-producing and alcohol-producing condensation, presented in Eqs. 2 and 3, respectively. In both cases, a siloxane network is formed. The continuous polycondensation reaction, also known as the aging process, is responsible for densifying the material, leading to the gel structure of silica. The evaporation of the solvent further facilitates the formation of a solid silica network.

$$2Si(OH)_4 \rightarrow Si-O-Si + 2H_2O \quad (Water\text{–}Producing\ Condensation)\ (Eq.\ 2)$$

$$Si(OH)_4 + ROH \rightarrow Si-O-Si + H_2O \quad (Alcohol\text{–}Producing\ Condensation)\ (Eq.\ 3)$$

The kinetics of the hydrolysis and condensation reactions are pH-dependent. At acidic pH, the hydrolysis process is catalyzed, with an optimum at pH 3. On the other hand, the condensation process is most effectively catalyzed at pH 8, as illustrated in Figure D.3. This pH dependency underscores the significance of controlling the reaction environment for optimal synthesis outcomes.

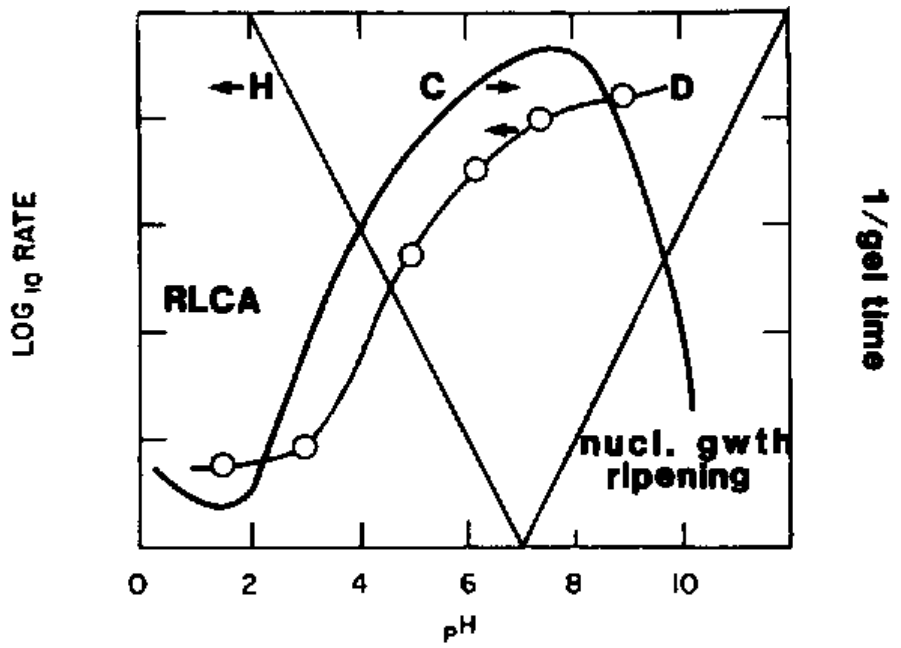

Figure D.3 Schematic representation of pH influences in the hydrolysis (H), condensation (C), and depolymerization (D) rates[14].

In contemporary research and industrial applications, the sol-gel method has been pivotal in fabricating mesoporous materials boasting a variety of morphologies. This versatility is achieved through the use of structure-directing agents such as cationic surfactants, triblock copolymers, and organic small molecules[6], often in conjunction with template methods. The sol-gel technique is frequently viewed as a nuanced adaptation of the Stöber process, sharing a foundational mechanism but diverging in its incorporation of surfactants as structural guides and its broader application in creating mesoporous structures. Werner Stöber's seminal work in 1968 laid the groundwork for synthesizing monodisperse silica particles[15], a method that has since evolved through numerous refinements to yield an array of monodisperse, ordered, nanosized silica particles.

3.2 Mesostructuration

The achievement of mesoporosity in silica involves selecting from various synthetic pathways, each leading to distinct structural characteristics.

3.2.1 Hard-Templating Method

Hard templating, often referred to as "nanocasting," is a template based method employed in the synthesis of mesoporous nanomaterials. The fundamental principle of hard templating involves replicating the porous structure of a sacrificial template, typically composed of materials like colloidal crystals, porous alumina, or other ordered materials. This template, acting as a mold, dictates the final architecture of the mesoporous structure, with its intricate network of pores and channels serving as a blueprint for the arrangement of mesopores in the silica material.

For silica mesoporous nanostructures, the synthesis process begins by impregnating the porous template with a silica precursor, typically tetraethyl orthosilicate (TEOS). This precursor fills the void spaces of the template. Following this, curing conditions are applied to transform the liquid precursor into a solid silica phase within the template's pores. The next step is template removal, which can be achieved usually through calcination or selective extraction methods [16]. This step sacrifices the template, leaving behind the mesoporous silica material with a structure that mirrors the original template.

3.2.2 Soft-Templating Method

The soft-templating uses no hard template solid instead it uses a liquid templates that are dissolved during the synthesis process. That-s why it is usually referred to as ‘Liquid crystal template approach’[17]. In this method, a surfactant, serving as a structure-directing agent, takes center stage as the template for synthesizing ordered mesoporous materials. The surfactant forms a mesostructured assembly while the silica precursors condense around the structure. Here, the use of different types of surfactant (e.g. cationic, anionic, or nonionic surfactants, and block-copolymers) can tune the pore size, structure, and morphology of the resulting mesoporous silica.

For instance, the mechanism used by Kresge et al. concerning the formation of the hexagonally arranged MCM-41 was based on a soft templating methods using hexadecyltrimethylammonium chloride (CTAC) surfactant[18]. In the true liquid-crystal

template mechanism (Figure D.4, pathway a), highly concentrated surfactant molecules aggregate and form a hexagonal array of cylindrical micelles. Subsequently, silica precursor is added and condenses around its structure. Nowadays, a concerted self-assembly mechanism is mostly accepted, where a mixture of surfactant molecules and silica precursor undergoes a cooperative assembly and form the same final mesostructure (Figure D.4, pathway b). In both cases, mesoporosity is obtained upon removal of the surfactant molecules by calcination or extraction.

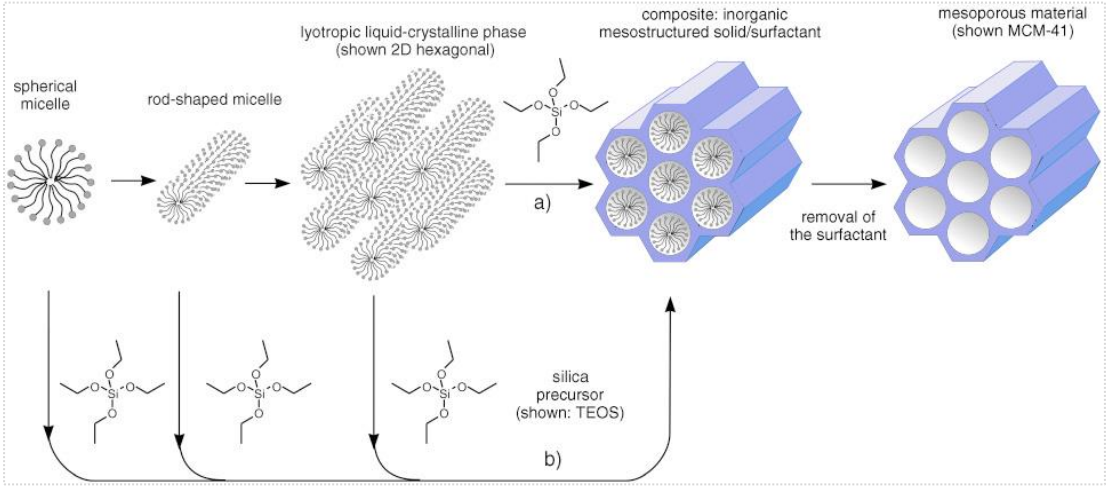

Figure D.4 Synthesis of mesoporous materials by surfactant structure directing agents: (a) true liquid-crystal template mechanism, (b) cooperative liquid-crystal template mechanism [19].

The arrangement of the resulting mesopores can be changed by varying the concentration of the surfactant as it can change the arrangement of the micelles from spherical, cylindrical up to planar bilayer form giving various pore geometries, such as 2D hexagonal, cubic, and lamellar structures (Figure D.5). The absence of a hard template simplifies the synthesis process and contributes to its designation as a more facile and adaptable method.

Figure D.5 Different structures of mesoporous M41S materials: a) MCM-41 (2D hexagonal p6mm), b) MCM-48 (cubic Ia3d), and c) MCM-50 (lamellar p2)[19].

3.3 Morphology

Morphology plays a crucial role in the performance of mesoporous silica nanomaterials, influencing their functionality in various applications. As previously mentioned, the pore geometry can be tuned by changing the surfactant/silica ratio. Also, the final morphology can be controlled to form typical shapes such as fibers, rods, monoliths, single crystals, spheres, and thin films. These changes in morphology are influenced by factors such as the types of silica precursors used, the types of surfactant micelles, the interactions between silicate species and surfactants, and the addition of inorganic salts, organic swelling agents, cosolvents, and cosurfactants.

For instance, in the field of catalysis, separation, and water treatment, mesoporous silica monoliths can be used directly as reactors[20,21].

The field of drug delivery has witnessed significant advancements through the utilization of mesoporous silica, particularly spherical particles. These materials stand out for their biocompatibility, biodegradability, and well-defined pore architecture, making them excellent carriers for therapeutic agents. The surface of hollow mesoporous silica nanoparticles (MSNs) can be functionalized with various stimuli-responsive elements, allowing for the controlled release of drugs in response to specific biological triggers such as pH, temperature, redox conditions, or enzymatic activity[22]. This ability to modulate drug release profiles tailors treatment regimens to the precise needs of therapeutic applications[23].

Additionally, mesoporous silica spheres have found extensive use in chromatography and electroanalysis[24,25]. They have been used in high-performance liquid chromatography (HPLC) packing for the separation of aromatic molecules[26] and large biomolecules such as proteins[27]. Furthermore, these materials have been instrumental in enhancing the sensitivity and specificity of electrochemical sensors for detecting a wide range of analytes[28].

The exploration of fibrous mesoporous materials, including the optimization of silica fibers and the development of nanorods and helical structures, has opened new avenues in material science[29]. By transitioning from traditional silica precursors (TEOS) to alternatives like tetrabutoxysilane (TBOS), researchers have achieved mesoporous silica fibers with controlled diameters and unique morphologies, expanding their potential applications[30,31].

Lastly, mesoporous silica thin films cover a wide range of applications, from coatings and insulators, membrane and separation science, photocatalysis, sensors, and preconcentration analysis, up to (nano)bio and biomedical applications.

3.3.1 Ordered Mesoporous silica film on electrode

As already mentioned, film morphology attracted researchers' attention due to its versatility and unique structures and functions especially for electrochemical application. They are conventionally prepared by the evaporation-induced self-assembly (EISA) method, a technique initially introduced by the research groups led by Brinker[32] and Ozin[33] in the late 1990s. This method was further refined and expanded upon by the collaborative efforts of Grosso and Sanchez[34]. The EISA process, as implied by its name, leverages the evaporation of solvents to drive the polycondensation of silica precursors around a supramolecular template, a process that unfolds in four distinct stages, as depicted in the accompanying Figure D.6.

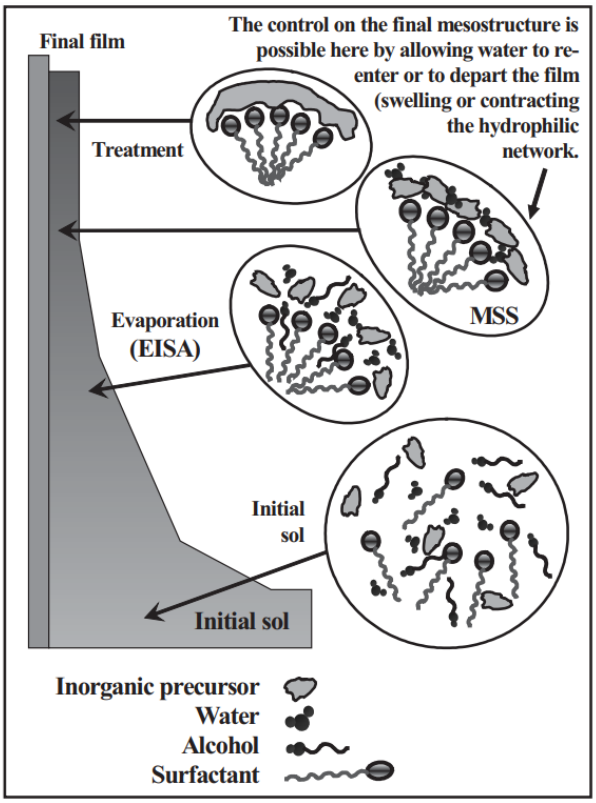

Figure D.6 Schematic representation of EISA of mesoporous inorganic material by dip coating[25,34].

In the EISA process, a homogeneous sol solution containing a soluble silica precursor (e.g., tetraethyl orthosilicate, TEOS) and a surfactant or block copolymer (e.g., cetyltrimethylammonium bromide, Pluronic P123, Brij-56) is prepared in a water/alcohol mixture. This solution, with an initial surfactant concentration below the threshold for bulk mesophase formation, is deposited onto a solid support. As the substrate is withdrawn, the solution coats the surface, and preferential alcohol evaporation triggers film formation through self-assembly and condensation, concentrated by the surfactant and silica species. The silica within the cast films continues to undergo hydrolysis and condensation reactions, solidifying the pore structure.

Common techniques for casting mesoporous thin films onto substrates include dip-coating, spray-coating, and spin-coating. The choice of support is crucial, as the film's resulting morphology is inherently dependent on its nature. Through EISA, a variety of pore structures can be achieved, ranging from 2D or 3D mesostructures to wormlike configurations in cases of less organized assemblies. Generally, 2D mesophases exhibit lower chemical and mechanical stability, and access to the pore channels is more challenging due to their parallel orientation to the surface. This orientation restricts the applications of these materials due to limited accessibility and mass transport rates (Figure D.7).

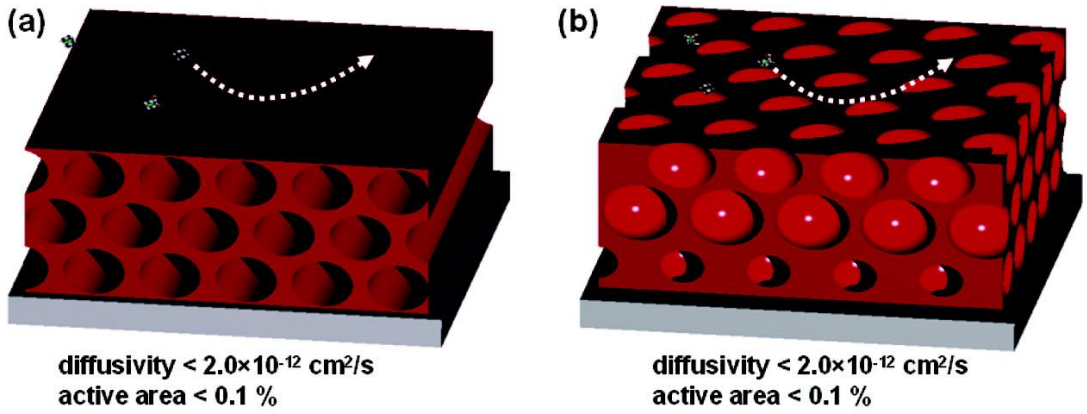

Figure D.7 (a) Representation of poor mass transport access of species through 2D hexagonal silica film and (b) face-centered cubic silica film [35].

From an application perspective, it is vital to develop devices with pores accessible from the surface, which are particularly promising for sensing and host-guest applications. Films with cylindrical mesochannels oriented perpendicularly to the

substrate present novel opportunities for such devices. However, fabricating vertically-aligned mesoporous silica films remains a considerable challenge.

3.4 Vertically aligned mesoporous silica film on electrode

The development of vertically aligned mesoporous silica films on electrodes has been a focal point in materials science, particularly for enhancing electrochemical applications. The quest for surface-accessible mesoporous structures dates back to 1998, when Zhao et al. first reported the synthesis of continuous mesoporous silica thin films with 3D-accessible pore structures. This breakthrough paved the way for further innovations in the field.

One notable approach for achieving vertical alignment was introduced by Teng et al., who utilized a Stöber solution—a mixture of tetraethoxysilane (TEOS), cetyltrimethylammonium bromide (CTAB), ethanol, and ammonia—for the growth of silica films. This method relies on the attachment of CTA^+ ions to form spherical micelles on negatively charged substrates, with hydrolyzed TEOS condensing on the micelle surfaces. The presence of ammonia catalyzes the transformation from spherical to cylindrical silica-CTAB structures, promoting vertical growth perpendicular to the substrate.

Other attempts have been reported. Techniques such as epitaxial-like growth on patterned substrates, scanning electrochemical microscopy, and the application of external fields (e.g., magnetic fields or radio frequencies) have been explored. Some methods even involve modifying the sol mixture with additives like decane to influence the film's structure. However, these approaches often come with significant drawbacks, including complex and time-consuming processes, elaborate substrate pre-treatments, limited pore orientation, and constraints on support types and geometries. Furthermore, achieving smaller pore sizes (below 5-6 nm) remains challenging, and there has been limited success in functionalizing the film surfaces to enhance their applicability in various electrochemical systems.

These challenges highlight the need for continued innovation and exploration of simpler, more versatile methods for fabricating vertically aligned mesoporous silica films.

3.4.1 Electrochemically-assisted Self-assembly (EASA)

Electrochemically Assisted Self-Assembly (EASA) represents a groundbreaking strategy in the fabrication of mesoporous films. This innovative method, pioneered by A. Walcarius and his team, has revolutionized the process of creating vertically structured mesoporous layers on conductive substrates[36]. Initially introduced in 2007, EASA has become a popular choice for modifying electrode surfaces with mesoporous silica thin films due to its efficiency and versatility. The core principle behind EASA, as depicted in Figure D.8 A, involves the application of a suitable cathodic potential to an electrode submerged in a hydrolyzed sol solution that contains a surfactant template, such as CTAB. The silica sol is initially kept at a pH of around 3–4, a value that makes hydrolysis faster than condensation.

The negative potential, typically around -1.3 V, triggers two significant phenomena. Primarily, it promotes the self-assembly of surfactants onto the electrode surface. Simultaneously, it generates hydroxide ions at the electrode-solution interface, leading to a local pH increase. The negatively charged silica clusters that form at pH 9–10 interact at the interface of the transient cationic hemimicelles that form at the interface. The process of silica condensation promotes the transformation of the hemicelles into cylindrical micelles forming the template for the vertically aligned mesopores (Figure D.8 B).

The pore organization and vertical orientation of the mesoporous silica film produced by EASA are regulated by the CTAB/TEOS ratio. Detailed studies, including one conducted by Goux et al., have identified three primary pore structures based on this ratio: amorphous (non-organized), weakly organized (wormlike structure), and a highly organized and oriented hexagonal structure, which is achieved within the CTAB/TEOS ratio range of 0.16 to 0.64. By maintaining a consistent cathodic potential (-1.3 V) and deposition time (20 seconds), the film thickness can be controlled by adjusting the TEOS concentration in the sol solution, which ranges from 50 to 350 mM, yielding a film thickness between 25 and 150 nm. The pore dimension can be increased by swelling with mesitylene[37] or using surfactants with a longer alkyl chain[38].

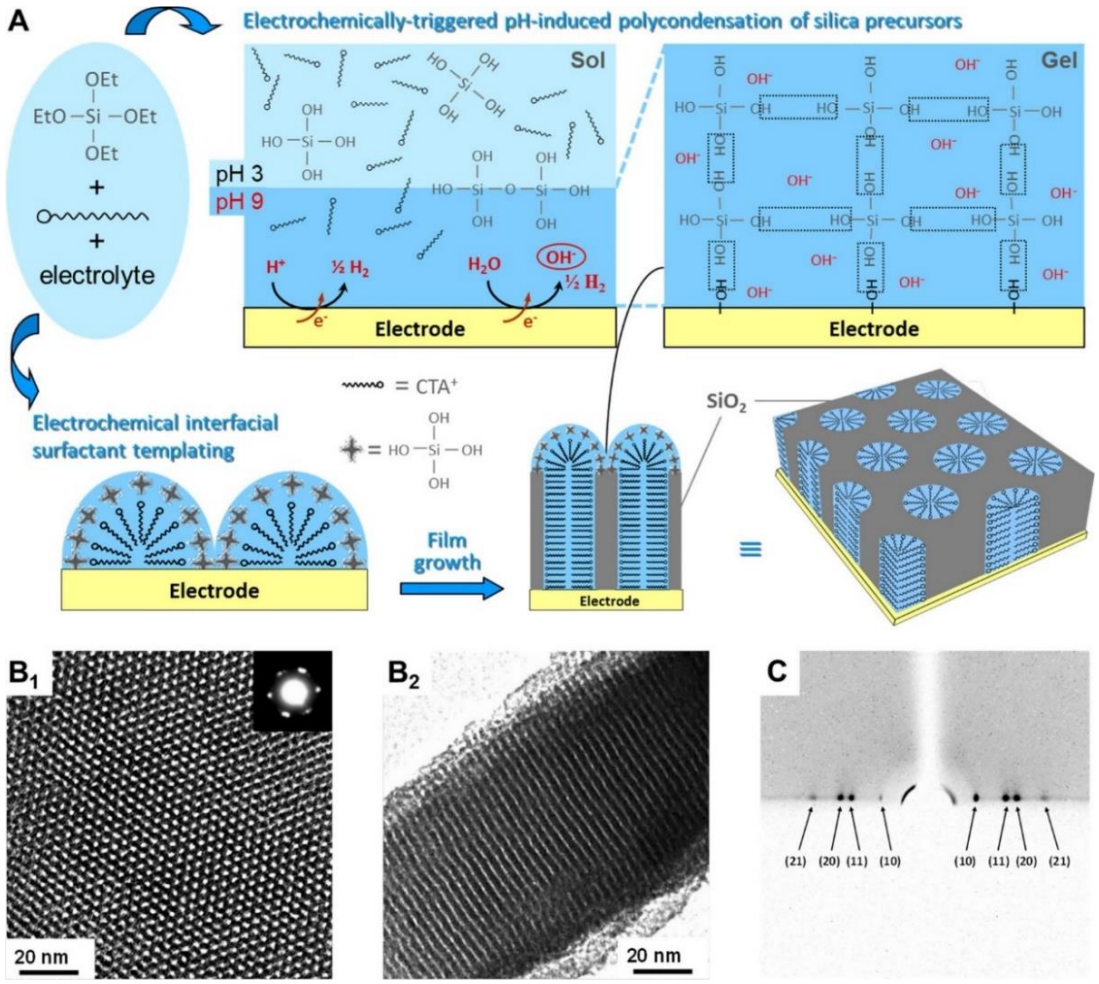

Figure D.8 (A) Schematic illustration of the EASA process. (B) TEM images of the ordered and oriented mesoporous silica film (B1) top view with electron diffraction pattern as inset; B2 cross-section). (C) Typical GI-XD pattern confirming the hexagonal packing of vertically aligned mesopore channels[39].

3.4.2 Electrochemical sensing at VMSFs modified electrode

Vertically aligned mesoporous silica films have emerged as a pivotal technology in the development of advanced electrochemical sensors. These films facilitate the regulated access of redox-active analytes to the electrode surface, thereby augmenting both the sensitivity and selectivity of the detection process.

A key feature of VMSFs is their size-selective permeability, attributed to the uniformity in shape and diameter of the mesopores within the films (Figure D.9 a). This sieving mechanism is critical for distinguishing analytes based on size. Li et al. showcased this property by illustrating the selective exclusion and permeation of ferritin, an iron-storage protein with a 12 nm diameter, through VMSFs with nanopores of different sizes[40]. Ferritin was able to permeate through 24-nm diameter mesopores, modified

with tetraethylene glycol (TEG) chains, while being excluded by smaller 19-nm nanopores. The TEG modification played a crucial role in minimizing non-specific adsorption, thereby enabling the size-dependent selectivity of the VMSFs (Figure D.9 b).

Beyond size exclusion, electrostatic interactions within the VMSFs significantly contribute to the selective sensing capabilities of modified electrodes (Figure D.9 c). The surface charge of the mesopores, which can be precisely determined using cyclic voltammetry (CV)[39], significantly affects the transport of charged species. This includes cationic, anionic, and neutral molecules, allowing for a nuanced control over the permeation process[40]. This precise control significantly improves the sensor's selectivity by effectively repelling interfering species through electrostatic exclusion. Moreover, the sensitivity of the sensor is markedly increased through a preconcentration mechanism, a direct consequence of the minimal nanopore size (2-3 nm in diameter) within the VMSFs. These small dimensions intensify electrostatic interactions between the solutes and the nanopore surfaces, facilitating the preconcentration effect and thus boosting sensitivity.

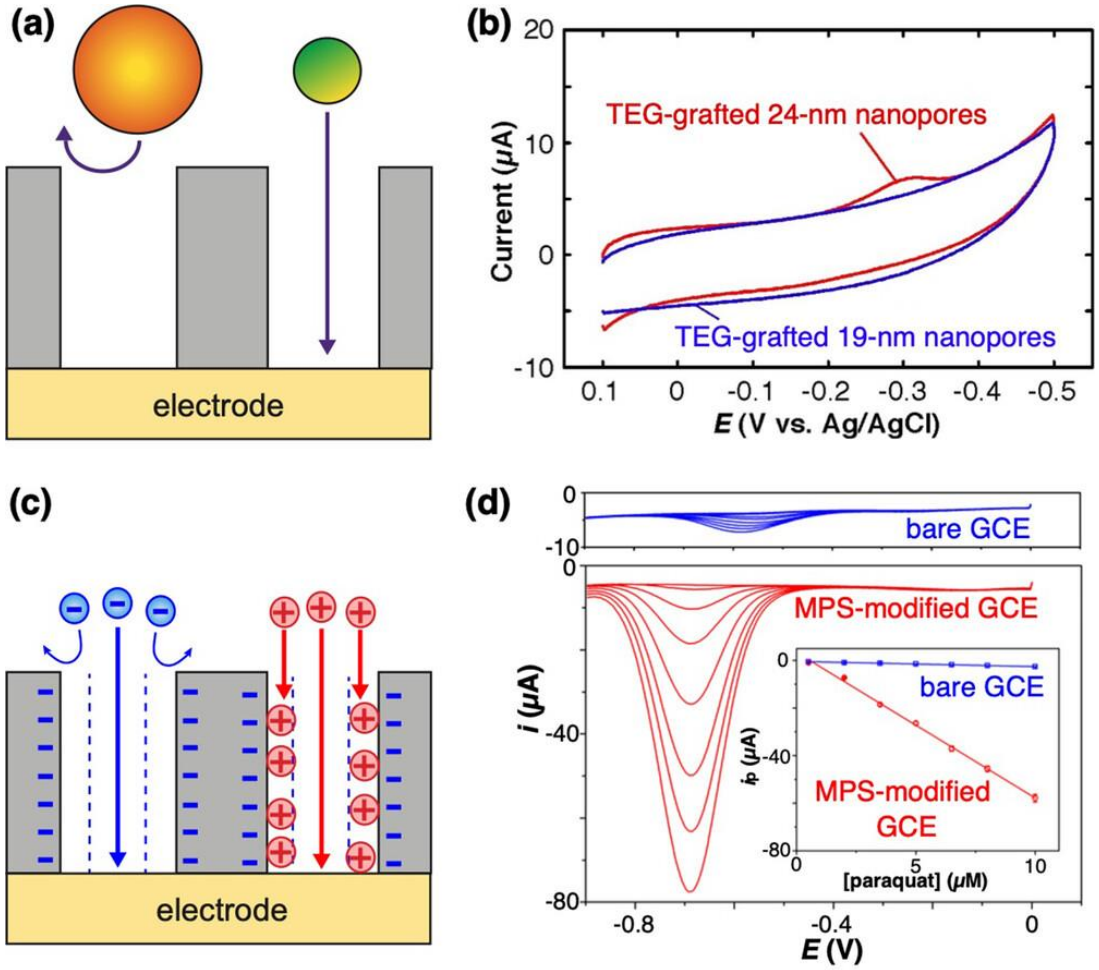

Figure D.9 (a) Size-selective permeation of redox-active analytes at an VMSF. (b) CV data of ferritin measured at VMSFs modified electrode with different pore diameters[40]. (c) Electrostatic exclusion (left) and preconcentration (right) of electroactive analytes at an VMSF. (d) DPV data and calibration curves of cationic paraquat measured at a bare GCE and an VMSF-modified GCE[41].

The significant impact of electrostatic effects on sensor performance is exemplified by the findings of Walcarius et al. [41]. Their research demonstrated the effective exclusion of anionic analytes like diclofenac and the preconcentration of cationic analytes such as paraquat in negatively charged VMSF-modified glassy carbon electrodes (GCEs). This electrostatically driven preconcentration led to an impressive 30-fold increase in the detection sensitivity for paraquat when compared to unmodified GCEs, underscoring the profound influence of electrostatic interactions on enhancing electrochemical sensor performance (Figure D.9 d).

Further evidence is provided by Yan et al., who achieved highly sensitive detection of doxorubicin in human whole blood samples using VMSF-coated GCEs[42]. The exceptional sensitivity of these modified electrodes was attributed to the mesoporous

film's antifouling properties and the electrostatic enrichment of cationic doxorubicin (Figure D.10 A).

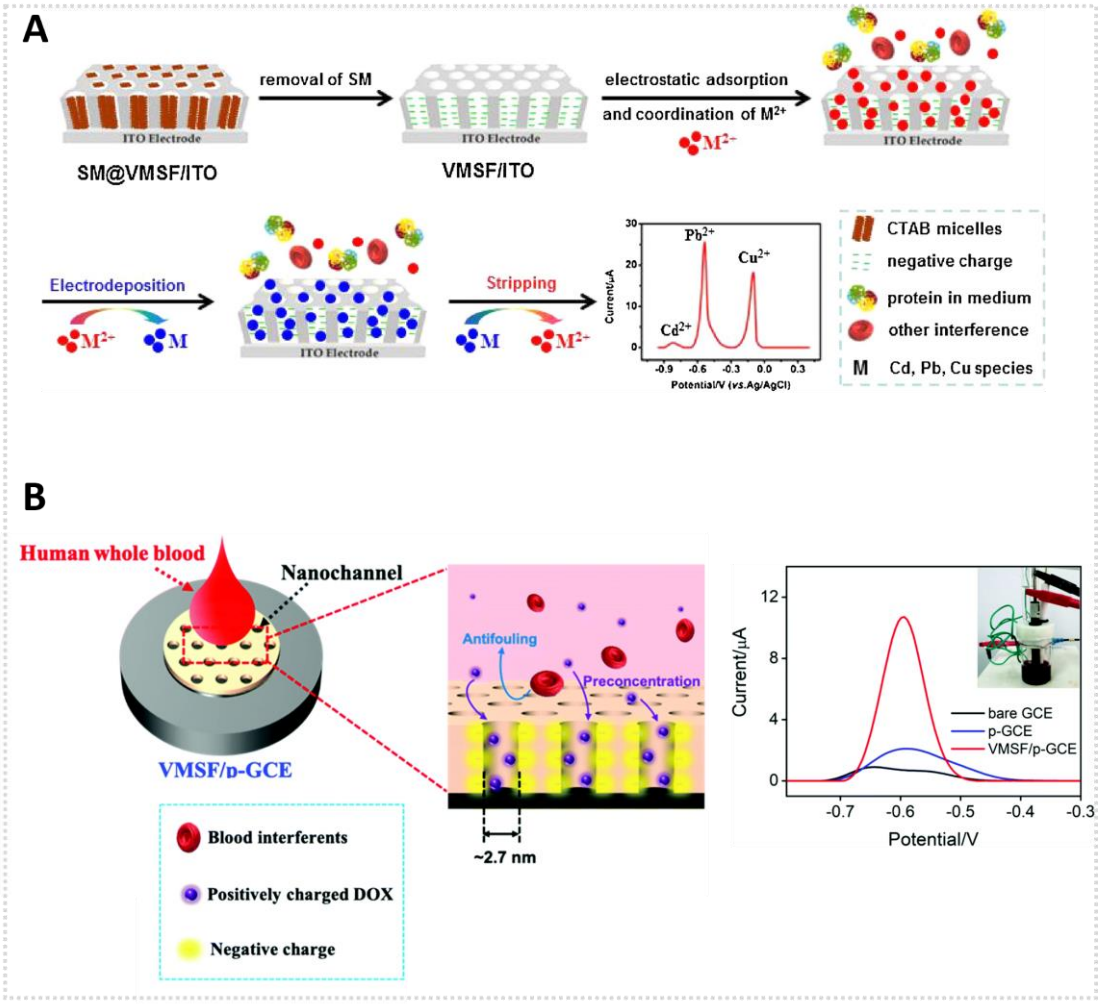

Figure D.10 (A) Schematic illustration of the preparation of VMSF/ITO sensor and its simultaneous detection of Pb^{2+}, Cu^{2+} and Cd^{2+} [43]. (B) Illustration of the meso-architecture of the VMSF/p-GCE for doxorubicin sensing [42].

Additionally, Chen et al. utilized VMSF-based resin nanoelectrodes for the detection of heavy metal ions such as Pb^{2+}, Cu^{2+}, and Cd^{2+} through stripping voltammetry [43]. The thin films not only served as effective antifouling layers in complex matrix samples but also significantly improved the detection sensitivity of these metal ions through the electrostatic enrichment of target cations within the negatively charged nanopores (Figure D.10 B).

In addition to these mechanisms, VMSFs have been employed before the removal of surfactants, introducing a novel sensing strategy based on the hydrophobic effect. Su and colleagues utilized surfactant-filled VMS films for the selective detection of

uncharged, hydrophobic analytes such as nitroaromatic pesticides and chloramphenicol[44]. The retention of surfactants within the mesopores led to the preconcentration of hydrophobic analytes, lowering the limit of detection (LOD) and enabling effective sensing in complex matrices like human whole blood, leveraging the sieving properties of the VMSF mesopores.

The functionalization of mesoporous silica films significantly broadens their applicability in electrochemical sensing by enabling the attachment of a diverse array of organic and inorganic groups, nanoparticles, small biomolecules, or ions[45]. This modification process alters the intrinsic properties of the films, tailoring them for more specific sensing applications.

Functionalization can be achieved through various methods, with co-condensation and post-grafting being the predominant techniques[46]. Co-condensation involves the integration of functional groups into the sol-gel solution, ensuring their uniform distribution throughout the material. Post-grafting, conversely, involves attaching functional groups to the surface of the mesoporous material after the film has been formed, which can enhance the accessibility and functionality of these groups.

A particularly effective approach for creating organically functionalized films without compromising their mesochannel structure or ordering is the combination of electrically assisted self-assembly (EASA) with click chemistry. This method preserves the integrity of the mesochannels while allowing for the introduction of functional groups.

When functionalizing with redox-active groups, such as ferrocene, it becomes possible to facilitate long-range electron transfer through the otherwise insulating silica matrix via electron hopping[47]. For example, ferrocene-functionalized VMSFs have been utilized in the indirect amperometric detection of non-redox-active anions[48] (Figure D.11 A), as well as in the selective sensing of biomolecules like cysteine over glutathione.

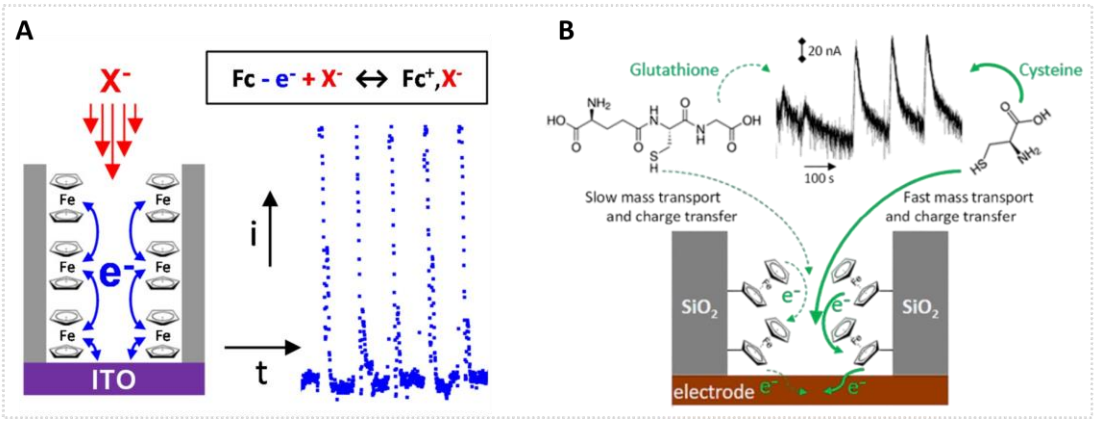

Figure D.11 (A) vertically-oriented, ferrocene-functionalized, mesoporous silica film on ITO electrode and, with description of the electron transfer mechanism involving the ingress of the electrolyte anion (X^-) upon ferrocene oxidation into ferricinium ion [48]. (B) Representation of flow injection analysis of 50 µM of glutathione and cysteine at a ferrocene-functionalized film electrode [49].

In a notable study by Maheshwar et al., the selective detection of cysteine was achieved by exploiting the slow oxidation kinetics of glutathione[49] (Figure D.11 B). By immobilizing ferrocene within the silica mesochannels, the sensor could selectively oxidize cysteine present in the solution at the ferrocene-functionalized films, while glutathione remained unreacted. This selective detection is a result of the combined effects of charge transfer kinetics and mass transport limitations, showcasing the potential of functionalized mesoporous silica films in enhancing the selectivity and sensitivity of electrochemical sensors.

References

[1] G. S. Day, H. F. Drake, H. C. Zhou, M. R. Ryder, *Commun. Chem.* **2021**, *4*, 1–4.

[2] N. Pal, D. Chakraborty, E. B. Cho, J. G. Seo, *Nanomaterials* **2023**, *13*, 2184.

[3] S. Shubhashish, A. S. Amin, Y. Dang, S. J. Karasik, H. S. Khanna, S. L. Suib, *ACS Appl. Nano Mater.* **2022**, *5*, 7078–7091.

[4] T. Kumeria, *ACS Biomater. Sci. Eng.* **2022**, *8*, 4025–4027.

[5] Q. Wei, F. Xiong, S. Tan, L. Huang, E. H. Lan, B. Dunn, L. Mai, *Adv. Mater.* **2017**, *29*, 1602300.

[6] K. Lan, D. Zhao, *Nano Lett.* **2022**, *22*, 3177–3179.

[7] S. S. Danewalia, K. Singh, *Mater. Today Bio* **2021**, *10*, 100100.

[8] K. Na, M. Choi, R. Ryoo, in *Microporous Mesoporous Mater.*, Elsevier, **2013**, pp. 3–19.

[9] N. Nassif, J. Livage, *Chem. Soc. Rev.* **2011**, *40*, 849–859.

[10] K. S. A. Butcher, J. M. Ferris, M. R. Phillips, M. Wintrebert-Fouquet, J. W. Jong Wah, N. Jovanovic, W. Vyverman, V. A. Chepurnov, *Mater. Sci. Eng. C* **2005**, *25*, 658–663.

[11] L. De Stefano, P. Maddalena, L. Moretti, I. Rea, I. Rendina, E. De Tommasi, V. Mocella, M. De Stefano, *Superlattices Microstruct.* **2009**, *46*, 84–89.

[12] T. Yanagisawa, T. Shimizu, K. Kuroda, C. Kato, *Bull. Chem. Soc. Jpn.* **1990**, *63*, 988–992.

[13] R. Narayan, U. Y. Nayak, A. M. Raichur, S. Garg, *Pharmaceutics* **2018**, *10*, DOI 10.3390/pharmaceutics10030118.

[14] C. J. Brinker, *J. Non. Cryst. Solids* **1988**, *100*, 31–50.

[15] L. P. Singh, S. K. Bhattacharyya, R. Kumar, G. Mishra, U. Sharma, G. Singh, S. Ahalawat, *Adv. Colloid Interface Sci.* **2014**, *214*, 17–37.

[16] H. Ghaedi, M. Zhao, *Energy and Fuels* **2022**, *36*, 2424–2446.

[17] F. Hoffmann, M. Cornelius, J. Morell, M. Fröba, *Angew. Chemie - Int. Ed.* **2006**, *45*, 3216–3251.

[18] S. Kumar, M. M. Malik, R. Purohit, *Mater. Today Proc.* **2017**, *4*, 350–357.

[19] F. Hoffmann, M. Cornelius, J. Morell, M. Fröba, *Angew. Chemie - Int. Ed.* **2006**, *45*, 3216–3251.

[20] A. Galarneau, A. Sachse, B. Said, C. H. Pelisson, P. Boscaro, N. Brun, L. Courtheoux, N. Olivi-Tran, B. Coasne, F. Fajula, *Comptes Rendus Chim.* **2016**, *19*, 231–247.

[21] V. Miglio, C. Zaccone, C. Vittoni, I. Braschi, E. Buscaroli, G. Golemme, L. Marchese, C. Bisio, *Molecules* **2021**, *26*, 1316.

[22] J. Wagner, D. Gößl, N. Ustyanovska, M. Xiong, D. Hauser, O. Zhuzhgova, S. Hočevar, B. Taskoparan, L. Poller, S. Datz, H. Engelke, Y. Daali, T. Bein, C. Bourquin, *ACS Nano* **2021**, *15*, 4450–4466.

[23] W. Zhao, H. Wang, H. Wang, Y. Han, Z. Zheng, X. Liu, B. Feng, H. Zhang, *Nanoscale* **2021**, *13*, 6394–6399.

[24] F. Hoffmann, M. Fröba, *Chem. Soc. Rev.* **2011**, *40*, 608–620.

[25] A. Walcarius, *Chem. Soc. Rev.* **2013**, *42*, 4098.

[26] G. Zhu, Q. Yang, D. Jiang, J. Yang, L. Zhang, Y. Li, C. Li, *J. Chromatogr. A* **2006**, *1103*, 257–264.

[27] A. Katiyar, S. Yadav, P. G. Smirniotis, N. G. Pinto, *J. Chromatogr. A* **2006**, *1122*, 13–20.

[28] M. Parra, S. Gil, P. Gaviña, A. M. Costero, *Sensors* **2022**, *22*, 261.

[29] Q. Huo, D. Zhao, J. Feng, K. Weston, S. K. Buratto, G. D. Stucky, S. Schacht, F. Schüth, *Adv. Mater.* **1997**, *9*, 974–978.

[30] B. Yao, D. Fleming, M. A. Morris, S. E. Lawrence, *Chem. Mater.* **2004**, *16*, 4851–4855.

[31] Y. Yang, M. Suzuki, S. Owa, H. Shirai, K. Hanabusa, *J. Mater. Chem.* **2006**, *16*, 1644–1650.

[32] C. J. Brinker, Y. Lu, A. Sellinger, H. Fan, *Adv. Mater.* **1999**, *11*, 579–585.

[33] H. Yang, N. Coombs, I. Sokolov, G. A. Ozin, *Nature* **1996**, *381*, 589–592.

[34] D. Grosso, F. Cagnol, G. J. D. A. A. Soler-Illia, E. L. Crepaldi, H. Amenitsch,

A. Brunet-Bruneau, A. Bourgeois, C. Sanchez, *Adv. Funct. Mater.* **2004**, *14*, 309–322.

[35] T. C. Wei, H. W. Hillhouse, *Langmuir* **2007**, *23*, 5689–5699.

[36] A. Walcarius, E. Sibottier, M. Etienne, J. Ghanbaja, *Nat. Mater.* **2007**, *6*, 602–608.

[37] C. Robertson, R. Beanland, S. A. Boden, A. L. Hector, R. J. Kashtiban, J. Sloan, D. C. Smith, A. Walcarius, *Phys. Chem. Chem. Phys.* **2015**, *17*, 4763–4770.

[38] N. A. N. Mohamed, Y. Han, A. L. Hector, A. R. Houghton, E. Hunter-Sellars, G. Reid, D. R. Williams, W. Zhang, *Langmuir* **2022**, *38*, 2257–2266.

[39] A. Walcarius, *Acc. Chem. Res.* **2021**, *54*, 3563–3575.

[40] W. Li, L. Ding, Q. Wang, B. Su, *Analyst* **2014**, *139*, 3926–3931.

[41] T. Nasir, G. Herzog, M. Hébrant, C. Despas, L. Liu, A. Walcarius, *ACS Sensors* **2018**, *3*, 484–493.

[42] M. Wang, J. Lin, J. Gong, M. Ma, H. Tang, J. Liu, F. Yan, *RSC Adv.* **2021**, *11*, 9021–9028.

[43] B. Cheng, L. Zhou, L. Lu, J. Liu, X. Dong, F. Xi, P. Chen, *Sensors Actuators B* **2018**, *259*, 364–371.

[44] Q. Sun, F. Yan, L. Yao, B. Su, *Anal. Chem.* **2016**, *88*, 8364–8368.

[45] A. Walcarius, *Curr. Opin. Electrochem.* **2018**, *10*, 88–97.

[46] B. Sartori, H. Amenitsch, B. Marmiroli, *Micromachines* **2021**, *12*, DOI 10.3390/MI12070740.

[47] N. Vilà, E. André, R. Ciganda, J. Ruiz, D. Astruc, A. Walcarius, *Chem. Mater.* **2016**, *28*, 2511–2514.

[48] C. Karman, N. Vilà, C. Despas, A. Walcarius, *Electrochim. Acta* **2017**, *228*, 659–666.

[49] H. Maheshwari, N. Vilà, G. Herzog, A. Walcarius, *ChemElectroChem* **2020**, *7*, 2095–2101.